Micro fluidised bed technology for the screening of carbon capture adsorbents (Chemical Engineering)

by

Awad Alamri

A thesis presented for the degree of

Doctor of Philosophy

School of Engineering

Newcastle University, UK

October 2023

Abstract

To accomplish global Net Zero emissions goals, a diverse portfolio of technologies, regulations, frameworks, and changes in behaviour will be required. Within this landscape, carbon capture is still relevant in reducing or entirely offsetting greenhouse gas emissions, particularly emissions that cannot be avoided in the immediate or long-term. Adsorption-based processes using solid sorbents are appealing due to their high flexibility, non-volatility and low energy regeneration burden. Ultimately, the success of adsorption-based processes depends on the development of the materials (rapid kinetics, high capacities, high stabilities, high selectivities, etc.) and gas-solid contacting technology (good mixing, low-pressure drop, etc.).

This thesis proposes that 3D-printed Micro Fluidised Bed Reactor (MFBR) technology can meet these requirements due to cost-effectiveness, high-throughput capability, minimal energy requirement, efficient heat/mass transfer characteristics, and enhanced safety measures. In the early phases of material development, only small volumes of samples are typically synthesised; it would be inefficient to mass-produce potentially poor-performing materials before their complete characterisation. Thus, the MFBR's primary function is to facilitate data collection of new materials under relevant operating conditions, thereby enabling informed decision-making. Accordingly, this thesis aims to develop the MFBR as a platform for low-cost and rapid screening of novel CO_2 adsorbents. To demonstrate this approach, 3D-printed micro fluidised beds are used to screen the performance of a commercially available hydrotalcite product (PURAL MG70, Sasol).

In its raw as-supplied state, this powdered hydrotalcite has significant cohesive characteristics that prevent fluidisation. Accordingly, detailed hydrodynamic experiments were first performed in order to find feasible MFBR designs and operating conditions for these Geldart C powders by studying the pressure drop characteristics. The hydrodynamic studies demonstrate that the fluidisation quality was significantly enhanced by employing a straightforward removal of fines through pre-sieving, specifically retaining particles larger than 53 μm (density of 2 g/cm^3), followed by pre-fluidisation. This improved quality included removing a significant hysteresis between increasing and decreasing the gas velocity, minimising the amplitude of the pressure drop overshoot prior to fluidisation, and ensuring that the whole bed was fluidised without gas bypassing (slugging). Furthermore, addition of a secondary inert Geldart A type particle (silica, with a mean particle size of 93 ± 10 μm and density of 2.65 g/cm^3) to the hydrotalcite powder

resulted in similar improved fluidisation quality. These treatments were valid in three different 3D-printed MFBRs (bed diameters of D_t = 10–15 mm) at all bed heights tested (H_s/D_t = 1–3). Following this, the adsorption process was studied using CO_2 breakthrough experiments, validated against independent TGA measurements. These breakthrough tests were conducted for a 10 mm bed diameter at various bed heights (H_s/D_t = 2–3), CO_2 concentration (8–16 vol%), superficial gas velocities (1.5–6 U_{mf}) and operating temperatures (25–60 °C). The results indicate that the measured CO_2 adsorption capacity increases as the gas velocity increases in the bubbling regime before decreasing again in the slugging regime. A maximum capacity of 0.76 mmol/g was measured when operating at $4U_{mf}$, 16 vol%, and 40 °C. The capacity declined at lower velocities (<3 U_{mf}) because of inadequate gas-solid mixing and declined at higher velocities (>4 U_{mf}) because of gas bypassing due to slugging. The maximum capacities observed agreed with independent TGA measurements at all conditions. This agreement defined the operating window for studying the adsorption kinetics (corresponding to operating under kinetically limited conditions). At 16 vol% CO_2 concentration, the desirable kinetically limited velocity range was 3 – 4 U_{mf}. At a lower CO_2 concentration of 8 vol%, the process was mainly diffusion-limited, which reduced the width of the operating window; only $4U_{mf}$ achieved the kinetically limited state. This highlights the importance of including hydrodynamic screening in the workflow of materials development using the MFBR platform.

Finally, the desorption kinetics were studied through the implementation of temperature swing adsorption, where adsorption was performed at 40 °C (which gave the highest capacities) and desorption was performed between 40 °C and 90 °C. At desorption temperatures of 40 °C, expectedly, a low 7% CO_2 recovery was observed. At 90 °C, the CO_2 recovery increased to 33% of the adsorbed CO_2. Raising the desorption temperature changes the thermodynamic equilibrium, destabilising the affinity of the CO_2 to the hydrotalcite by overcoming the activation energy of weak Van der Waals forces or chemical interactions with the surface. The maximum 'desorbed capacity' was measured to be 0.24 mmol/g at 90 °C. Based on the results obtained in this thesis, it can be concluded that 3D-printed micro fluidised beds can be used for the development of carbon capture sorbents, offering insights for decision-making and design.

Keywords: 3D-printed Micro-Fluidised Bed, Gas-solid Fluidisation, Carbon Capture, Hydrotalcite, Pressure Drop Analysis, Kinetics Screening

Declaration

I, Awad Alamri, hereby certify that this thesis is my original work and that it has not been used for any other academic purpose or degree. All sources and references have also been properly cited.

Awad Alamri

2023

Acknowledgements

I would like to express my heartfelt gratitude to my academic mentors, Dr. Vladimir Zivkovic and Dr. Jonathan McDonough, whose constant guidance and unwavering support were invaluable throughout my doctoral studies. Their wealth of expertise, dedication, and invaluable ideas influenced the direction of my research and my progress greatly. I appreciate their patience, support, and willingness to share their knowledge. Their assessment of my work, helpful input, and aid in overcoming research problems have all played an important role in my academic career. I appreciate their faith in my abilities and their encouragement to push me towards success in research and personal development. Working with such outstanding mentors has been an honour.

I dedicate this thesis to my late parents, particularly my mother, who, although she is no longer with us, provided constant support and encouragement during the initial stages of my Ph.D. Her faith in my abilities and her sacrifices for my education have left an unforgettable impact on my journey for knowledge. I am grateful to my wife, Amal, for her continuous support, as well as to my son, Yazeed, and daughters, Sadeem and Jana, for their patience and encouragement throughout my studies. Their love and sacrifices have been critical to my accomplishments, and I am grateful for their contribution to my success.

Finally, I want to express my heartfelt gratitude to all of my brothers and sisters who have constantly supported me during my Ph.D. journey.

Table of Contents

List of Figures

List of Tables

Publications and Conferences

Publications

- Awad Alamri, Jonathan McDonough, Vladimir Zivkovic, Fluidisation behaviour and wall effects of cohesive hydrotalcite powder in a micro-fluidised bed by Powder Technology 415 (2023) 118192.

- Awad Alamri, Jonathan McDonough, Vladimir Zivkovic, Screening of a carbon capture adsorbent using a 3D-printed Micro fluidised bed. *In development*, to be submitted to Chemical Engineering Journal.

Conference Presentations

- Awad Alamri, Jonathan McDonough, Vladimir Zivkovic. Fluidisation of a Geldart C Powder in a Micro-Fluidised Bed". Oral presented at 9th World Congress on Particle Technology on September 18-22, 2022, in Madrid, Spain, in-person.

- Awad Alamri, Jonathan McDonough, Vladimir Zivkovic. Hydrodynamic testing of fluidisation of CO_2 adsorbent in MFB". Abstract was accepted for Oral Presentation at 24th International Conference on Fluidised Bed Conversion on May 8-11, 2022, in Gothenburg, Sweden.

Nomenclature

A	Cross-sectional area of the column (m^2)
C_{Outlet}	Outlet CO_2 Concentration (vol %)
C_{Inlet}	Inlet CO_2 concentration (vol%)
d_p	Particle diameter(m)
D_t	Bed diameter(m)
g	Gravitational acceleration (9.81 m/s^2)
H_b	Bed height during fluidisation (m)
H_s	Static bed height (m)
K_1	Adsorption rate constant (Pseudo-first order model)
K_2	Adsorption rate constant (Pseudo-second order model)
K_f	Adsorption rate constant (Fractional-order model)
m_1	Empirical coefficient
m	Total bed mass (kg)
n	Empirical coefficient
q_e	The equilibrium CO_2 uptake (mmol/g)
$q_t(\text{exp})$	The CO_2 uptake at time t (mmol/g)
$\tilde{q}(\text{exp})$	The mean CO_2 uptake (mmol/g)
$q_t(\text{model})$	The model- predicted CO_2 uptake value at time t
R_e	Reynolds number
R^2	Coefficient of determination
T	Temperature (°C)
U_g	Gas velocity (m/s)
U_{mb}	Minimum bubbling velocity (m/s)
U_{mf}	Minimum fluidisation velocity (m/s)

U_{ms}	Minimum slugging velocity (m/s)
V_p	Volume of particle bed (m^3)
V_t	Total volume of the bed [including voids] (m^3)

Greek Letters

ΔP	Total pressure drop of fluidised bed system (Pa)
ΔP_B	Pressure drop across fluidised bed (Pa)
ΔP_{bed}	Pressure drop due to buoyant weight of the particle bed (Pa)
ΔP_E	Excess pressure drop (Pa)
ΔP_{os}	Pressure drop overshoot (Pa)
ΔP_w	Extra pressure drop resulting from wall friction (Pa)
μ_g	Dynamic viscosity of fluidising gas (Pa.s)
ε	Voidage
$\sigma_{\Delta P}$	Standard deviation of pressure drop signal (Pa)
ρ_g	Density of fluidising gas (kg/m^3)
ρ_p	Particle density (kg/m^3)
$\Delta\tau$	Breakthrough time (s)
τ_{95}	The time required to reach 95% of the total concentration value (s)
τ_{05}	The time required to reach 5% of the total concentration value (s)

Abbreviations

AM	Additive Manufacturing
ASU	An air separation unit
BC	Breakthrough Curve
BT	Breakthrough Time
CFB	Circulating Fluidised Bed
CCS	Carbon Capture and Storage
FB	Fluidised Bed
IGCC	Integrated Gasification Combined Cycle
IR	Infrared
LDF	Linear Driving Force
LDHs	Layered Double Hydroxides
MBA	Moving-Bed Adsorption
MFB	Micro Fluidised Bed
MFB-TGA	Micro fluidised Bed Thermogravimetric Analysis
MTO	Methanol-To-Olefins
MG70	Hydrotalcite – PURAL
MMO	Mixed Metal Oxides
PC	Pulverized Coal
PDMS	Polydimethylsiloxane
PSA	Pressure Swing Adsorption
TGA	Thermogravimetric Analysis
TSA	Temperature swing adsorption
UV light	Ultraviolet light
VSA	Vacuum Swing Adsorption
BPEI	Branched Polyethyleneimine

Chapter 1. Introduction

1.1 Carbon Capture

In many developing countries, growing urbanisation and industrialisation have caused significant rises in greenhouse gases, especially CO_2, leading to climate change and global warming (Biniek *et al.*, 2020). The impacts of climate change including food security, global agricultural production, rising sea levels, soil and water degradation, migration, severe cyclones, and economic damage, are harmful (Rabbani *et al.*, 2013; Kumar *et al.*, 2018). Therefore, to solve these problems, it is necessary to reduce CO_2 emissions and devise strategies for preventing environmental degradation. One of the most common techniques to achieve this is carbon capture. The main aim of carbon capture processes is to diminish the association between economic development and greenhouse gas emissions by effectively capturing CO_2 emissions from various sources besides relying on renewable energy. This could encourage the achievement of a more sustainable and environmentally conscious economic growth direction (Álvarez *et al.*, 2017). These technologies offer a viable path to decarbonising energy-intensive sectors, such as steel production, cement manufacture, and power generation, which are some of the principal sources of CO_2 emissions (McDonough *et al.*, 2018). Different techniques and technologies are used in each strategy to selectively extract CO_2 from flue gases, providing flexibility and allowing carbon capture to be adapted to various emission sources and industries depending on the requirements. Carbon capture includes a variety of approaches, such as precombustion capture, post-combustion and oxy-fuel combustion capture. The post-combustion capture, for example, includes eliminating CO_2 from flue gases after combustion of the fuel has occurred (Krishnamurthy *et al.*, 2021). Precombustion capture, on the other hand, focuses on catching CO_2 before the fuel is burned, while oxy-fuel combustion yields flue gas mostly composed of CO_2 rather than air by burning the fuel in pure oxygen, simplifying the capture procedure (Kanniche *et al.*, 2010).

Post-combustion carbon capture systems involve several types (Mukherjee *et al.*, 2019), including absorption, where CO_2 is dissolved in a liquid solvent (Cousins *et al.*, 2011); adsorption, where CO_2 is captured by adherence to solid sorbents (Monazam *et al.*, 2013); membrane separation, in which CO_2 is selectively removed from the gas stream (Kárászová *et al.*, 2020); cryogenic separation, where CO_2 is condensed using low temperatures (Font-Palma *et al.*, 2021); and hybrid technologies, which employ a combination of different methods. Each

approach has benefits and disadvantages, and the selection is influenced by criteria such as capture efficiency, gas composition, cost-effectiveness, and scalability (Kanniche *et al.*, 2010). The main barrier to early CCS (Carbon Capture and Storge) implementation is the high energy penalty. Hence, several studies have been conducted to develop low-energy demand capture methods (Mukherjee *et al.*, 2019; Rogelj *et al.*, 2021). Ultimately, there has been increased worldwide effort to seek alternative, less expensive carbon capture technologies, where the industrial sector has shown an interest in working on CO_2 footprint control (Anwar *et al.*, 2018).

1.1.1 Carbon Capture Using Adsorption Process

Adsorption can be employed for CO_2 capture from exhaust gases and other emission sources, where CO_2 binds to the surface of solid adsorbent materials. Adsorption and desorption are implemented regularly to adsorb and regenerate CO_2 from adsorbent materials. Adsorption is a technique that can be utilised for capturing carbon from emission sources, including iron/steel and cement refineries (McDonough *et al.*, 2018). The adsorption technique has several advantages, including process simplicity, low operating costs, extensive operational flexibility, moderate operating conditions, and a broad operating temperature range (Lee and Park, 2015; Chao *et al.*, 2021; Raganati *et al.*, 2021).

Physical and chemical adsorption are the two distinct categories of the adsorption process. Physical adsorption describes the binding of CO_2 onto the surface using weak van der Waals forces. In contrast, chemical adsorption occurs when CO_2 is attached to the surface by forming strong chemical bonds (Ben-Mansour *et al.*, 2016; Allangawi *et al.*, 2023). This process offers a potentially effective strategy for capturing and reducing carbon emissions. However, the extent to which it outperforms competing methods depends upon the specific operating conditions in which it is used. Adsorption demonstrates its advantages in situations where certain characteristics are of utmost importance. In situations where the concentration of carbon dioxide (CO_2) is comparatively low, or the objective is to collect small quantities from various gas streams, the use of adsorption may provide a more cost-effective, and efficient alternative when compared to energy-intensive techniques, such as chemical absorption (Chao *et al.*, 2021; Allangawi *et al.*, 2023).

Adsorption systems also have the benefit of being more compact, which makes them suitable for applications with limited space (Vasta, 2023). Nevertheless, it is essential to recognise that

adsorption may not consistently surpass alternative methodologies, particularly in scenarios involving raised CO_2 concentrations or where a quick mass transfer is important. Therefore, the decision between adsorption and other methods should be made carefully, taking into account factors such CO_2 concentration, limitations in infrastructure, and specific objectives of the project. This emphasises the importance of adopting a customised approach to carbon dioxide capture that aligns with the specific requirements of each individual condition so that Net Zero can be reached.

1.2 Carbon Capture Using Fluidised Beds

The adsorption process can be performed in fixed, moving, or fluidised bed technologies (McDonough *et al.*, 2018). In fluidised beds, when the drag force on the solid particles exerted by the fluid exceeds the particle weight, they become suspended whereby they behave as a well-mixed fluid themselves. In the case of an adsorption process, this is accomplished by rapidly introducing a gas into the bed to overcome the gravitational pull on the particles (Yates, 2013). Compared to fixed-bed platforms, fluidised beds present several benefits for carbon capture, including improved gas-solid contact that ensures consistent mixing and reduction of dead zones leading to improved mass and heat transfer (Li *et al.*, 2017).

The development and improvement of fluidised-bed-based carbon capture technologies have garnered considerable focus in recent years, particularly in the selection and characterisation of appropriate adsorbents, knowledge of the interactions between gases and solids, and investigation of new reactor designs and methods of operation. Fluidised bed techniques could be of significance in effectively expanding the use of carbon capture technology from experimental settings in laboratories to real-world industrial implementation. The scalability of these technologies becomes apparent when they are used in industrial settings since the concepts that may be proven in the laboratory could successfully apply to bigger reactors without compromising the fundamental processes. Through a systematic process of carefully adjusting variables in controlled micro fluidised bed systems, researchers aim to improve the interactions between gases and particles, with the goal of optimising the adsorption process. Using the micro fluidised bed carbon capture technique provides for studying the effect of various operating conditions for instance flow regime, gas flow rates, temperature, and concentration on the adsorption of carbon dioxide (CO_2) which could provide a reliable basic framework for scaling up carbon capture, accommodating diverse environments, and

facilitating a seamless transfer from laboratory experimentation to commercial implementation (Raganati *et al.*, 2021).

Fluidised bed carbon capture technology has the potential to decrease CO_2 emissions from the combustion of fossil fuels such as natural gas, coal, and oil, as well as from chemical reactions, including the cement-production process. Further, small-scale micro fluidised bed (MFB) technology could have a distinctive function in developing solid adsorbent materials by providing a scalable, fast, controlled, and cost-effective tool for investigating and improving the interactions between sorbent surfaces and gas molecules. However, the implementation of MFB technology faces capacity, selectivity, and energy-efficient regeneration challenges.

1.3 Why Employ Micro-Fluidised Beds?

The concept of microfluidic able channels with a small internal diameter was first proposed by Potic *et al.* (2005). Subsequently, a range of definitions for micro-fluidised beds has been proposed, with the key criteria for classification being the diameter of the bed, which spans from 1 mm (Zivkovic and Biggs, 2015) to 15.5 mm (Guo *et al.*, 2009; McDonough *et al.*, 2019). The notion of a gas-solid MFB was later introduced by Liu *et al.* (2008) (Han *et al.*, 2021; Qie *et al.*, 2022).

Over the past 20 years, studies of MFB have identified the main operational behaviours, such as wall effect, fluidisation regimes, residence time distribution, diffusion resistance, back mixing, and gas/solid mixing (Han *et al.*, 2020; Qie *et al.*, 2022). MFBs are characterised by their high mass/heat transfer rates, excellent mixing, cost effectiveness, short response times, temperature consistency, and good gas plug flow (Geng *et al.*, 2018). MFBs have been employed in various applications, such as chemical reactions, catalyst production, and materials screening. Soft lithography, micro-machining, additive manufacturing, and capillary systems may all be used to fabricate MFBs using materials such as Perspex, quartz, stainless steel, and polymer (Zhang *et al.*, 2021b).

Micro-fluidised beds (MFBs) have been identified as a suitable choice for the examination of carbon capture sorbents in this thesis. First, MFB systems allow for scale reduction as they function on a smaller scale than traditional fluidised bed systems (Qie *et al.*, 2022). This decrease in size allows researchers to investigate carbon capture performance using smaller quantities of adsorbent material; this is beneficial in the case of new and costly sorbents or those

in limited supply due to the reduction in expenditure, costs, waste, and energy required for testing. Second, the controlled experimental platform offered by MFBs allows one to evaluate the effects of various process Parameters on carbon capture performance and determine the optimal operating conditions. This data can be used to Optimize the planning and implementation of large-scale carbon capture systems, resulting in increased efficiency and cost-effectiveness. Third, MFBs can rapidly screen a wide range of sorbent materials and assess the carbon capture performance of multiple sorbents in parallel or simultaneously. This expedites the screening process, assisting in identifying potential sorbents for further studies and development. Fourth, studies have found that MFBs enhance the mass/heat transfer properties (Wang *et al.*, 2020a). This increases the carbon capture efficiency and promotes sorbent regeneration, decreasing the overall energy needs and operating expenses of the carbon capture development pipeline. Such interactions are crucial in determining the efficiency of carbon capture solid sorbents, including Parameters such as their sorption capacity, kinetics, and stability.

Overall, MFBs are a valuable tool for investigating carbon capture sorbents because of their small size, enhanced control, detailed evaluation of gas–particle interactions, ability to simulate plant conditions, fast screening capabilities, and utility in optimising processes and designs. These benefits help address the global challenge of reducing CO_2 emissions and minimising climate change by contributing to the advancement of knowledge and the development of effective carbon capture techniques.

As mentioned previously, micro-fluidised bed reactors have several benefits over traditional fluidised bed platforms for studying carbon capture solid sorbents. Employing MFB systems facilitates the investigation of fluidisation dynamics, sorbent characterisation, process intensification, and kinetic studies, which all contribute to the advancement of more efficient and effective carbon capture technologies. These enable researchers to conduct smaller scale, yet fundamental studies, to acquire greater knowledge of the adsorbent features and the behaviour of fluidisation gas/solid. In this project, the MFB is developed as a platform to examine the performance of promising carbon capture adsorbent candidates, and by using MFB, investigators can obtain insight into the adsorption selectivity, capacity, and stability of various sorbents by analysing the behaviour of solid sorbent, to help investigators determine how to improve the effectiveness and efficacy of carbon capture processes.

1.4 Research Aim and Objectives

The overall aim of this project is to develop the MFB as a platform for fast and reliable screening of carbon capture adsorbents using commercially available hydrotalcite materials as a case study. These are considered as a suitable candidate for CO_2 capture from effluent gas streams since they have the following benefits: fast adsorption and desorption kinetics, high thermal and mechanical stability, high CO_2 adsorption capacity, high CO_2 selectivity, high-cost efficiency for manufacturing, adjustable composition, substantial surface area, and simple manufacturing process (León *et al.*, 2010; Aschenbrenner *et al.*, 2011; Suescum-Morales *et al.*, 2022). The ability of the material to withstand harsh conditions, alter its chemical composition, and provide numerous active sites for the adsorption of CO_2 makes it an excellent candidate for further study and optimisation.

The key advantages of the MFB (Micro Fluidised Bed) in this carbon capture materials development context include the ability to gain a deeper understanding of the effects of mass transfer and mixing on the kinetics, relevant to full scale implementation, and the ability to use only small amounts of material. The latter is especially relevant to the early stages of materials development where usually there is limited availability of novel high-capacity variants.

Another aim of this project is to quantify the differences between micro- and macro-fluidisation and find optimal conditions for the materials screening to address these competing considerations. The key originality of this research lies in applying MFB technology (small-scale) to study gas-solid adsorption/desorption for carbon capture and using 3D printing to assist in the development of MFB technology itself. The main objectives are as follows:

a) Identify suitable affordable treatments that enable the micro-fluidisation of cohesive hydrotalcite powders.
b) Study the hydrodynamics of cohesive hydrotalcite powders in different 3D-printed MFB designs by measuring the influences of particle size, gas velocity, bed diameter, and static bed height on the pressure drop.
c) To identify optimal fluidisation conditions and understand where regime transitions occur when using cohesive hydrotalcite powders using pressure drop data.

d) To screen the CO_2 adsorption kinetics of hydrotalcite in an Optimized 3D-printed MFB using breakthrough experiments, including investigating the impact of CO_2 concentration, gas flowrate, temperature, and bed loading.

e) To study desorption kinetics via the TSA approach, including investigating the impact of desorption temperature.

1.5 Thesis Structure

Chapter 2. Literature Review

Presents an overview and general background of carbon capture technologies, addressing post-composition carbon capture techniques. Provides details on the adsorption process and fluidised bed techniques comprising conventional and micro-fluidised applications that are relevant to the experiments in this thesis. Furthermore, previous studies on MFBs (e.g., hydrodynamic and kinetic studies of gas/solid fluidisation) are reviewed in order to establish a foundational comprehension of the principles governing gas and solid fluidisation and carbon capture techniques. This evaluation aims to highlight the problems and constraints encountered in previous studies. The assessment of previous research endeavours Optimizes the performance of MFB systems. The significance of this chapter resides in the analysis of previous investigations on MFBs with regard to gas/solid fluidisation, and the identification of research gaps, including the use of 3D printing micro fluidised beds to screen carbon capture adsorbent.

Chapter 3. Methodology

Outlines the methodology and describes the experimental setup, comprising the 3D-printed micro-fluidised bed reactors, equipment, and measurement techniques. The chapter also examines the precise operating settings and parameters explored in the research. The chapter is divided into four main sections: (1) 3D-printed MFB and setup; (2) hydrodynamic study; (3) adsorption kinetics study; and (4) desorption kinetics study. The materials and equipment used, along with their specifications, are also presented. In the hydrodynamic study, the impact of the particle size, bed diameter, static bed height, and gas flow rate is examined in detail to find the optimum regime for the kinetics experiment. Subsequently, the effects of the CO_2 concentration, gas flow rate, static bed height, and temperature on kinetic screening are

explored. Finally, the effects of temperature on the desorption capacity in the desorption kinetic screening are investigated.

Chapter 4. Hydrodynamic Results

Cohesive powder fluidisation in a micro-fluidised bed (MFB) is discussed. The characteristics of gas/solid fluidisation are analysed via pressure drop data, and the influence of various bed configurations, particulate sizes, bed heights, and gas flow rates on the hydrodynamic performance of the MFBR presented. The findings will serve as a guide for selecting suitable experimental operating conditions for the kinetic tests in chapters 5 and 6, including an optimum fluidisation regime (bubble regime) because the bubble regime behaviour improves gas-solid mixing and mass/heat transfer, enhancing carbon uptake.

Chapter 5. Adsorption Kinetics

Experimental results related to the adsorption capacity, breakthrough time, and selection of empirical kinetic models are presented. The chapter analyses the impact exerted by various conditions such as CO_2 concentration, gas flow rate, bed loading, and temperature on the adsorption performance.

Chapter 6. Desorption Kinetics

Focuses on examining the desorption kinetics of the hydrotalcite within the MFBR on the efficiency of regeneration. The chapter provides an analysis of the effect of temperature and desorption conditions on the desorption process. The study contributes to the estimation of desorption efficiency and regeneration potential, which is an essential factor in enhancing carbon capture processes and selecting suitable adsorbents for real-world application.

Chapter 7. Conclusion and Future Work

Summarises the key research results and explores their consequences and impact. Recommendations for prospective future studies and development opportunities using MFBs for carbon capture are also given, highlighting additional exploration and development areas.

Chapter 2. Literature review

2.1 Introduction

Climate change is one of the main issues currently concerning the world, and its impact has only grown over time (Liu *et al.*, 2008; Ram, 2013; Ammendola *et al.*, 2017). According to United Nations Data, the global population is predicted to surpass 9 billion by 2050, increasing the demand for energy and natural resources (Khraisheh *et al.*, 2020). In addition, almost all everyday human activities result in the generation of CO_2, exacerbating its effect (Adamu *et al.*, 2020; Rogelj *et al.*, 2021). The CO_2 concentration in the atmosphere is steadily raising because the natural carbon cycle is unable to counteract the resulting CO_2 emissions (Dantas *et al.*, 2010). The natural carbon cycle regulates CO_2 levels in the Earth's atmosphere. However, during past decades, the amount of CO_2 generated by human activity was twenty times less than the amount released by natural sources. In recent years, natural and industrial sources have become about equal (Songolzadeh *et al.*, 2012). Anthropogenic carbon dioxide sources include, but are not limited to, industrial process emissions, the burning of fossil fuels, land use change, waste treatment, and soil degradation (Choi *et al.*, 2009). Therefore, there is considerable research interest in controlling and reducing CO_2 emissions.

Policymakers have recognised the necessity of limiting carbon dioxide (CO_2) emissions, which are the main component of human greenhouse gases (Anwar *et al.*, 2018). The European Union and United Kingdom intend to decrease carbon emissions by 80% before 2050 (Khraisheh *et al.*, 2020). The European Union's target is to shift towards a carbon-neutral economy, a net-zero greenhouse economy, and reduce gas emissions by the year 2050. Consequently, carbon dioxide management has become a research industry during the last several decades. Universities worldwide are conducting research and development efforts to achieve this goal. As of 2011, over 190 countries have signed and approved the agreement, and they have started taking concrete steps to decrease greenhouse gas emissions (CO_2, CH_4, NO_x, and SF_6) (Anwar *et al.*, 2018). CO_2 has received the most attention since it has the highest emission levels of the four main greenhouse gases (Yu *et al.*, 2008).

Carbon dioxide emissions may be reduced by a combination of (i) carbon capture and storage (CCS); (ii) reducing the utilisation of fossil fuels through the transition to renewable energy sources (which may be challenging); (iii) improving the efficiency of existing fossil fuel-based

processes; and (iv) increasing the CO_2 partial pressure in the exhaust gas, that could enhance the power efficiency of the previous step (Font-Palma *et al.*, 2021). Carbon capture and storge (CCS) is regarded as the most encouraging technology that may handle the CO_2 issue in the short term. It enables the continued use of fossil fuels and the decreasing of emissions from fossil fuel combustion, buying time for the discovery of a suitable alternatives to fossil fuels. Carbon capture and storage can effectively reduce CO_2 emissions through the shift to low-carbon options (Adamu *et al.*, 2020).

2.2 Carbon Capture

Since the industrial revolution, CO_2 emissions and their negative impacts have increased (Zhao *et al.*, 2021), making carbon capture one of the few techniques to control and reduce them. CO_2 could be captured from industrial plant exhausts in a variety of ways, including through oxy-fuel, pre-combustion, and post-combustion processes (Wilberforce *et al.*, 2021). However, each technique has its own pros and cons, making it challenging to find a method that is both highly effective and widely usable (Hu *et al.*, 2020; Khraisheh *et al.*, 2020).

2.2.1 Pre-Combustion

CO_2 can be separated from the fuel before composition through a technique known as pre-combustion capture (Kanniche *et al.*, 2010). The process involves the partial oxidation of fossil fuel followed by its reaction with steam to generate a syngas consisting of carbon monoxide (CO) and water vapour (H_2O) which is then converted into CO_2 and hydrogen (H_2) via the water-gas shift reaction (Chao *et al.*, 2021). The CO_2 can then be separated for storage or reuse (Kanniche *et al.*, 2010).

The cost of pre combustion carbon capture could be about $60 per tonne (Management, 2023) This process may be subjected to the hydrating process (Chao *et al.*, 2021), which is known as "integrated gasification combined cycle" (IGCC) (Kanniche *et al.*, 2010). Solid sorbents, solvents, or membranes can be applied to capture CO_2 from an effluent gas in the pre-combustion process (Chao *et al.*, 2021). Chemical solvents, particularly amines such as MDEA, Selexol, or Rectisol, have been used to separate CO_2 in gasification plants for decades (Madejski *et al.*, 2022). Moreover, pre-combustion technology has also employed a membrane for carbon separation (Jansen *et al.*, 2015) that might be manufactured from various materials, such as non-mineral, porous inorganic, and polymeric membranes (Scholes *et al.*, 2010). This

technique can be appealing, particularly when used with a chemical solvent, due to its performance as a combination of chemical adsorption and filtration. However, many issues have arisen during the development of this technology, including vapour and dust influences that lead to membranes' physical degradation (Kanniche *et al.*, 2010). Pre-combustion capture is often more efficient than oxyfuel and pre-combustion due to the higher concentration of CO_2 produced, but the capital expenditures of the base gasification process are frequently higher than those of ordinary pulverising coal power stations (Kanniche *et al.*, 2010). Additionally, excessive energy for regeneration provides a further drawback of this process, which has a negative influence on the efficiency of the power plant (Singh *et al.*, 2003; Røkke and Langørgen, 2009).

2.2.2 Oxy-fuel Combustion

Abraham *et al.* (1982) were the first to suggest using oxygen during combustion for CO_2 capture in the energy sector. In oxy-fuel combustion process, the fuel undergoes burning in pure oxygen rather than air, and the flue gas produced is primarily constituted of CO_2 and minor contaminants such as sulphur oxide (SO_x) (Kanniche et al., 2010). The inlet gas mixture could have a $15 - 50\%$ CO_2 concentration, in contrast to post-combustion technology, which usually involves exhaust gas flows of 5-15% CO_2 concentration (Kanniche *et al.*, 2010; Jansen *et al.*, 2015; Krishnamurthy *et al.*, 2021). This approach has undergone further research to make it a viable alternative to existing carbon capture techniques. For new and current conventional pulverised coal (PC) power plants, oxy-fuel combustion is considered a viable option to post-combustion carbon capture, with the capacity to capture all CO_2 (Nemitallah et al., 2017).

The primary benefit of oxygen combustion is that it significantly enhances the partial pressure of CO_2 in the combustion exhaust gases by preventing their dilution with nitrogen in the air (Chao *et al.*, 2021). This approach is currently under development, and cost evaluations must be determined while considering all effective application aspects (Habib *et al.*, 2011). It is more suited for CO_2 storage without the separation of nitrogen (Gopan *et al.*, 2014; Nemitallah *et al.*, 2017; Ahn and Kim, 2020). Generally, oxy-fuel combustion occurs at a temperature of 100-300 °C and a high pressure of 20-30 bar and

An air separation unit (ASU) is used in the oxy-fuel combustion process to generate an oxygen-rich stream rather than air for combustion (Jansen *et al.*, 2015). Several additional processing units are also needed to convert the pulverised coal-fired power plant to oxygen fuel, including

an air separation facility to supply the virtually pure oxygen combustion process, a CO_2 treatment facility, and ducts and fans to control flame temperature (Gopan *et al.*, 2014). A near-pure CO_2 stream can be produced from carbon in order to be stored (Ahn and Kim, 2020). The CO_2 can be captured from the flue gas via the condensation of water, requiring only a small amount of energy (Nemitallah *et al.*, 2017). However, oxygen production requires a significant amount of energy (7– 10% of the entire system input). In this technique, a flue gas stream with a high proportion of CO_2 and H_2O (around 80%) permits a very straightforward CO_2 separation procedure by condensing off the H_2O (Wang *et al.*, 2007a). Oxy-fuel combustion capture has a number of drawbacks however, including a high energy need for producing pure oxygen and the lack of a comprehensive process for preparing the fuel prior to its commercialisation (Chao *et al.*, 2021)

2.2.3 Post-Combustion

Post-combustion processes have attracted the largest amount of attention (Chao *et al.*, 2021; Raganati *et al.*, 2021), and involve separating the CO_2 from the flue generated after conventional combustion has taken place. This process is applicable to oil, conventional coal, or gas-fired power plants, combined natural gas and natural gas cycle flue gas capture, and many other industrial processes with significant CO_2-containing flue emissions, such as the steel and cement industries (Samanta *et al.*, 2011; McDonough *et al.*, 2018). Popular post-combustion separation approaches include absorption, adsorption, cryogenics, and membranes.

Ultimately, among the three approaches, post-combustion is perhaps more favourable for several reasons. It can be retrofitted easily into existing plants. without requiring significant modifications and can be implemented more quickly than the other methods (Kanniche *et al.*, 2010; Allangawi *et al.*, 2023). Its maintenance does not halt the power plant's operation, and it can be readily adjusted or managed. Additionally, it can produce high-purity CO_2 (>99%) with high CO_2 capture ratios (>90%) (Najmi *et al.*, 2016). Popular post-combustion separation approaches include absorption, adsorption, cryogenic processes, and membrane separation (Chao *et al.*, 2021; Font-Palma *et al.*, 2021). Further details on post-composition approaches are presented in section 2.3.

2.3 Post-Combustion Carbon Capture Techniques

2.3.1 Absorption

CO_2 can be captured from gas streams using liquid solvents through chemical or physical absorption processes (Kanniche *et al.*, 2010; Chao *et al.*, 2021). Absorption is currently the most used and mature CO_2 capture process due to its high absorption capacity and good CO_2 selectivity. Absorption procedures are classified based on the type of absorbent used, including aqueous ammonia absorption (Kim *et al.*, 2012; Zhang and Guo, 2013), alkanolamines absorption (Mondal *et al.*, 2012), dual-alkali absorption, chilled ammonia process (Yu and Tan, 2013), (Darde *et al.*, 2009), and sodium carbonate (Na_2CO_3) slurry absorption. Intensive study has been performed to address the challenges faced using absorption processes. Two areas of research have been focused on developing more cost-effective and efficient processes and improving the performance of absorbents (Chao *et al.*, 2021).

Nevertheless, it has several drawbacks, including high cost, strong corrosion produced by the liquid solvent, high energy requirements for solvent regeneration, high toxicity, and high absorbent loss due to low stability. Moreover, the requirement for compression of the captured CO_2 along with the requirement to handle large gas volumes due to the low concentration and partial pressure of CO_2 in flue gas are further challenges (Kanniche *et al.*, 2010; Chao *et al.*, 2021). These barriers have limited the uptake of this mature technology into the capture of medium and large scale industries, such as coal-fired power plants (Ochedi *et al.*, 2020).

2.3.2 Cryogenic Distillation

Cryogenic distillation is a carbon capture technique that uses a gas separation unit. In this process, the gas is compressed and cooled at high pressures and low temperatures in a distillation column. For CO_2 separation, the efficiency can reach up to 90–95% of CO_2 recovery, which largely depends on the temperature and pressure used (Font-Palma *et al.*, 2021). However, cryogenic distillation techniques are not a practical option for CO_2 separation from flue gas in post-combustion (Kanniche *et al.*, 2010). This is because it is not economically feasible to compress the flue gas, which typically only contains 15% CO_2, to the pressures necessary for CO_2 liquefaction. Additionally, the flue gas stream must be pre-dried before undergoing the process (Vitillo *et al.*, 2017; He *et al.*, 2023). Ultimately, this technique is too energy-intensive (Ochedi *et al.*, 2020).

2.3.3 Membrane Separation

Post-combustion CO_2 capture using membrane-based semi-permeable or permeable materials that would enable selective carbon dioxide (CO_2) transport and capture from the post-combustion flue gas is another option (Ochedi *et al.*, 2020). Membrane separation is a novel carbon capture process that does not require chemicals or regeneration. It is straightforward to use, and the capital costs are reasonable (Wilberforce *et al.*, 2021). Through membrane processes, gas molecules are selectively separated from the mixture. Selectivity and permeability are used to measure membrane performance, which are mainly functions of the membrane nature, as well as conditions that can be applied, such as pressure, temperature, and concentration. Permeance (gas flux) is a more recent term than permeability which describes the volumetric flow rate of a specific gas that permeates through a unit membrane's surface area (Siagian *et al.*, 2019). Selectivity is identified by the membrane's preference for allowing the permeation of one gas over another. It can be more desirable for a membrane to obtain a rising gas flux throughout the membrane while maintaining selectivity (Madejski *et al.*, 2022).

The membrane can be classified based on the manufacturing material's nature, which involves inorganic (ceramics, zeolites, carbon), organic (polymers), and mixed matrix membranes. In general, all these types of membranes have pros and cons in terms of CO_2 capture performance, operation cost, and operation life (Kárászová *et al.*, 2020; Madejski *et al.*, 2022). There are two types of inorganic membranes, porous and nonporous. Organic membranes offer greater thermal and mechanical stability, whereas inorganic membranes have greater selectivity and less CO_2 permeability. The production of inorganic membranes is more expensive because of the difficulty of producing them without defects over large surface areas. Hybrid and polymer membranes are the most researched due to their low cost, high membrane processability, and high selectivity separation (Kárászová *et al.*, 2020; Madejski *et al.*, 2022).

Although there are many membrane investigations, most membrane applications are still in early phases of development. For example, efficient membrane separation requires a higher initial pressure (20% CO_2 concentration or higher), which is dubious considered the low partial CO_2 pressure in flue gas post combustion flue gas (it can be as low as 4%). Whilst multistage membrane systems might proposal a solution, carbon separation by a membrane is more expensive than using absorption by primary amines at low concentrations (Kárászová *et al.*, 2020), which is already a mature technique. Moreover, to use commercial membranes at high

temperatures, extra pre-treatment steps are required, such as cooling and compression (Siagian *et al.*, 2019). Other shortcomings include low selectivity, low processing capacity, and poor stability (Scholes *et al.*, 2010).

2.3.4 Adsorption

Adsorption is an alternative low-cost post-combustion carbon capture approach. Here, gas molecules, ions and atoms are attracted to a solid adsorbent through a combination of chemisorption and physisorption. Chemisorption involves chemical forces (*e.g.,* covalent bonding) and is characterised by its high selectivity, but significant energy to break the chemical bonds for the sorbent regeneration process (McDonough *et al.*, 2018; Madejski *et al.*, 2022). Meanwhile, physisorption occurs by weaker physical attraction forces between the gas (CO_2) and the adsorbed surface, such as the Van der Waals force, and takes place at lower temperatures than chemisorption (Chao *et al.*, 2021; Font-Palma *et al.*, 2021). Whilst physisorption is more weakly binding, the regeneration cost is also lower.

The most common adsorbent materials are zeolites, activated carbons, hybrid ultra-materials (HUMs), and metal-organic frameworks (MOFs) (Madejski *et al.*, 2022). The principal characteristics for sorbent selection include high selectivity, a large surface area, and easy regeneration ability. By selecting specific sorbents, adsorption may provide a very pure CO_2 stream with a small pressure drop compared to other techniques, while consuming less energy and producing little parasitic pollution and by-products (Upendar *et al.*, 2014; Chaiw *et al.*, 2016; Peredo-Mancilla *et al.*, 2018).

The regeneration process can be carried out through a variety of techniques, including pressure swing (PSA), temperature swing (TSA), and vacuum pressure swing (VPSA) (Madejski *et al.*, 2022). During PSA, CO_2 is captured at high pressures and then desorbed at low pressures; higher pressures typically increase the driving force, enabling high saturation of the sorbent material. Similarly, in TSA, adsorption occurs at low temperatures and regeneration occurs at high temperatures by applying steam or hot N_2 or CO_2, since CO_2 is usually more weakly binding at higher temperatures. Any additional adsorbed pollutants such as NO_x and SO_x may be eliminated, resulting in the production of highly concentrated CO_2 (Madejski *et al.*, 2022). In either method, adsorption is reversible meaning the adsorbents can be recycled numerous times (Raganati *et al.*, 2021).

TSA can be implemented directly or indirectly. Popular direct approaches involve the use steam or heated CO_2 and/or N_2 sweep gases. High purity CO_2 can also be recovered using steam as the sweep gas by condensing the water afterwards. Indirect heating can be achieved using an embedded heat exchanger within the bed or through the use of microwave heating. These methods also reduce the amount of purge gas needed, leading to higher purity CO_2. Nevertheless, the methodologies employed in TSA have a number of limitations, such as potential modifications to the chemical/physical and characteristics of the adsorbent, loss of heat to the surrounding equipment, and an extended duration required for regeneration (Zeng *et al.*, 2022). TSA has a higher rate of recovery than other approaches and requires less energy than PSA, It is a simple method that could be utilised effectively with the MFB reactor device (Raganati *et al.*, 2021; Zeng *et al.*, 2022).

Adsorption effectiveness overall depends on the development of readily regenerable solid sorbents with superior CO_2 adsorption selectivity and capacity (Kim *et al.*, 2016c; Khraisheh *et al.*, 2020), and on the development of the gas-solid contacting technology. Adsorption can occur in three types of reactors: fixed bed (typically packed beds containing solid sorbents in random or structured arrangements), moving bed systems (which contain solid sorbents which can move between vessels for adsorption and regeneration processes) (MacDowell *et al.*, 2010; McDonough *et al.*, 2018; Yaghoobi-Khankhajeh *et al.*, 2018; Mesfer *et al.*, 2020), or fluidised beds (where adsorbent particles are suspended in a flue gas at high velocities) (Yaghoobi-Khankhajeh *et al.*, 2018).

2.3.4.1 Fixed Beds

In the fixed bed mode, desorption occurs in the same column as adsorption once the sorbent is saturated with CO_2 (Shafeeyan *et al.*, 2014). Here the sorbent will saturate with a moving front from the inlet to the outlet where eventually CO_2 will breakthrough. Fixed beds support PSA and TSA (Mesfer *et al.*, 2020). Advantages of fixed beds include no particle attrition, and no need for additional mechanical systems. Moreover, the operation of fixed beds are generally simpler than fluidised beds (Yaghoobi-Khankhajeh *et al.*, 2018). Limitations of the fixed bed approach are the repetitive valve shifting required during cyclic operation and the complexity of setting the heat integration strategy (Chao *et al.*, 2021). The disadvantages of a fixed bed are its limited scalability and poor heat and mass transfer (Raganati *et al.*, 2021).

In recent years, a significant number of studies have focused on CO_2 adsorption via fixed-bed reactor using simulation and experimental methods (Moreira *et al.*, 2006; Lamia *et al.*, 2008; Hickman *et al.*, 2016; Mesfer *et al.*, 2020). Ben-Mansour and Qasem (2018) used gas mixtures of 20% CO_2/N_2 to obtain the breakthrough curves of the following temperatures (28, 50, 100, and 150 °C) with a total pressure of 1.02 bar. The solid adsorbent used was activated carbon, which was pre-treated by flowing helium through it for two hours at a rate of 30 mL/min and 423K temperature. The mass transfer rate was represented applying the linear driving force model (LDF), and the adsorption kinetics model was developed via considering the mass, momentum, and energy balances. Their findings supported activated carbon's high selectivity for CO_2 adsorption (Mukherjee *et al.*, 2019).

2.3.4.2 Moving Beds

A moving bed system incorporates the movement of solid particles through the bed in a regulated (controlled) manner (Cann *et al.*, 2021). In general, solid particles are fed into the bed from one side, while the spent solid particles are continuously withdrawn from the other (Jung *et al.*, 2018b). Mechanical techniques (involving conveyor belts, for example) and gravity can be used to transport particles. Such systems offer continuous operation and are commonly employed in adsorption, catalytic, and ion exchange processes. While moving bed techniques involve continuously moving solid particles, fluidised and fixed beds have suspended and stationary particles, respectively; the former thus enables a continuous process, while the latter two can only be used in batch or continuous mode (Kim *et al.*, 2013).

Compared to fixed beds, the moving-bed adsorption (MBA) cycle has numerous benefits for CO_2 adsorption. Moving beds offer fast and high mass and heat transfer rates with low pressure drop (Kim *et al.*, 2013). Additionally, they have a lower solid circulation rate compared to fluidised bed. This is because a large, rich load is created when the sorbent and gas move against each other (Kim *et al.*, 2013). On the other hand, significant challenges include mechanical solid conveyance, solid particle attrition, a large bed cross-section, and a low superficial gas velocity (which limits the flue gas processing capacity) (Jung *et al.*, 2018b).

Several studies have been carried to model MBA for carbon capture (Jung *et al.*, 2018b; Zhao *et al.*, 2021). As a novel and energy-efficient carbon capture method, Kim *et al.* (2013) proposed a heat-integrated MBA configuration. The moving bed allowed for the creation of a temperature profile within the adsorption bed, enabling cooling water to carry the heat of adsorption and be

released at high temperatures. Following the additional heating, the discharged cooling water could then be utilised for the desorption bed as a heating medium. Cann *et al.* (2021) proposed capturing CO_2 with a moving packed bed of cold bed material rather than multiple packed beds operating in cycles (Kim *et al.*, 2013; Zhao *et al.*, 2021). Further, certain US patents (US 7594956 and US 5169607) characteristics a moving bed for CO_2 capture that is implemented as a parallel plate heat exchanger and is able of treating flue gases across a wide temperature range of 80 to 500 °C. However, the specifics of the process are not defined in patents, causing evaluation challenging. Further research has yet to be conducted on these ideas (Chao *et al.*, 2021).

2.3.4.3 Fluidised Beds

The development of gas-solid fluidised beds can be tracked back to the 1920s (Zhang *et al.*, 2014). Gas-solid fluidised beds have been extensively utilised across different industries, covering chemical processes such as combustion, gasification , fluid catalytic cracking, and or physical processes such as granulation, drying, and mixing (Fuchs *et al.*, 2019; Luo *et al.*, 2022). This is because they exhibit superior gas-solid interaction properties and high mass and heat transfer rates between gases and particles (Yu *et al.*, 2011; Webley, 2014; Anwar *et al.*, 2018; McDonough *et al.*, 2019; Shen *et al.*, 2019), making them ideal candidates for handling the large volumes of flue gases in CO_2-producing processes (Raganati *et al.*, 2021; Girimonte *et al.*, 2022).

Research on gas-solid fluidised beds encompasses many aspects, including reactor design, performance optimisation scale-up, and the discovery of new applications (Tan *et al.*, 2017; Shen *et al.*, 2020). Development is achieved through experimental methods, modelling, or a combination of both (Wang and Fan, 2011; Sabouni *et al.*, 2013; Álvarez *et al.*, 2017; Zivkovic *et al.*, 2017). The fluidisation behaviour is influenced by three factors: the characteristics of the granules, such as particle size distribution ,the size and density of the particles, and particle surface characteristics (Kongkitisupchai and Gidaspow, 2013); fluid properties, such as gas density and gas flowrate; and the fluidised bed design itself, such as the cross-sectional area, bed shape, and bed length. Identifying optimal conditions for all of these parameters in the physical process, such as absorption, heating, and mixing particles, or chemical processes, such as gas-solid reaction and solid-liquid reactions, contributes to achieving efficient gas-solid particle contact (Macdonald *et al.*, 2017).

In a fluidised bed carbon capture process, a flue gas moves upward at high velocities through a column of adsorbent, suspending the adsorbent particles once the drag force exceeds the buoyant weight (Girimonte *et al.*, 2017). This results in a particle bed with good solid-gas mixing, but also high particle-particle and particle-wall collisions. Further, in circulating fluidised beds (CFBs), the sorbent is normally moved frequently to a regenerator column and returned to the absorber column. (Girimonte *et al.*, 2017). Particle collisions can lead to mechanical degradation of bed material.

A large volume of research has focussed on optimising the CO_2 removal efficiency in multistage fluidised bed reactors (Raganati *et al.*, 2014; Jung *et al.*, 2018a; Das *et al.*, 2019). These studies investigate the impact of several factors, including solid circulation rate, bed height, carbonation and regeneration temperature, water content, and other variables, on the efficiency of CO_2 capture in three bubbling fluidised-bed reactors. These reactors consist of two carbonation reactors and one regeneration reactor, equipped with a screw-conveyor system to provide dependable conveyance. (Kongkitisupchai and Gidaspow, 2013; Nam *et al.*, 2020; Ren *et al.*, 2022). Moreover, the adsorption/desorption of CO_2 in CFBs have been investigated using various solid sorbents (Chalermsinsuwan *et al.*, 2010; Veneman *et al.*, 2012; Jaiboon *et al.*, 2013; Zanco *et al.*, 2018; Lee *et al.*, 2019; Rongtao *et al.*, 2019). The sorbent's CO_2 capture capacity varies significantly depending on the flow regimes in the fluidised bed. The bubbling and turbulent regime seem to provide the superior CO_2 capture capacities (Jaiboon *et al.*, 2013). Therefore, when designing and operating such fluidised bed units, it is critical to understand particle physical properties and their interactions with the flow characteristics.

The fundamental advantages of using fluidised beds include superior mixing and mass transfer, homogeneous temperature distribution, scalability, and pressure drop management in comparison with fixed and moving beds. Particle movement promotes homogeneous temperature distribution, efficient mixing, and solid–gas interactions. Due to these benefits, fluidised beds are preferred in gas–solid separations, catalytic reactions, and carbon capture systems (Chao *et al.*, 2021; Dhoke *et al.*, 2021).

The bubbling regime of a fluidised bed is characterised by the creation of small spherical or ellipsoidal bubbles that rise evenly and are distributed uniformly across the particle bed at low gas velocities(Wang *et al.*, 2011). The form and size of the bubbles rely on many factors, including the gas viscosity and density, and the particle size and density (Shrestha and Zhou,

2021). Particles within the bubbles exhibit chaotic behaviour in their motion, resulting in effective gas–particle contact and superior mixing. In addition, it is crucial in fluidised bed operations and is frequently favoured due to its predictable and controlled behaviour, enabling optimal performance in numerous industrial applications, such as carbon capture (Choi *et al.*, 1988; Jaiboon *et al.*, 2013).

In the next sections, a general introduction of gas/solid fluidisation involving the Geldart classification of particles and feature behaviours of various flow regimes will be provided. Next, the development of micro-fluidised beds (MFBs) will be summarised including the recent application of 3D printing for MFB fabrication. Following the summary of MFB research activities for carbon capture, the aim and objectives of this thesis will be identified.

2.4 Solid Adsorbents for Carbon Capture

The majority of the studies have focused on the material categorisation, utilising a relatively tiny number of solid sorbents under ideal lab conditions. Furthermore, the energy requirement has not been widely addressed, which is regarded as a critical process indicator for evaluating the economic performance of a realistic carbon capture system (Raganati *et al.*, 2021).

In recent years, several researchers have studied solid sorbents as a possible option for use on an industrial scale (Jaiboon *et al.*, 2013; Kongkitisupchai and Gidaspow, 2013; Wang *et al.*, 2014). Systems based on lithium, calcium, and magnesium are just a few examples of solid sorbents for carbon capture. Due to the global availability and cheap cost of raw materials, calcium-based solid sorbents are the most common kind of solid sorbent. Moreover, Mg $(OH)_2$ and MgO are the two compounds with the highest CO_2 sorbent potential. However, they attract impurities, such as SO_x, NO_x, and H_2S, which must be removed before adsorption (Chao *et al.*, 2021). Zeolites, activated carbons, hydrotalcites, MOFs, alkali-doped metal oxides, amine-functionalised adsorbents, and other compounds can also be used to adsorb CO_2, depending on their chemical composition's function (Chao *et al.*, 2021; Raganati *et al.*, 2021; Allangawi *et al.*, 2023).

The solid sorbent must meet crucial requirements for the CO_2 capture process to be economically and practically viable. These specifications include: high CO_2 adsorption capacity, repeatable solid sorbent regeneration capability over several cycles, high CO_2 selectivity, high mechanical strength, rapid kinetics for adsorption and regeneration, high

chemical tolerance (stability against contaminants and moisture), and simplicity of manufacturing (Kárászová *et al.*, 2020; Chao *et al.*, 2021).

In the practical application of adsorbent materials, the adsorption capacity is linked to several factors, including the structure of the adsorbent material, such as the geometry and size of the sorbent material (*e.g.,* associated, or cylindrical cracks or cages, or cylindrical or interconnected cages or slits), and the interna; accessibility of the active sites for adsorption on the surface. The chemical composition of the adsorbent material is also important, and all of these factors must be considered with cost in mind. Tuning the structure of the sorbent is a viable method for improving CO_2 adsorption capacity, but it requires a complicated and challenging process of sorbent choice (Lee and Park, 2015).

Generally, it is necessary to remove impurities in the flue gas prior to the carbon capture process, which may otherwise result in a considerable reduction in the capacity of CO_2. Gas molecules are separated due to changes in equilibrium concentration, adsorption kinetics, and molecular sieving processes, which enables effective and distinct CO_2 adsorption.

2.4.1 Hydrotalcites

Hydrotalcite was first identified in Sweden in 1842 (Dębek *et al.*, 2017). It was member of the clay mineral family and are an example of layered double hydroxides (LDHs) – these consist of positively charged metal hydroxide layers alternating with interlayers of anions and water molecules, which create an environment suitable for CO_2 capture. The general formula of hydrotalcites $[M_{1-x}^{2+}\ M_x^{3+}\ (OH)_2\ ]^{x+}\ x + \ (A^{\ n-})_{x/n}\ mH_2O$ where "A" represents the interlayered anions, and M^{3+} and M^{2+} represent trivalent and divalent cations, respectively. Moreover, the parts $(A^{\ n-})_{x/n}\ mH_2O$ and $[M_{1-x}^{2+}\ M_x^{3+}\ (OH)_2\ ]_2$ represent the composition of interlayer gaps and brucite-like layers, respectively (Aschenbrenner *et al.*, 2011; Bhatta *et al.*, 2015; Dębek *et al.*, 2017; Suescum-Morales *et al.*, 2022).

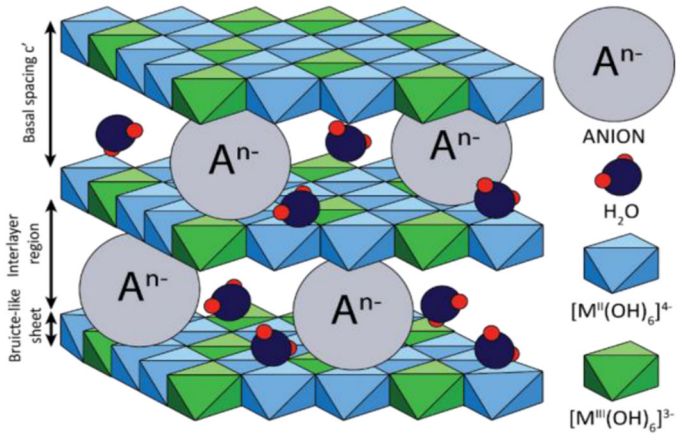

Figure 2.1. The Schematic Structure of Layered Double Hydroxides (Dębek *et al.*, 2017).

Figure 2.1 depicts the overall organisation of LDHs. Metal cations occupy the centres of octahedra, with hydroxide ions at the vertices; shared edges connect the octahedra to create an endless sheet (Evans and Slade, 2006; Dębek *et al.*, 2017). Since the chemical structure of both the interlayer gallery anions and the inorganic layers can be precisely controlled, LDHs exhibit highly variable characteristics and show potential use in a variety of applications, including the production of catalysts, CO_2 -capture materials, polymer–LDH nanocomposites, flame-retardant additives, luminescent substances, and magnetic materials (Dębek *et al.*, 2017; Daniel and Thomas, 2020; Mallakpour *et al.*, 2020). In addition, LDHs have long been investigated as adsorbents (Aschenbrenner *et al.*, 2011). They are thought to be efficient at adsorbing CO_2 because of their large surface area and the availability of basic sites near the surface.

Hydrotalcite powder particles range from a few manometers to several tens of micrometeors in diameters, and their size is affected by the way they are produced (Jose *et al.*, 2018; Veerabhadrappa *et al.*, 2021; Suescum-Morales *et al.*, 2022). In industrial-scale applications, well-defined particle diameters and structured forms are essential. Recently, hydrotalcites have been considered an suitable candidate for CO_2 capture from effluent gas due to several advantages, including high manufacturing cost effectiveness, mechanical / thermal stability for circulation between adsorption and desorption processes, fast adsorption and desorption kinetics, high CO_2 adsorption capacity: rapid/reasonable conditions for regeneration and high CO_2 selectivity, even in the presence of water vapour (Oliveira *et al.*, 2008; McDonough *et al.*, 2018).

Although they display promise for carbon capture in industrial applications considering the above-mentioned advantages, they cannot be used to their maximum potential due to limited control of particle size control and stability (Veerabhadrappa *et al.*, 2021). Utilising powders also presents limitations concerning mass and heat transfer, resulting in decreased carbon removal. Therefore, designing and developing novel synthetic techniques or post-synthesis modifications is necessary to achieve the desired particle size while enhancing or maintaining the carbon capture specifications. The rational design and enhancement of the post-synthesis development of LDH-based materials is a promising approach for attaining desired particle sizes and enhancing the stability and porosity of mixed metal oxides (MMOs). Scholars have conducted several studies on LDH-derived CO_2 adsorbents with the natural mineral MgAl–CO_3, investigating the chemical composition of LDHs, the influence of co-existing gases, the synthetic conditions and methods, the adsorption mechanism and kinetics, the effect of alkali metal doping, and techno-economic which involves evaluating costs, examining the impact of co-existing gases, determining the ideal synthesis conditions, comprehending adsorption mechanisms, and studying kinetics (Aschenbrenner *et al.*, 2011; Nishimura *et al.*, 2013; Bhatta *et al.*, 2015; Coenen *et al.*, 2019). Hydrotalcites adsorb CO_2 through physisorption (via weak Van der Waals forces) and chemisorption. CO_2 adsorption onto a partially carbonated hydrotalcite-like Al–Mg compound in a fixed bed has been studied at different temperatures, flow rates, and gas concentrations (Moreira *et al.*, 2006). This demonstrates that mass transfer and axial dispersion may increase with rising temperature in a fixed bed mode.

The adsorption capacities of LDHs with varying amounts of aluminium were evaluated, demonstrating that the quantity of adsorbed CO_2 increased as the aluminium content decreased (Reijers *et al.*, 2006). The effect of adsorption temperature on CO_2 capture capacity was also considered. Higher temperatures led to lower adsorption capacities due to decreases in the distance between LDH layers and the amount of CO_2 that could be absorbed. Physical adsorption, comprising interactions with basic sites generated by LDH decomposition, was the predominant method of CO_2 adsorption (Moreira *et al.*, 2006; Coenen *et al.*, 2019). Many authors (Moreira *et al.*, 2006; Oliveira *et al.*, 2008; Ortrud Aschenbrenner a and Somsak Supasitmongkol a, 2011; Kim *et al.*, 2016c; Coenen *et al.*, 2019) have investigated such materials for CO_2 capture, and their validity in enhanced adsorption/desorption (Aschenbrenner *et al.*, 2011). A thorough analysis of such adsorbents, discussing their benefits and drawbacks and possible industrial uses, is still required.

2.5 Fundamentals of fluidisation

Fluidisation is an important process for solid-gas contact and is widely used across various industrial processes. Fluidisation technology has been developed for quite some time. In 1922, German inventor Fritz Winker developed the first fluidised bed to produce synthetic fuel from coal (Szöllösi-Janze, 2001). Fluidisation refers to a mechanism in which a bed of solid particles begins behaves like fluids when they come into contact with a gas/liquid (Formisani *et al.*, 2001). This process begins when a gas or liquid is injected through a particle bed at a flowrate where the fluid drag force becomes equal to the buoyant weight of the particle (Pell, 1990). As a result, the bed is converted from a fixed-state to fluidised-state where the particles move freely (Pell, 1990). The fluidisation process can generally occur in three ways: by using liquid, gas, or a combination of both to improve gas-solid mixing and enhance the speed and quality of chemical reactions (Ullah *et al.*, 2013). Within the fluidised bed, particles are subjected to three main forces: the particle-wall interaction force or particle-particle force, gravitational force (i.e., particle weight), and the interaction drag force of gas particles (Deen *et al.*, 2007; Wang *et al.*, 2015). Among these forces, gravity dominates for high density particles (Wang *et al.*, 2015)), leading to a high viscosity bed (Pan *et al.*, 2022). When particles have a high density, they experience a stronger gravitational pull. Consequently, they have a tendency to interact more vigorously with both each other and the surrounding fluid. This heightened interaction results in greater resistance to flow and an increased apparent viscosity (Pan *et al.*, 2022; Bai *et al.*, 2023).

Gas–solid fluidised beds may be operated in various flow regimes: the “bubbling” and “slugging” regimes. In the former, low gas velocities produce small spherical or ellipsoidal bubbles that are distributed evenly across the bed, as mentioned earlier; the latter, on the other hand, occurs at higher gas velocities, leading to significantly larger elongated bubbles or slugs that are unequally distributed and that rise sporadically through the bed. Furthermore, the bubbling regime is preferable for effective gas–particle interaction and heat and mass transfer. The distinction between bubble-borne particles and particles in the particulate phase of a fluidised bed is crucial in understanding the behaviour of particles within the bed (Fanucci *et al.*, 1979; Zhu *et al.*, 2023). The bubbles influence the movement of particles within the bed, with particles moving upwards in the wake of the bubbles, downwards around the bubbles, and between them, especially near the walls (Werther, 2000; Zhu *et al.*, 2023). On the other hand, particles in the particulate phase of the bed are influenced by the movement of the bubbles and

the gas flow. At low gas velocities in the range of fluidisation, the rising bubbles contain very few solid particles, and the remainder of the bed has a much higher concentration of solids, known as the emulsion phase of the fluidised bed (Kono *et al.*, 1986; Wu *et al.*, 2021; Zhu *et al.*, 2023). As the gas velocity is increased, the bubbles become more frequent, and the bed becomes more highly agitated, but the particles remain in the bed, representing the bubbling fluidisation phase (Wu *et al.*, 2021). In contrast, the slugging regime may be less efficient due to bed height and flow oscillations. (Shaul *et al.*, 2012). These regimes are formed based on characteristics such as gas velocity, density, particle size, and bed geometry, and analysing these aspects is crucial for optimal efficiency in fluidised bed systems.(Bi and Grace, 1995).

There are four main particle classifications as shown in Figure 2.2, Geldart A (Aeratable), Geldart B (Bubbly-ready), Geldart C (Cohesive), and Geldart D (Spoutable) (Shi *et al.*, 2014; Chladek *et al.*, 2018). This categorisation is based on the relationship between particle diameterand the difference between the density of particles and gas, as shown in Figure 2.2. Particles in Group D are extremely coarse and/or dense, which includes gravel and coffee beans (particle diameter> 500 μm, particle density > 4000 kg/m^3) (Shaul *et al.*, 2012). The next group is Geldart B, which consist of relatively large particles (particle diameter of 40–500 μm, particle densities of 1400–4000 kg/m^3), such as sand and powder. The B/D boundary is largely empirical; according to Geldart (Ram, 2013), the differentiating characteristic can be based on the bubble properties (Molerus, 1982). Typically, the inter-particle forces within group B can be insignificant (neglected) compared to the particle weight. The formation of bubbles occurs either at or slightly above the minimal fluidisation point. The third group, Geldart A, refers to well-fluidised aeratable powders (typical diameters are 40–200 microns with densities < 1400 kg/m^3). Bubbles start to form when the superficial gas velocity is just above U_{mf} (Sande and Ray, 2014). Group A beds expand significantly between the minimum fluidisation and minimum bubbling points, resulting in a particle (or homogenous) fluidisation phase. This particulate fluidisation regime distinguishes group A particles from the others. Finally, Geldart C refers to the cohesive powders like talc or concrete. The particle density and diameter are typically much less than 1400 kg/m^3 and 20–40 μm respectively. Group C particles form large aggregates due to strong adherence between particles. Spouting is common, and bubbles are not typically observed (Molerus, 1982; Lee *et al.*, 2020).

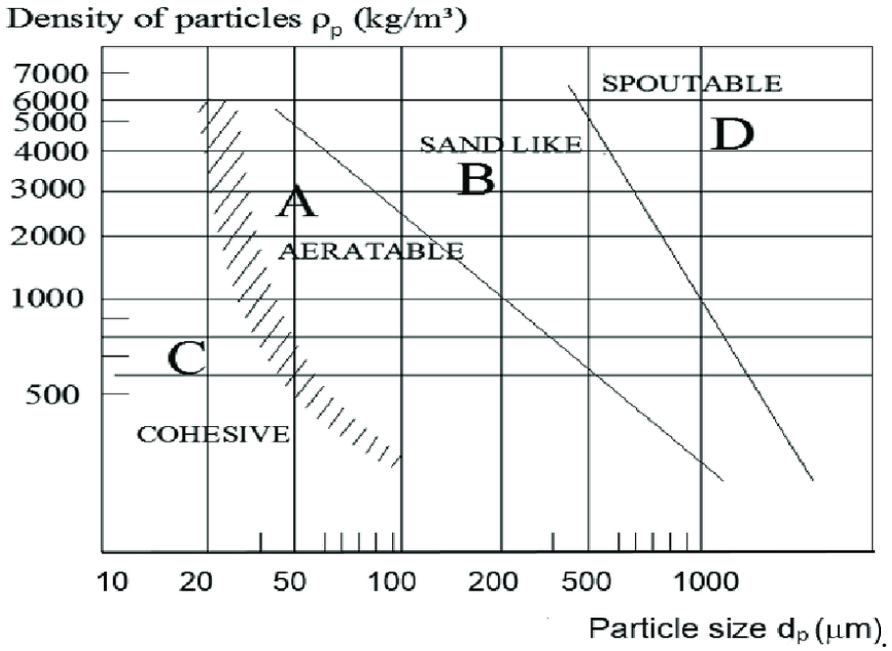

Figure 2.2. Geldart classification of particles, where solid lines indicate demarcation between Geldart A, B, and D groups; and dashed lines indicate Geldart C and Geldart A group boundaries. Adapted from (Yehuda and Kalman, 2020).

Whilst hydrotalcites are a promising candidate for carbon capture, they are also classified as Geldart C due to their typical small particle size. The strong Van der Waals cohesive forces relative to the particle size/drag causes the particles to stick together resulting in poor fluidisation (Shi *et al.*, 2021). Preventing agglomeration and channelling that otherwise lead to poor gas-solid contact is one of the key challenges for the hydrotalcite material.

The hydrodynamic investigation of gas-solid fluidised beds primarily concentrates on describing flow regime characteristics and identifying flow regime transition velocities (Zivkovic *et al.*, 2017). The key transition velocities involve the minimum fluidisation velocity, the minimum bubbling velocity, the minimum slugging velocity, the onset of osculation, and the minimum slugging velocity.

2.6 Fluidisation Regimes

The hydrodynamic investigation of gas-solid fluidised beds primarily focuses on defining flow regime characteristics and finding flow regime transition velocities (Zivkovic *et al.*, 2017). The key transition velocities involve the minimum fluidisation velocity, minimum bubbling

velocity, minimum slugging velocity, onset of turbulence (also called the critical velocity), and transition velocity to fast fluidisation (where particles are entrained in the gas) (Jaiboon *et al.*, 2013). Following the minimum fluidisation velocity, increasing the gas velocity will produce particulate, bubbling, slugging, turbulent or fast fluidisation (McDonough *et al.*, 2020). These regimes are a function of the sorbent particles properties (*e.g.,* size and density) and applied gas velocity. Furthermore, these regimes can be divided into circulating and non- circulating ones. Non-circulating processes include fixed bed and bubbling, slugging and turbulent fluidisation. Fast fluidisation would only be used in the circulating fluidisation system (Jaiboon *et al.*, 2013). Figure 2.3. shows the behaviour of different regimes.

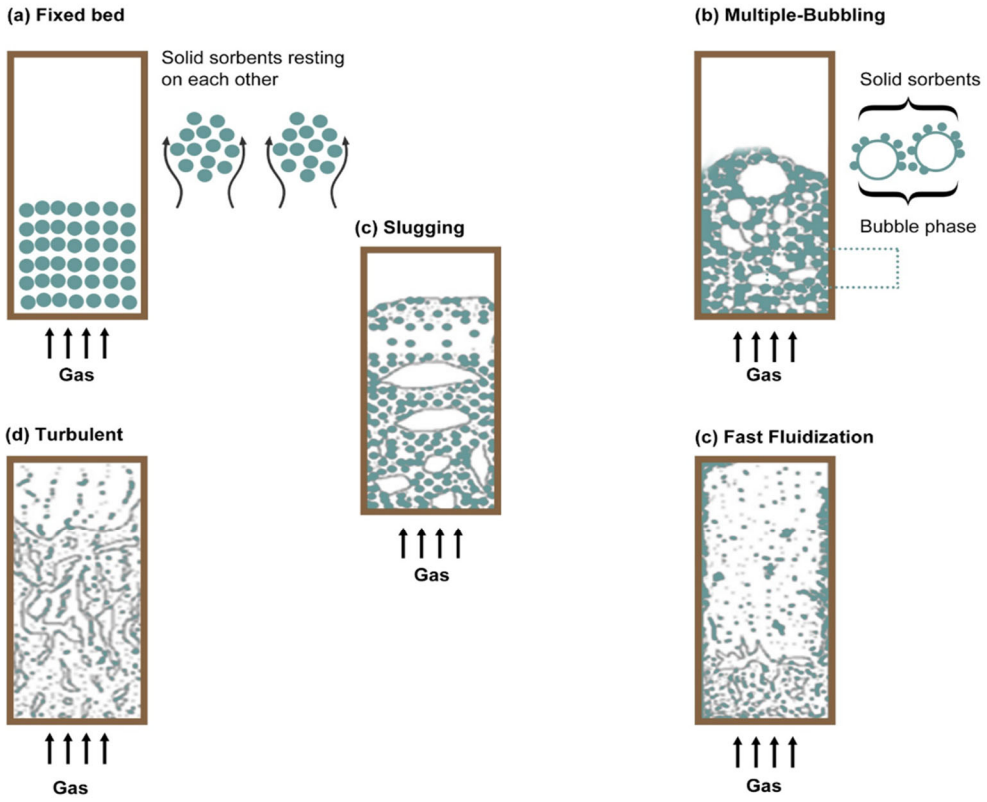

Figure 2.3. Schematics presentation of different regimes inside fluidised bed. Adapted from (Smolders and Baeyens, 2001).

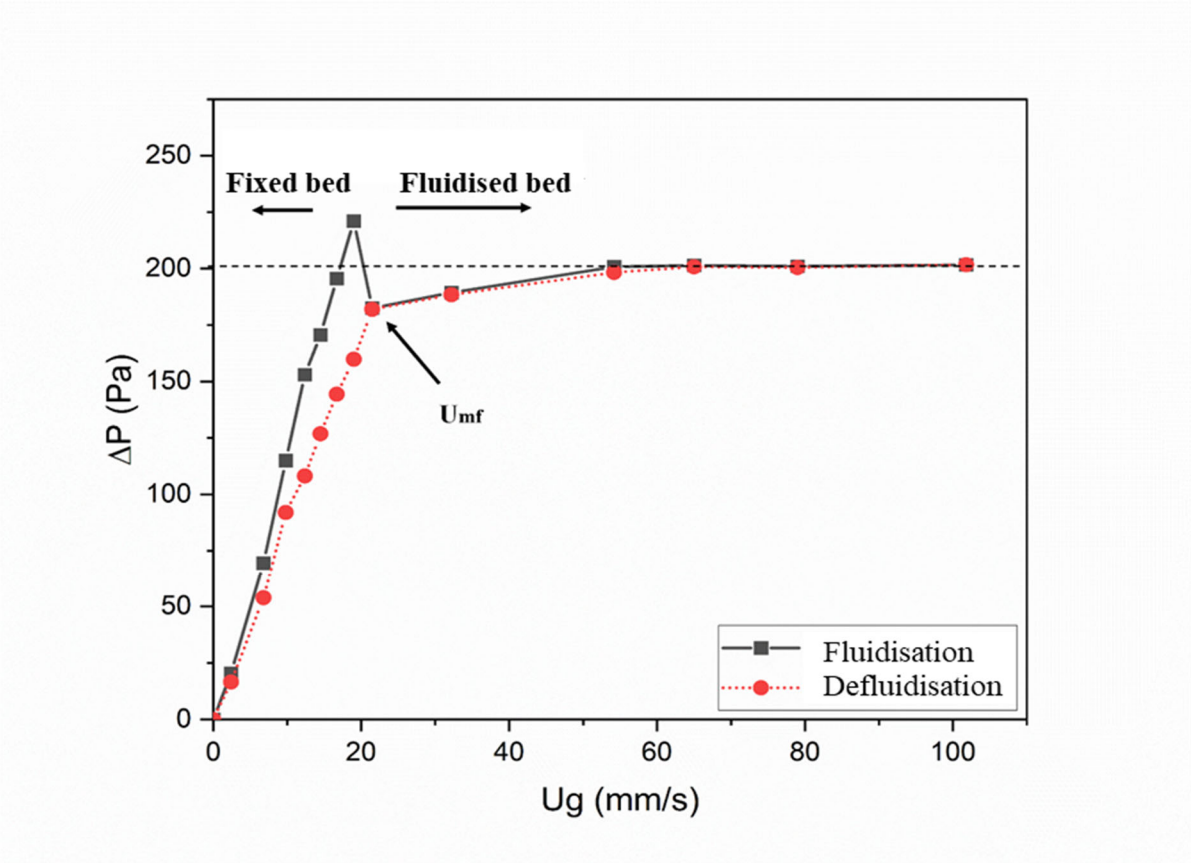

Figure 2.4. A typical pressure drop profile for gas-fluidised bed including lines used to identify the minimum fluidisation velocity. (U_{mf}) is determined from the intersection of the pressure drop extract from packed bed and that in the fluidised bed (defluidisation).

- Fixed bed. The particles inside the fixed bed have no motion, and the gas flow rate and pressure drop have a direct relationship. Furthermore, the minimum fluidisation velocity (U_{mf}) is the interception between pressure drop extracted from packed bed ($\triangle P_{Ergun}$) (Ergun equation represented in equation 1) which increases with increased gas velocity (Rao *et al.*, 2010; Li *et al.*, 2018) and pressure drop of fluidised bed (ΔP_b), which remains constant with an increase in gas flowrate, whose magnitude can be estimated using Equation 2 (the buoyant weight of particles in the bed) as shown in Figure 2.4. This point identifies when the fixed bed changes to the fluidised bed regime (particles start moving which leads to minor bed expansion (Liu *et al.*, 2008). Here $\triangle P_{Ergun}$, and ΔP_b represent pressure drop anticipated by the Ergun equation and pressure drop caused by buoyant weight of the particle respectively, μ is the gas viscosity, $\rho_g$is gas density respectively, d_p is particle

diameter, u_g is gas velocity, ϵ is voidage, ρ_g is particle density and H is static bed height (McDonough *et al.*, 2019).

$$\frac{\triangle P_{Ergun}}{H} = \frac{150\mu u_g}{{d_p}^2}\frac{(1-\epsilon)^2}{\epsilon^3} + \frac{1.75\rho_g {u_g}^2}{d_p}\frac{1-\epsilon}{\epsilon^3} \quad (1)$$

$$\Delta P_b = (1-\varepsilon)(\rho_p - \rho_g)gH \quad (2)$$

- Bubbling regime. Following the minimum fluidisation velocity, small bubbles are observed and rise from the distributor to the surface, leading to a slight improvement of gas/solid mixing and higher residence time of gas, which enables higher CO_2 capture. Additionally, particle bed height has minimal variation due to small gas bubbles erupting from the surface, leading to slight fluctuations in the pressure drop. A fluidised bed's bubbling regime is characterised by creating small, spherical, or ellipsoidal bubbles that rise evenly and distribute uniformly across the particle bed during low gas velocities. In the foaming regime, the form and size of bubbles rely on many factors, including gas viscosity and density, particle size, and density. Particles within the bubbles are in movement and exhibiting chaotic behaviour, resulting in effective gas-particle contact and superior mixing. The bubbling regime is appropriate for various applications, including catalytic reactions, solid mixtures, and heat and mass transfer processes. It is a crucial flow regime in fluidised bed operations and is frequently favoured due to its predictable and controlled behaviour, which enables optimal performance in numerous industrial applications, such as carbon capture (Lim *et al.*, 2016; Tan *et al.*, 2017).
- Slugging regime. When the gas flowrate continues to increase, the bubble size increases due to coalescence of smaller bubbles, possibly reaching the size of the fluidised bed cross-sectional area. At this instance, the bubbling flow regime changes to slugging flow regime. Here, the particle bed height has larger fluctuations (rise/fall), less gas/solid mixing (since the bulk of the gas phases 'misses' the particles), and decreased gas residence time. Together these lead to poorer CO_2 capture capacity (Jaiboon *et al.*, 2013).
- Turbulent regime. When the gas flow rate continues to increase, a turbulent regime will form where the ability distinguish between separate particle and gas phases disappears, resulting in homogeneous conditions. This results in a more consistent dispersion of gas

bubbles throughout the system. The shift towards this uniform regime is marked by the presence of relatively small gas bubbles that are evenly distributed across the system. The variation of bed height decreases again, becoming constant. All previous regimes, including the turbulent regime, occur in non-circulating micro-fluidised bed (McDonough *et al.*, 2019).

- Fast fluidised regime. Within this regime, particles are entrained in the gas and are ejected from the bed at high velocities. Here the surface disappears entirely. This regime is used in circulating fluidised bed devices. When compared to other regimes, the fluidised bed has a relatively small pressure drop, and the particles act as though they are in a dense, cloudy condition, producing a homogenous phase with the gas (Nam *et al.*, 2020).

2.7 Micro-Fluidised Beds (MFBs)

2.7.1 Introduction to MFBs

MFBs were initially described by the concept of small hydraulic diameters or as general small-scale fluidised beds in a conventional engineering perspective, with visible changes in hydrodynamic features (Zhang *et al.*, 2021b; Qie *et al.*, 2022). Research on MFB dates back to the 1980s when Scott and Piskorz (1982) utilised small fluidised reactor for studying biomass pyrolysis (Tsutsumi *et al.*, 1995; Qie *et al.*, 2022), Funazukuri *et al.* (1986) used in 1986 similar fluidised bed reactor for the pyrolysis of cellulose and specifically referred to it as a "micro-fluidised bed." (Han *et al.*, 2020). However, following these early studies there was a hiatus of micro-fluidised bed development.

Then, Potic *et al.* (2005) revived the idea of MFBs with a small internal diameter of just a few millimetres, (Zhang *et al.*, 2021b). Later, various definitions of micro-fluidised were introduced based on bed size ranging from 1 mm (Zivkovic *et al.*, 2013) to 15.5 mm (Guo *et al.*, 2009). The concept of gas-solid MFB was proposed by Liu *et al.* (2008). Following that, significant efforts have been made in the field of MFB research over the last two decades, leading to a better understanding of MFB features including low gas back mixing , low diffusion resistance, and adequate interphase mixing, as well as their characteristics such as residence time distribution (Qie *et al.*, 2022). Potic et al.'s work is frequently cited as the pioneering work in the field (Zhang *et al.*, 2021b)

The MFB is gaining popularity as a rapid screening tool for numerous engineering processing (Zhang *et al.*, 2021b). This is due to their low cost and energy consumption, enhanced safety, and excellent heat and mass transfer. Compared to large scale fluidised beds, MFB requires less specialised operating equipment and training (Wang and Fan, 2011; McDonough *et al.*, 2018; Wang *et al.*, 2020a). Additionally, gas back-mixing is significantly reduced, temperature distributions are homogenous, and reactants are distributed in both axial and peripheral directions in MFB. The MFB can function as a miniature modular reactor for creating high-value fine chemicals used in various sectors such as biological, chemical, culinary, and medicinal. MFB can also be applied in various environmental sustainability usage such as carbon capture and wastewater treatment (González *et al.*, 2001; Kim *et al.*, 2016b). The previous hydrodynamic characteristics make the micro-fluidised bed a perfect isothermal differential reactor, making it a useful and potent addition to the current reaction analysers, particularly for characterising complicated and potent exothermic chemical reactions (Yu *et al.*, 2013; Geng *et al.*, 2018). It can be used to test catalysts, improve catalyst formulations, and study the effects of operation factors on product yields in low-cost, quick-run trials (Potic *et al.*, 2005). MFB is employed to analyse the kinetics of the fundamental reactions, and the scale-independent kinetic models that are developed can direct the design of industrial fluidisation reactors (Wang *et al.*, 2017; Zhang *et al.*, 2021b). MFBs, unlike large-scale fluidised beds, can be ramped up linearly by correctly integrating multiple micro-reactors, enabling large output capacities (Wang and Fan, 2011). The findings from small-scale fluidised beds can be employed to the design and operation of large fluidised beds because they closely resemble the circumstances of large-scale fluidised bed operations (Wang *et al.*, 2020a; Zhang *et al.*, 2021b).

It is proposed that micro fluidised bed reactor (MFBR) technology would be useful to study particle fluidisation behaviour, gas/solid reaction kinetics and reaction characteristics for carbon capture applications (Qie *et al.*, 2022). The advantages of this technology involve cost effective experiments, low energy requirement, enhanced safety (minimising large-scale trials), and potentially easier scale up of the results compared to micro-packed bed screening platforms. Furthermore, MFBRs provide high rates of mass/heat transfer between gas and solid and enable the real-time monitoring of gaseous outputs via online gas analytical mechanisms (Wang *et al.*, 2017) .

However, the success of MFBR depends on identifying suitable conditions for sorbent screening. Scalability and poor fluidisation quality remain significant challenges that need to

be addressed (Wang *et al.*, 2017). To develop novel CO_2 adsorbents, the MFBR can play a crucial role. By enabling the data collection under more real-world conditions compared to small-scale packed beds, it can aid in decision-making and design. The hydrodynamic characteristics of MFB are crucial for bed design and optimisation, and cylindrical or rectangular bed columns with various diameters can significantly influence fluidisation performance.

Research on gas-solid fluidised beds covers many aspects, including the design, scaling up, optimisation performance, and the development of novel applications. Experimental and Numerical approaches, or a combination of the two, are commonly used research methods (Zivkovic *et al.*, 2013). Various kinds of MFBs using fabrication techniques such as additive manufacturing, micro-machining, soft lithography, and capillary systems have been reported to date (McDonough *et al.*, 2019; Zhang *et al.*, 2021c; Alamri *et al.*, 2023).

2.7.2 Hydrodynamics Gas-Solid MFBs

Following Potic *et al.* (2005), Xu and colleagues advanced the field by expanding the applications of gas-solid MFB to applications in pyrolysis, gasification, and combustion while additionally characterising the hydrodynamic Parameters (*i.e.*, column size, particle size, fluidisation velocities) (Zhang *et al.*, 2021b; Zhipeng Qie 2022). Moreover, numerous others such as Liu *et al.* (2008), Zivkovic *et al.* (2013), and McDonough *et al.* (2019) have continued the development of MFB technology based on liquid-solid, liquid-solid-gas, and gas-solid micro-fluidisation. Further studies have focused on minimum bubbling and fluidisation velocities, bed expansion, and the distinct characteristics of micro-fluidised beds compared to macro fluidised beds (Potic *et al.*, 2005; Guo *et al.*, 2009; Rao *et al.*, 2010; McDonough *et al.*, 2019; Alamri *et al.*, 2023).

MFBs are characterised by the concept of small-scale fluidised beds in traditional engineering contexts, exhibiting several evident changes in the hydrodynamic behaviour compared to ‘conventional’ larger scale beds. Although the commonly accepted threshold between micro- and macro-fluidisation is usually 1 mm (Günther and Jensen, 2006; Zivkovic and Biggs, 2015), descriptions of MFB reside along a broad range of bed diameters ranging from sub-500 μm (Zivkovic and Biggs, 2015) up to several centimetres (Potic *et al.*, 2005; Wang and Fan, 2011). Although micro and macro fluidised beds share features such as high rates of heat transfer and

temperature uniformity, micro fluidised beds have some unique characteristics due to an enhanced wall effect.

Micro fluidised beds exhibit a greater ratio of surface area to volume compared to macro beds, leading to enhanced friction between the bed and walls (Loezos *et al.*, 2002). This friction between the particles and the wall creates an additional external force on the bed that provides a stabilising effect. This is commonly referred to as wall effects in the wider literature. The wall effect can result in undesirable behaviours for example the delayed initiation of fluidisation, delayed initiation of bubbling (Guo *et al.*, 2009; McDonough *et al.*, 2019), and a high-pressure drop overshoot right prior to fluidisation, needs additional energy per unit volume to overcome particle-wall attraction and particle-distributor attraction (adhesive forces) and inter-particles attraction (cohesive forces) (Hsu *et al.*, 2018). Positive influences are also reported. For example, Wang *et al.* (2011) discovered that a micro-structured fluidised bed reactor operates under turbulent fluidisation regime with considerably lower gas flow rates than conventional fluidised bed reactors.. Hence, it is usually essential to carry out hydrodynamic investigates before the kinetic screening test to comprehend the behaviour of the bed and find where regime transitions occur. This procedure provides for the identification of a suitable operational window. This ensures that a suitable operating window can be determined for each unique solid material while suppressing unwanted slugging, spouting and channelling.

Pressure drop analysis was used to study flow regimes and wall effects (Jaiboon *et al.*, 2013; McDonough *et al.*, 2019) and high-speed camera visualisation (Liu *et al.*, 2008; McDonough *et al.*, 2019). The wall effect and surface forces are not just connected to bed dimensions but also related to particle size and form (Liu *et al.*, 2008; Han *et al.*, 2021). The bed wall effect in MFBs exhibits an inverse relationship with bed diameters, as it augments the surface area-to-volume ratio when the bed diameter decreases. Consequently, this leads to increased friction between particles and the wall surface. As a result, the wall effect becomes more pronounced, leading to a deviation from the Ergun equation for pressure drop and resulting in higher pressure drops compared to conventional fluidised beds governed by the same equation. However, there is an insignificant relationship between the bed wall effect in MFBs with static bed height and particle size, when the bed diameter exceeds 20 mm. Liu *et al.* (2008), together with, Guo *et al.* (2009) noted that in the case of a rise in bed diameter from 12 to 20 mm, there is a clear reduction in minimum bubbling and fluidisation velocities. However, when the bed diameter higher than 20 mm, there is little increase in both velocities mentioned. Therefore, a MFB with

a diameter smaller than 20 mm could be appropriate for use in this study. However, when employing bubbling fluidised bed for analysing CO_2 capture, a high pressure drop (approximately 2500 Pa to 9450Pa) was gained (Wang *et al.*, 2011; Zhang *et al.*, 2014; Lim *et al.*, 2016). Generally, literature has shown that pressure drop decreases with channel diameter according to experiments. Using low pressure will contribute to decreasing the energy consumption (Geng *et al.*, 2018).

Properties of gas solid fluidisation were reported in a recent studied by Han *et al.* (2021). When the bed diameter particle diameter ratio, D_t/d_p, exceeded 150, there were barely any changes in the fluidisation behaviour characterised by the normalised pressure drop, $\rho_p/(mg/A)$, minimum fluidisation velocity, U_{mf}, and minimum bubbling velocity, U_{mb}. When D_t/d_p= 150, the MFB behaviour became distinct from the full-scale FB behaviour. Though Guo *et al.* (2009) recommend maintaining $D_t/d_p = 100$ to observe micro fluidisation phenomena reliably. It is evident that many hydrodynamic experiments have been conducted for MFBs to determine specific velocities, regime maps, and wall-effect using pressure drop (Chen *et al.*, 2013).

On this basis, the MFB reactor structure, particle fluidisation properties, wall effect, gas-solid back-mixing feature, and operating stability have all been thoroughly studied (Yu *et al.*, 2010). The wall effect also lead to virtually plug-like flow of gas in micro-fluidised beds (Dang *et al.*, 2014; Shi *et al.*, 2021). Specifically, it induces the development of a boundary layer proximate to the solid walls, which, in turn, fosters the establishment of laminar flow conditions, resulting in a consistent flow of gas within the central region of the bed. This phenomenon effectively restrains gas back mixing, ensuring even distribution of temperature and reactants (Han et al., 2021), which can substantially increase reaction selectivity and conversion (Guo *et al.*, 2016). Notably, micro fluidised beds are distinguished by their capacity to achieve a gas flow pattern closely resembling plug flow, thereby augmenting the selectivity of reactions compared to their macro fluidised counterparts. The axial gas dispersion coefficients, intimately connected with the characteristics of the bed, serve as indicators of the diminished extent of back mixing (Han et al., 2021).

Gas bypassing of the particles, resulting from slugging, spouting, and channelling, is a crucial consideration since it can significantly influence gas-solid reactions. Therefore, gas residence time distributions within MFBRs have been investigated as well to determine the influence of

wall effects on back mixing (Dang *et al.*, 2014; Guo *et al.*, 2016; Geng *et al.*, 2018). For example, (Geng *et al.*, 2018) reported that MFBs with diameters of 15–21mm and static bed heights of 20 mm of silica sand can approach plug flow. This indicates that the gas flow behaviour and degree of gas back-mixing may differ between conventional and small beds. In traditional bubbling fluidised beds, the gas velocity and particulate movement dictate the degree of gas back-mixing. Due to the particles' rapid downward movement resulting from the splitting and reforming of bubbles, gas entrainment, and gas back-mixing are exacerbated by increased gas velocity. However, if high gas velocities result in turbulent fluidisation, gas back-mixing decreases significantly. In the context of micro fluidised beds, the absence of large bubbles and the shallow particle bed prevent the formation of large bubbles. The increased gas flow rate observed at higher gas velocities results in a relative decrease in gas transport in the descending direction. This characteristic is desirable for MFBRA (Micro Fluidised Bed) applications. When gas velocities are increased in micro-fluidised beds, gas back-mixing is reduced. Bed parameters such as the interior diameter and static, particulate bed height may also affect gas back-mixing. It has been discovered that an increase in the height of the static particle bed results in a greater degree of gas back-mixing (Geng *et al.*, 2018).

2.7.3 MFBs as Reaction Analysers

Several scholars suggest that MFBs are suitable for the purpose of small-scale screening experiments and gas solid reactions (Yu *et al.*, 2010; Yu *et al.*, 2011; Li *et al.*, 2020; Wang *et al.*, 2020a). The Institute of Process Engineering (IPE) at the Chinese Academy of Sciences (CAS) has proposed a new analytical method for studying gas-solid reaction characteristics and identifying reaction kinetics using the MFB as the reactor (Yu *et al.*, 2010). The advantages include low energy requirement and enhanced safety (Amiri and Shahhosseini, 2018; Li *et al.*, 2020; Nam *et al.*, 2020). Various self-made gas-solid reaction testing apparatuses and many customised instruments, such as thermal gravimetric, microscopic, electrical, and magnetic analysers have been used to measure or analyse gas-solid reactions. The most widely used are TGA (thermogravimetric analyser) (Lim *et al.*, 2016), FB and MFB (micro-fluidised bed) (Dang *et al.*, 2014; McDonough *et al.*, 2020).

The so-called Micro Fluidised Bed Thermogravimetric Analysis (MFB-TGA) has been successfully developed to study gas−solid reaction characteristics and kinetics (Wang *et al.*, 2020a). This newly designed MFB-TGA offers a new method for assessing fast adsorption

kinetics within an FBR (Wang *et al.*, 2020a). In reality, TGA-based methods are used to measure the mass loss or thermal difference of a specimen as a function of temperature and time during a predefined heating programme. Before the heating process begins, the sample must be placed in a reaction cell. As a result, the reactions that occur in TG instruments suffer greatly from external diffusion. Certain energy materials, in particular biomass and coal, are inappropriate for examining with TGA owing to the rapid change in their compositions with rising temperature (Yu *et al.*, 2010). Further, TGA requires precise measuring of reaction rate, which can be influenced by poor heating rates (Lim *et al.*, 2016; McDonough *et al.*, 2020). For example, the isothermal reaction rates of char gasification with CO_2 in a micro fluidised bed reaction analyser (MFBRA) were compared to TGA. When the limits on heat and mass transfer were eased, it was observed that the rate of reaction in the MFBRA was faster than in TGA (Zeng *et al.*, 2014).

The fluidised beds used for investigating kinetic reactions are mostly large scale (defined by inner diameters of > 5cm with bed heights of several Meters), leading to significant mass transfer resistances that produce deviations of the measured kinetic data from the intrinsic kinetic rates, depending on alteration of the composition of the effluent gas (Yu *et al.*, 2010; Lim *et al.*, 2016). Amiri and Shahhosseini (2018) found that the capacity and saturation time in MFB-TGA was respectively 1.4% higher and 17% lower than a conventional scale fluidised bed reactor. This is because more contact occurs between the solid and gas within micro fluidised beds, which improves the CO_2 adsorption. Further, desorption of CO_2 in a micro fluidised bed occurred 17% quicker than in a fluidised bed. Moreover, for 10-cycles of CO_2 adsorption-regeneration, the adsorbent attrition in the micro fluidised bed was 2.1% compared to 10.7% for the large scale fluidised bed (Amiri and Shahhosseini, 2018). It is clear the performance of micro fluidised bed is superior to fluidised bed and TGA in terms of measuring accurate solid reaction kinetics. Furthermore, the fluidised bed enables the screening of the adsorption and regeneration of solid sorbent in a single experiment.

A novel Compact Micro Fluidised Beds (CMFB) reactor has also been suggested to decrease pressure drop and improve adsorption performance for CO_2 capture utilising solid sorbents (Li *et al.*, 2017). With the adoption of more MFB reactors in fundamental studies, the exploration of the MFB reaction analyser for gas-solid reaction analysis has become increasingly exciting and appealing due to apparent properties , for example, high heat and mass transfer, good feedstock flexibility and easy scale-up (Zhang *et al.*, 2021b). Guo *et al.* (2016) developed and

characterised a multistage reaction analyser (MFB-MIRA) based on a MFB for online analysis of multistage gas-solid reactions.

Ultimately, although several studies have used large scale fluidised beds for carbon capture adsorption and regeneration (Yi *et al.*, 2007; Oliveira *et al.*, 2008; Yu *et al.*, 2013; Li *et al.*, 2020), whilst many other studies report on the hydrodynamic of MFBs, little research has been conducted on screening gas/solid adsorption and desorption kinetics in MFBs. Furthermore, although some studies have investigated CO_2 capture using MFBs, they have mostly relied on modelling or the use of MFB-TGA, with few specific experimental investigations (Yu *et al.*, 2013; Li *et al.*, 2017; Amiri and Shahhosseini, 2018).

2.7.4 3D Printing Technology for MFB Development

It is vital to decrease the fabrication time to accelerate MFB design and development. Whilst materials such as polydimethylsiloxane (PDMS) produce high-quality devices for experimentation, these often require significant personell, spacious and expensive processing equipment, whilst also being slow and requiring high levels of technical expertise (Zhang *et al.*, 2021a). A number of alternative fabrication techniques, including soft lithography, micro-machining, additive manufacturing, and capillary technologies, have been used to fabricate various designs of MFBs.

Zivkovic *et al.* (2013) manufactured microfluidic beds containing micro-channels produced from a PDMS chip using a straightforward, affordable, and rapid lithography technique. Using a Perspex block equipped with such a distributor, Do Nascimento *et al.* (2016) developed and manufactured a sturdy MFB by reducing millimetre channels. Additive manufacturing (AM), also called 3D printing, provides a new opportunity to investigate novel fluidised bed designs that might have been impossible or difficult to produce using traditional production processes.

Employing 3D printing to build micro-fluidised beds presents several benefits, such as fast production, low costs, precision design, the ability to manufacture complicated geometries, the possibility of scaling up the process, and no specialist training requirements (Zivkovic and Biggs, 2015; Zhang *et al.*, 2021a). 3D printing technology allows for fabricating 3D objects via the successive addition of layers of material on top of each other under the control of a computer system (McDonough *et al.*, 2019). Recently, 3D printing techniques have made it possible to fabricate complex MFBs that could be challenging to design and fabrication using existing

conventional equipment. Customised fluidised beds or flexible fluidised bed parts can also be 3D-printed to create plug-and-play configureurations for faster and more efficient applications (McDonough *et al.*, 2019).

McDonough *et al.* (2019) were the first to use 3D-printing to manufacture mini- and micro-fluidised beds. Silica and glass particles (Geldart A and B) were subsequently fluidised in various designs to map the fluidisation characteristics (McDonough *et al.*, 2019). The advantages of 3D printing necessitate only minimal training (Zhang *et al.*, 2021a). The time required to fabricate a simple device, *e.g.* a MFB with a diameterof 10 mm and a height of 150 mm requires, in a matter of hours at low costs.

Moreover, Zhang *et al.* (2021a) constructed and examined a 3D-printed micro-fluidised bed to study the hydrodynamics of bubbles and compare the fluidisation characteristics of 3D-printed particles with those of fungal pellets. Their research demonstrated that when gas flow rates increased in a liquid–gas system, the flow regime varied from bubbling to multiple other regime types. The authors also examined how operational factors, including the gas flow rate, surface gas sparger size and liquid velocity, and affect the bubble size, volume fraction and velocity. Additionally, the study provided insights into the fluidisation performance of fungal pellets in a 3D-printed micro-fluidised bed (MFB) and the possible uses of 3D printing technology in fluidised bed research. Furthermore, Jamei *et al.* (2023) explored the development and effectiveness of a small-scale platform for testing carbon capture adsorbents using a 3D-printed swirling fluidised bed (TORBED) reactor. The efficacy of a commercial sorbent made from branched polyethyleneimine (BPEI) for capturing CO_2 from flue gas streams was evaluated, confirming fast data collection and high sorbent capacity, and examined the impact of various operational parameters on the performance of the TORBED system.

Jiang and Fatah (2022) employed stereolithographic 3D printing to fabricate two 4-mm MFB reactors using resin and glass materials, aiming to examine the impact of wall roughness on the hydrodynamic properties of MFBs. The researchers also investigated the influence of particle size and mechanical vibrations on the fluidisation characteristics of various particle cohorts. The findings indicated that an optimal level of wall roughness effectively mitigated the occurrence of slugging in fluidisation. Applying mechanical vibrations mitigated or eliminated the occurrence of the plugging phenomenon, thereby enhancing the quality of particle fluidisation. Moreover, miniaturised fluidised beds present a promising opportunity to reduce

the time and cost requirements associated with raw materials, thereby enhancing the cost efficiency of manufacturing high-value chemical commodities. In addition, Zhang *et al.* (2021c) investigated the fluidisation properties of fungal granules using the 3D-printed MFB platform, aiming to elucidate the hydrodynamic behaviour of pellets and investigate the possible applications of MFBs in bioproduction and bioprocessing. The study found that the static bed voidage of fungal pellets was higher than the typical value and that several factors, including the pellet mass and gas flow rate, affected the hydrodynamic characteristics, such as the minimum fluidisation velocity. The research demonstrated the viability of implementing MFBs in fungal fermentation and bioproduction procedures, offering vital insights into the practical development of fluidised bed bioreactors.

2.8 Research Gap and Novelty

Whilst hydrotalcites are a promising candidate for CO_2 capture, with numerous studies reporting on the behaviour and performance in both adsorption and desorption experiments (Moreira *et al.*, 2006; Oliveira *et al.*, 2008; Aschenbrenner *et al.*, 2011; Kim *et al.*, 2016c; Coenen *et al.*, 2019), no research has been performed to investigate the kinetics of hydrotalcites for carbon capture using the MFB platform. This is an important problem to tackle because the adsorbent material is still in development, is produced in small quantities, and has not been tested in a fluidised bed because it is a cohesive powder. Therefore, this study tested hydrotalcite powders in a micro fluidised bed in order to minimise the solid sorbent quantity required for testing and to investigate the possibility of fluidising prior to kinetic screening.

This project used laboratory experiments to screen industrial hydrotalcite samples to evaluate their carbon capture potential using MFB technology. This also required the study of fluidisation hydrodynamics to define the optimal conditions for carbon capture tests to ensure the observation of intrinsic adsorption and desorption kinetics rather than mass transfer effects. Here additive manufacturing was used to expedite the process.

This study also represents the initial step toward conducting a techno-economic analysis of carbon capture systems. As mentioned earlier, MFBs possess unique fluidisation characteristics and exceptional gas-solid phase mixing capabilities. However, MFBs are smaller in size than conventional FB reactors by up to 1,000–10,000 times (Knowlton *et al.*, 2005). Therefore, it is crucial to understand the variable correlation between plant scale FBs and MFBs, as the results found from MFB could offer substantial guidance for the creation of full-scale FBs at a much

smaller cost. Typically, the procedure for scaling up MFBs involves three stages (Rüdisüli *et al.*, 2012):

1. Construction of lab-size FBs reactor to investigate and/or optimise operating parameters, flow regimes, and kinetic data.
2. Construction of pilot-scale reactors (diameters of ~0.5 m) that offer a smooth transition from lab to industrial plant scale.
3. Construction of the final large-scale FB system (diameters of > 1 m)

Experiments based on MFBs may determine the effects of operating parameters including temperature, concentration, and pressure on the efficiencies of the adsorption and desorption reactions. It is proposed that the small-scale experiments can guide the design and optimisation of full-scale reactors (Wang *et al.*, 2021). It has been found that using MFB-TGA investigates in turbulent or bubbling regimes with minimal diffusion constraints can help develop kinetic models of pyrolysis and gasification that aid in CFD simulations for scaling up FBs. For instance, CFD simulations were used to examine the scaling-up process of a methanol-to-olefins (MTO) unit, which relied on MFB-TGA tests for the kinetics. The outcome demonstrated that the modelled total methanol conversions at various scales were equivalent to those measured experimentally at small-scale. Thus, the work in this thesis offers the potential to bypass part 2 of the scale-up methodology above, which could introduce significant cost savings and accelerate the uptake of post-combustion carbon capture technologies to help meet the Net Zero objectives. Figure 2.5 summarises the themes discussed in this literature review. The overall aim of this project is to develop a MFB platform for fast and reliable screening of adsorbents for carbon capture using hydrotalcites as a model material. This study also seeks to identify general design rules for a wide range of gas-solid fluidisation applications beyond carbon capture, such as catalytic reactions and general adsorption processes.

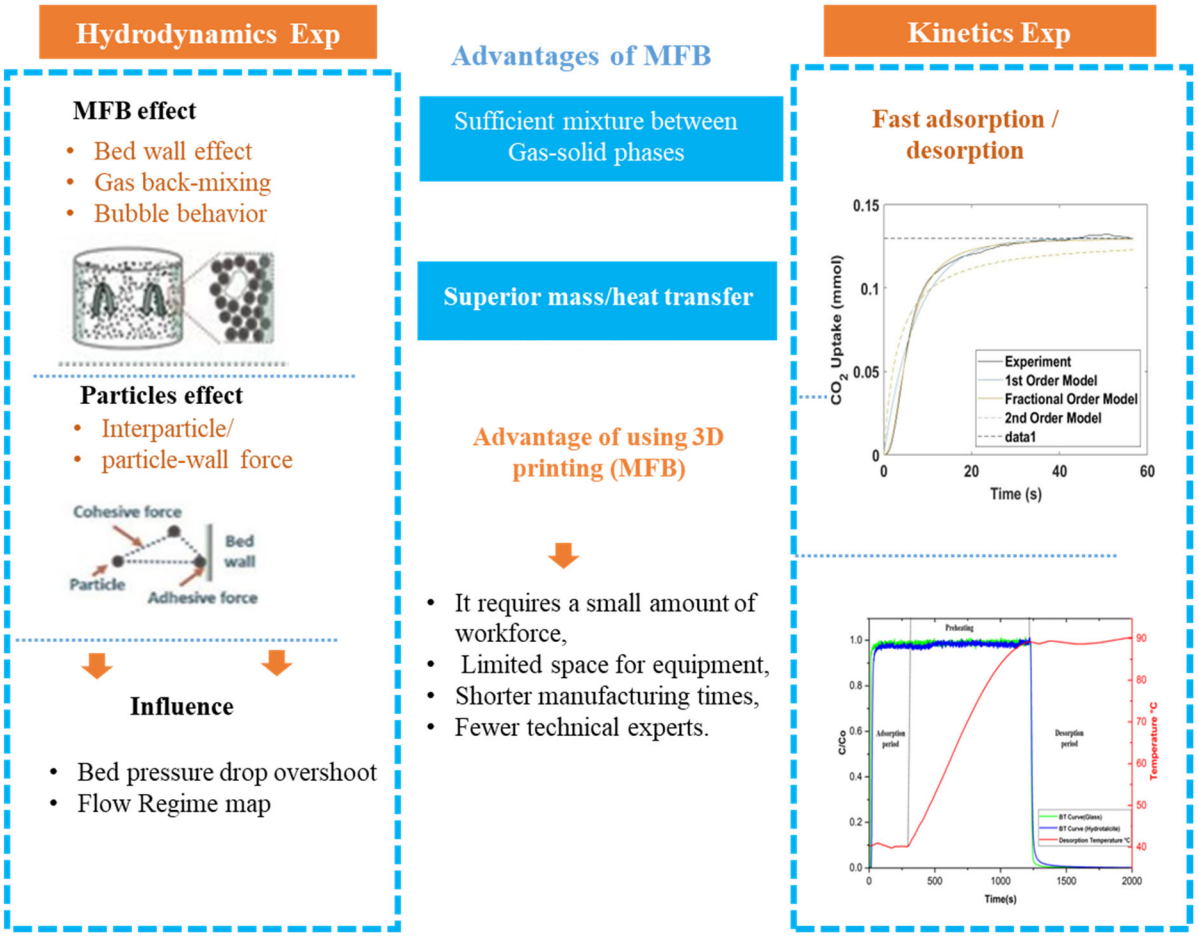

Figure 2.5. Summary of advantage of MFB in the context of carbon-capture screening from the literature review.

Chapter 3. Methodology

3.1 Introduction

This methods chapter is divided into four sections: design and fabrication of the micro-fluidised beds (MFBs) via 3D printing, investigation of the hydrodynamics of a candidate hydrotalcite material inside different MFBs, kinetic screening of adsorption of the hydrotalcite benchmark material using breakthrough experiments, and investigation of temperature swing adsorption in an MFB for regeneration of the hydrotalcite.

3.2 Design and Fabrication of MFBRs using 3D Printing

3.2.1 MFB Designs

Generally, an MFB has a square, rectangular, or circular shape for laboratory and industrial usage. Circular channels offer superior axial uniform solid distribution and prevent particle accumulation in sharp corners (Shen *et al.*, 2019). In contrast, square-shaped channels enable easier flow visualisation (McDonough *et al.*, 2019). For the purposes of this research, circular-shaped channels were used to minimise any corner effects.

The CAD models of the designs used for the hydrodynamics study are shown in Figure 3.1a–c, whilst an illustration of a wholly constructed 3D-printed MFB is depicted in Figure 3.1d. The fabrication involved dividing each bed into two halves and utilising a Form2 or Form3 stereolithographic 3D printer. Two types of resin were used for this purpose: the 'Clear V4' resin and the high-temperature resin. The higher parts, which had circular cross-sections, had heights of 150 mm and bed diameters of 10 mm, 12.5 mm, and 15 mm, respectively. The selection of these dimensions was made considering the need to find a balance between limiting the quantity of material required to fill the bed to prevent waste and ensuring that sufficient material was available to enable meaningful observation of reaction kinetics for subsequent CO_2 breakthrough studies. However, when estimating the length, consideration must be given to making sufficient room for producing different regimes, such as slugging, and the length must be compatible with Form 2/3 printer. A bed diameter of 5 mm produced enhanced wall effects and produced a greater error when measuring the capacity. A bed diameter of 20 mm saturated the pressure drop sensor at low velocities and used a greater amount of material.

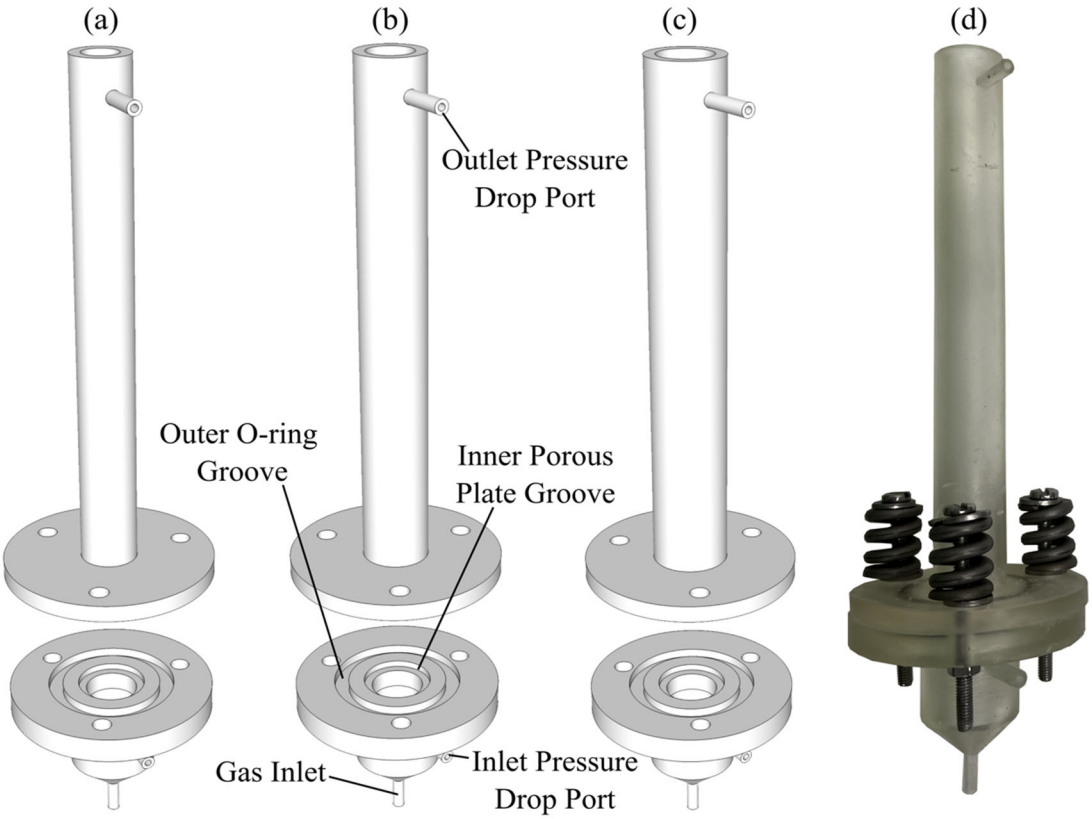

Figure 3.1. CAD models of the 3D-printed MFBRs: (a) D_t = 10 mm, (b) D_t = 12.5 mm, (c) D_t = 15 mm; (d) Example of a fully assembled 3D-printed reactor (the springs on the bolts were used to minimise the stress on the polymer that would otherwise easily shatter if the bolts were over-tightened).

The bottom section of each Micro Fluidised Bed, referred to as the plenum, had a gas supply connection and exhibited a steady increase in diameter. Starting at 2 mm at the entrance, the diameter of this design was progressively expanded to match the final diameter of the equivalent top part. In addition, every plenum section comprised a groove facilitating the insertion of a porous polyethylene plate (with a thickness of 2.5 mm and a pore size of 45 µm) between the two parts, serving as the distributor. To mitigate particles escaping from the bed, a steel mesh with a 26 µm aperture was installed across each pressure port and positioned above the upper section. Ultimately, every plenum was equipped with a groove designed to accommodate an O-ring, establishing an airtight seal between the two components.

3.2.2 Fabrication of MFBRs using 3D Printing

Reducing fabrication time is vital because it accelerates the MFB design and development process, whilst avoiding the need for significant personnel, spacious and expensive processing equipment and high levels of technical expertise (Zhang *et al.*, 2021a; Zhang *et al.*, 2021c). Numerous fabrication methods and materials for MFB construction have thus far been documented in the literature. In recent years, the manufacture of MFB via 3D-printing has become a popular topic, (Zhang *et al.*, 2021a) because additive manufacturing can create extremely complex and/or unique geometries at substantially lower costs and in less time than traditional manufacturing methods. SketchUp software was used in this study to design each fluidised bed, and 3D printing (using the stereolithography approach) was used to fabricate them. The stereolithography method creates 3-dimensional solid objects layer-by-layer through photopolymerisation of a liquid resin using UV light. The whole process is described as follows:

a. Applying Google SketchUp, a 3D CAD model of the MFB is designed (Figure 3.2a).)
b. The CAD model is transformed to the stl file format (Figure 3.2b)
c. The stl model is divided into separate layers and transformed into the tool pathways for the printer using the Pre-Form software (Figure 3.2c)
d. The MFB was manufactured using a Form Labs Form2 or Form3 (Figure 3.2d)
e. MFBs were post-processed, which involved cleaning in IPA in a Form Wash bath to remove excess uncured resin, drying, and post-curing in a Form Cure at 60 °C for 15 minutes (Clear 4) or 80 °C for 120 minutes (High Temp V2), (Figure 3.2e).

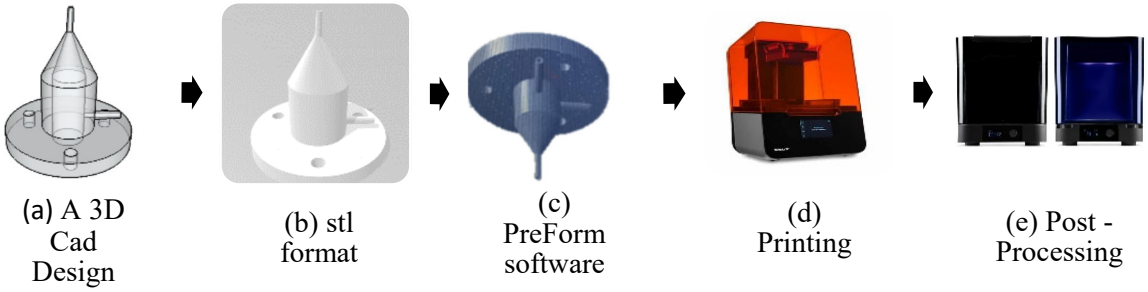

Figure 3.2. (a-e). The process of designing and fabricating an MFB.

3.3 Hydrodynamic Experiment

3.3.1 Materials & Equipment

Figure 3.3 illustrates a simplified experimental diagram that was utilised to analyse the behaviour of the hydrotalcite material in each micro-fluidised bed (MFB) system using conventional pressure drop data. The fluidising particles were fluidised using compressed air at a pressure of 1 barg, regulated by a P3A-EA12BERNP regulator. The flow rate can be adjusted within the range of 0 to 900 mL/min by employing a parallel configuration of float Meters, denoted as Omega. The pressure decrease across the bed was measured using a pressure transducer (Sensirion, SDP816) with a range of 0–500 Pa and a temporal resolution of 4.6 ms. A porous plate distributor design was used inside each MFB to provide uniform air distribution across the bed to increase the fluidisation quality. This approach is common for small scale applications, such as exploring properties of fluidisation in research labs. In order to facilitate the measurement of the pressure drop, pressure ports were incorporated in each fluidised bed as already described above. Each pressure port was covered with fine mesh (26μm) to prevent particles from escaping from the bed and clogging the sensor.

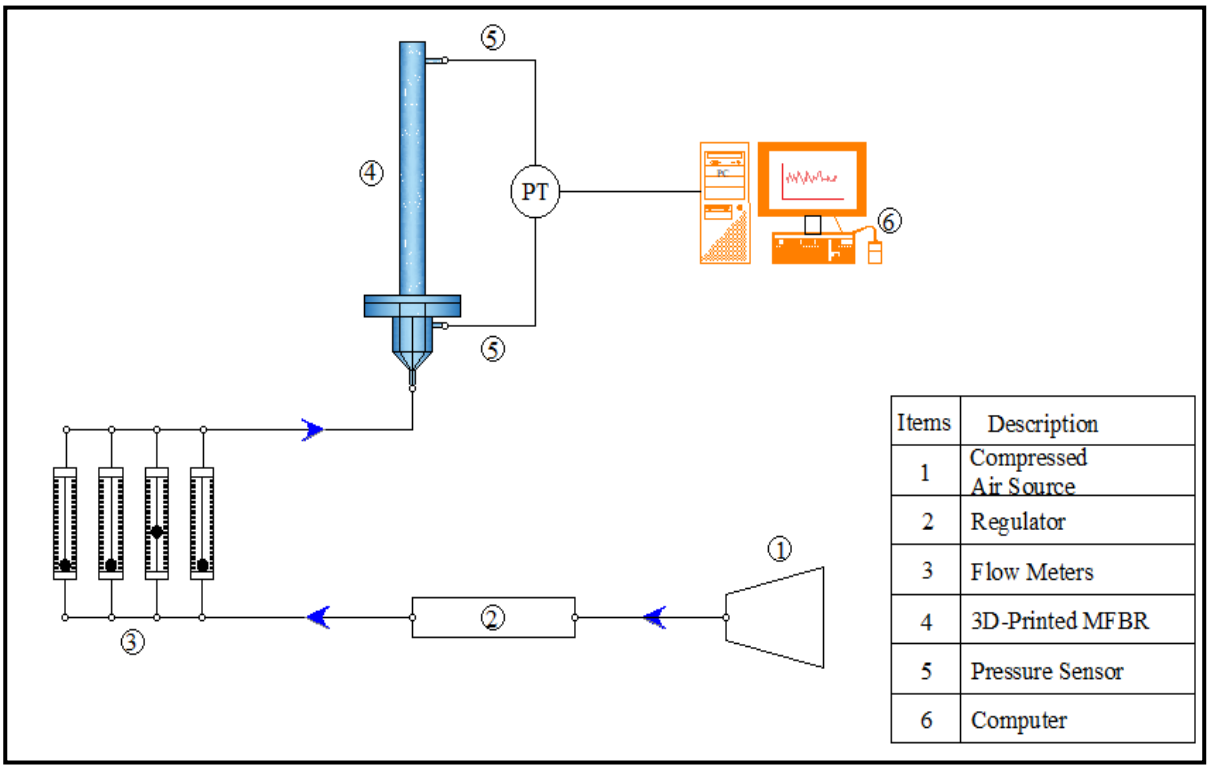

Figure 3.3. Simplified schematic of the hydrodynamic experiment rig.

3.3.2 Overview of Procedures

Before starting the experiment, the micro-fluidised bed reactor (MFBR) was filled with pure hydrotalcite or pure silica corresponding to static bed height ratios (H_s/D_t) of 1, 2, or 3. Furthermore, the experimental setup involved utilising mixtures of these two materials in proportions of 1:2 or 2:1, maintaining a H_s/D_t ratio of 2. In this study, the bed height (H_s) was defined as the height at which the bed settled after being lightly vibrated or tapped to ensure particle compaction. During the fluidisation investigations, the pressure drop data were recorded for 30 seconds at each gas flow rate via fluidisation and defluidisation processes. The fluidisation involved slowly increasing the gas flow rate, while the defluidisation experiments conducted immediately thereafter involved incrementally decreasing the flow rate. A period of stabilisation for the bed was allowed at each flow rate before recording the pressure drop data. The combination of fluidisation and defluidisation facilitated the measurement of the pressure overshoot and wall effects through hysteresis analysis; an illustrative instance is depicted in Figure 3.4.

The column was filled with pure hydrotalcite or pure silica, with static bed height ratios of H_s/D_t = 1, 2, or 3. In addition, a 1:2 or 2:1 mixture of the two materials was utilised with a static bed height of H_s/D_t= 2. The bed height H_s was defined as the height at which the bed settled after being lightly vibrated or tapped to ensure particle compaction. For each experiment, pressure drop data were recorded for 30 s at each gas flow rate, which the gas flow rate was incrementally increased (fluidisation), followed by 'defluidisation' in which the flow rate was incrementally decreased. Before recording pressure drop data at each flow rate, the bed had a few minutes to stabilise at each flow rate. Combining fluidisation and defluidisation experiments could quantify the magnitude of the pressure wall effects and overshoot via hysteresis; see Figure 3.4 for an example.

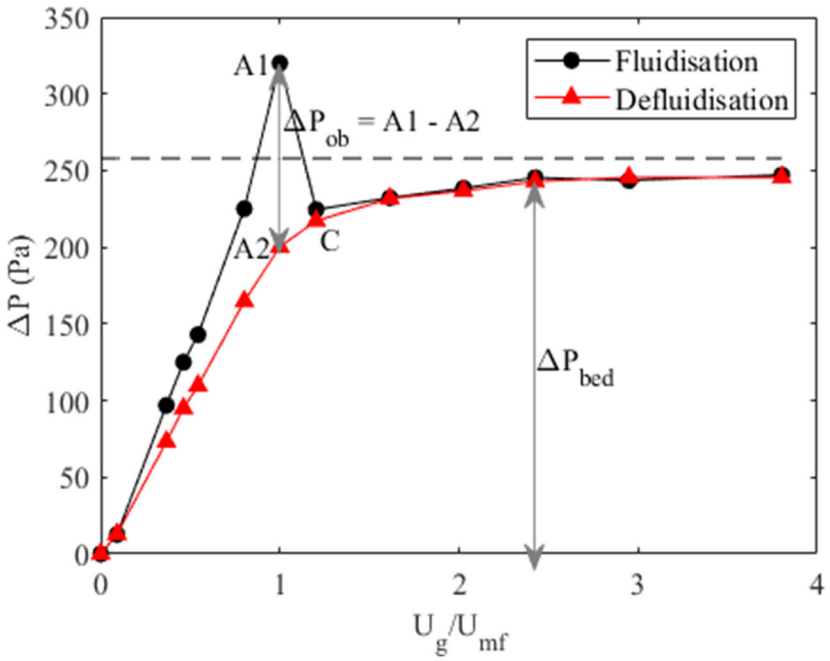

Figure 3.4. Example of fluidisation and defluidisation pressure drop profiles. The pressure overshoot is clearly present during the fluidisation run whilst absent in the defluidisation run; D_t= 15 mm, H_s/D_t = 3, pre-sieved hydrotalcite (d_p = 53–90 µm).

3.3.3 Fluidisation of Hydrotalcite

This study utilised a commercially available hydrotalcite powder with Geldart C characteristics, namely PURAL MG70 from Sasol. Hydrotalcite has emerged as a promising option for capturing CO_2 from effluent gas. This is because of its many benefits, such as its high CO_2 adsorption capacity, fast adsorption and desorption kinetics, thermal and mechanical stability for cyclic adsorption and desorption processes, superior CO_2 selectivity even in the presence of water vapour, and cost-effectiveness in the manufacturing sector (Aschenbrenner *et al.*, 2011; Rossi *et al.*, 2016; Suescum-Morales *et al.*, 2022). This material was chosen because, in addition to the previously mentioned benefits, it is undergoing development and is commercially available in limited quantities. The powder as supplied presented as a talc-like substance and had a density of 2 g/cm^3 and a quoted particle size distribution of <25 μm (45.9%), <45 μm (76.4%), <90 μm (99.6%).

Fluidising PURAL MG70 (cohesive granules) without using assisted approaches, such as Vibrators, applied fields (acoustic, magnetic, electric), and mechanical stirrers, poses numerous difficulties. They are subject to agglomeration, which limits fluidisation. In addition, cohesive particles can cause bed instability because of the growth of cohesive bridges or ineffective regions within the bed, resulting in irregular gas distribution (Visser, 1989; Raganati *et al.*, 2018). Consideration can be given to alternative, low-cost, and uncomplicated methods for addressing these obstacles. Sieving out tiny particles is one method for improving the fluidity of cohesive granules. Mixing with small amounts of Group A particulates can homogenise the bed, reduce attrition, and occupy interstitial spaces, enhancing fluidisation hydrodynamics (Kamranian Marnani *et al.*, 2019). These methods offer prospective solutions for enhancing the fluidisation of cohesive particles without relying on assisted techniques. The raw powder was extremely difficult to fluidise due to its "stickiness," so various strategies for improving fluidisation quality were taken into consideration. The powder was initially sieved via a basic sieve shaker (Retsch Gmbh, MESH S-STEEL) using a range of tray filters (32, 45, 53, 63, 75, and 90 μm). This allowed to remove powder with varying particle diameters in the range of 53–90 μm. Second, an inert secondary particle was added to disrupt the strong forces between the hydrotalcite particles; specifically, an inert silica material with a density of 2.65 g/cm^3 and an average particle size of 93±10 μm was used. This Geldart A material has previously achieved

satisfactory fluidisation in 3D-printed MFBRs (McDonough *et al.*, 2019). Before conducting the actual investigations, the bed was fluidised for several minutes.

3.3.4 Pressure Drop Analysis

3.3.4.1 Flow Regime *map*

The pressure drop data is applied to determine the flow regime transition velocities occurred (Shi *et al.*, 2021) which includes: minimum fluidisation velocity, minimum bubbling velocity, and minimum slugging velocity.

a. Minimum Fluidisation Velocity

The determination of minimum fluidisation velocity is crucial for gas/solid fluidised bed applications because this velocity identifies when the bed changes from fixed to fluidised. Operating higher than U_{mf} allows uniform mixing and improves heat and mass transfer (Guo *et al.*, 2009). It can be determined visually, *e.g.,* via high-speed camera, or non-visually. The non-visual approaches are common in the literature (Vollmari *et al.*, 2016; Hsu *et al.*, 2018; McDonough *et al.*, 2019) because pressure drop analysis is a reliable technique for investigating hydrodynamic experiments in a fluidised bed, with several advantages over other methods such as high-speed cameras. Pressure drop analysis has the advantage of providing quantitative data regarding the fluidisation behaviour of the bed and the pressure drop across the bed as a function of fluid velocity, such as the minimum fluidisation velocity (Sau *et al.*, 2007; Dang *et al.*, 2014; Shi *et al.*, 2021). High-speed cameras, on the other hand, are advantageous for visualising the fluidisation behaviour of the bed, but they may not provide quantitative data regarding fluidisation behaviour and may not capture all characteristics of fluidisation behaviour, such as pressure overshoots across the bed. Therefore, pressure drop analysis is a valuable tool for analysing hydrodynamic experiments in a fluidised bed, and it can provide crucial insights into the fluidisation behaviour of the bed. The most common method uses the pressure drop data, which represents the relation between pressure drop and superficial gas velocity (Bizhaem and Tabrizi, 2013; Dang *et al.*, 2014; McDonough *et al.*, 2019).

In this study, pressure drop data was used to determine U_{mf}. According to the Ergun Equation (Equation 1), the pressure drop rose linearly with increasing superficial gas velocity throughout low gas flow rates in the packed bed regime (Sau *et al.*, 2007; Shi *et al.*, 2021). Then, following the minimum fluidisation velocity, the pressure drop remained constant, this amount of which can be anticipated by applying the buoyancy weight of particles in the bed Equation 2 (McDonough *et al.*, 2019); see Figure 3.5.

$$\frac{\Delta P}{H} = 150\frac{\mu_g U_g (1-\varepsilon)^2}{d_p^2 \varepsilon^3} + 1.75\frac{(1-\varepsilon)}{\varepsilon^3}\frac{\rho_g U_g^2}{d_p} \tag{1}$$

$$\Delta P = (1-\varepsilon)\big(\rho_p - \rho_g\big)gH \tag{2}$$

The minimum fluidisation velocity, U_{mf}, is then defined by the intersection of the pressure drop in the packed bed and constant pressure drop regimes, which is characterised by the buoyant weight in Equation 2, as depicted in Figure 3.5.

Additionally, U_{mf} could be predicted applying empirical correlations based on experimental observations of MFBRs found in the literature. For example, Equation 3 has been derived for U_{mf} (Guo *et al.*, 2009; Qie *et al.*, 2022).

$$U_{mf} = \left[\frac{H_s}{d_p} exp\left(-6.312 + \frac{242.272}{\frac{D_t}{d_p}}\right) + 1\right] \frac{(7.169 \times 10^{-4}){d_p}^{1.82}\big(\rho_p - \rho_g\big)g}{{\rho_g}^{0.06}\,{\mu_g}^{0.88}} \tag{3}$$

H_s/d_p refers to the static bed height over particle diameter, while $D_t\ /\ d_p$ represents bed diameter over particle diameter. Additionally, ρ_g, ρ_p, and μ_g denote gas density, particle density, and gas viscosity, respectively.

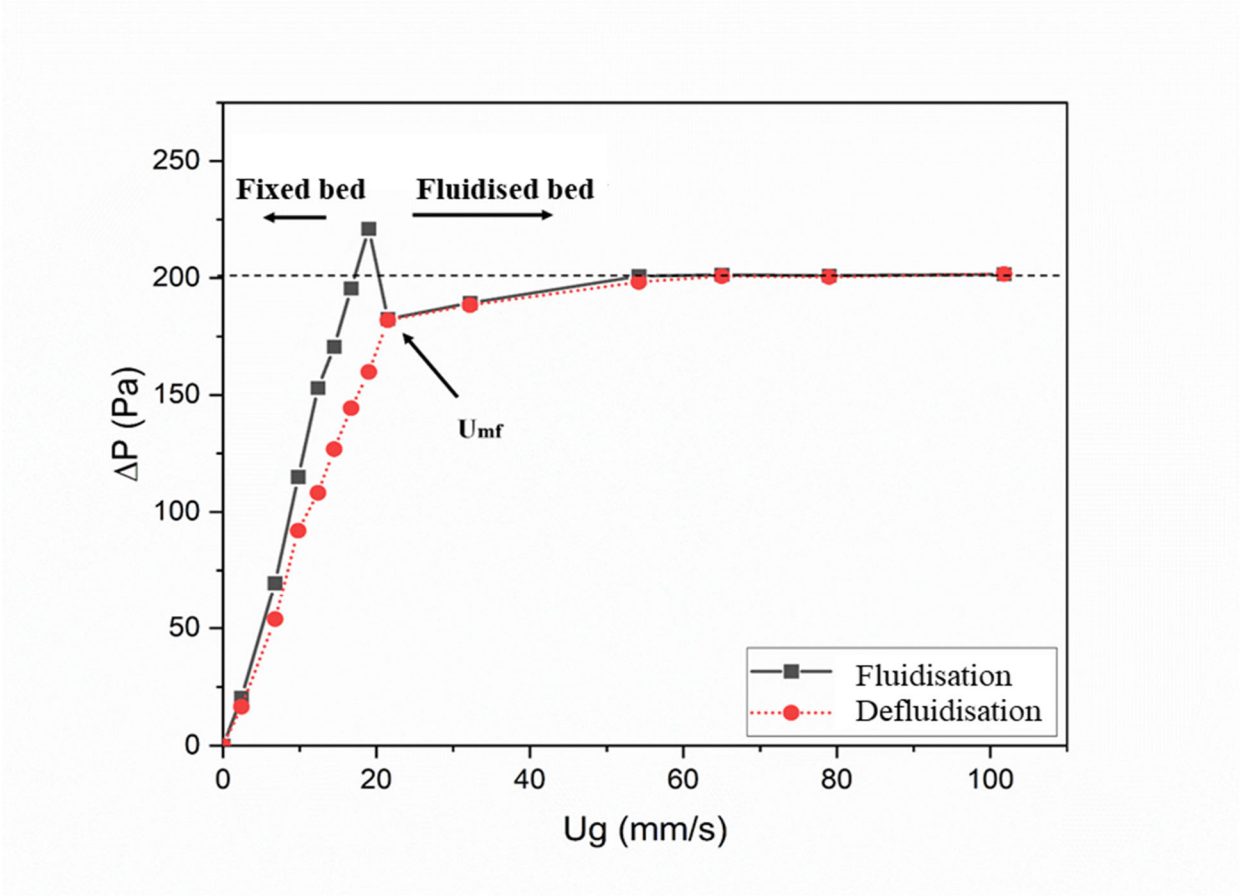

Figure 3.5. Example of pressure drop at different superficial gas velocities.

b. Minimum Bubbling Velocity

Following the attainment of the minimum fluidisation velocity, small bubbles emerge and rise from the distributor to the surface, which substantially impact the flow patterns in the MFB. These promote improved gas-solid mixing and higher contacting time of the gas with the solid, which both improve CO_2 capture by promoting effective mass transfer. The eruption of small gas bubbles from the surface leads to slight fluctuations in the pressure drop (Cornelius Emeka Agu, 2017; Kong *et al.*, 2017), which can be easily detected. The flow behaviour of bubbles/particles is influenced by the ratio of static bed height to bed diameter of the MFB. Generally, in this regime the bubbles form and separate from the gas distributor and subsequently move up throughout the MFB. The coalescence, breakup, and re-coalescence of bubbles could occur between bubbles during the formation of different regimes. The presence

of bubbles leads to the development of particle circulation patterns, which play a crucial role in achieving bed homogeneity (Wang *et al.*, 2011; Cornelius Emeka Agu, 2017). In this experiment, the point at which the standard deviation of the pressure drop increases above zero marks the minimum bubbling velocity, U_{mb} as shown in Figure 3.6. This is due to the fact that signal fluctuations occur by bed motion, indicating the existence of small bubbles in the initial stages of fluidisation (Kong *et al.*, 2017; McDonough *et al.*, 2019). In addition, U_{mb} can be estimated via empirical correlations derived from published studies of MFBRs. For instance, Equation 4 was derived for , U_{mb} (Han *et al.*, 2021).

$$\frac{U_{mb}}{U_{mf}} = 1.099 - 5.21\frac{H_s}{D_t}\left[exp\left(\frac{0.7}{\frac{D_t}{d_p}}\right) - 1\right] \tag{4}$$

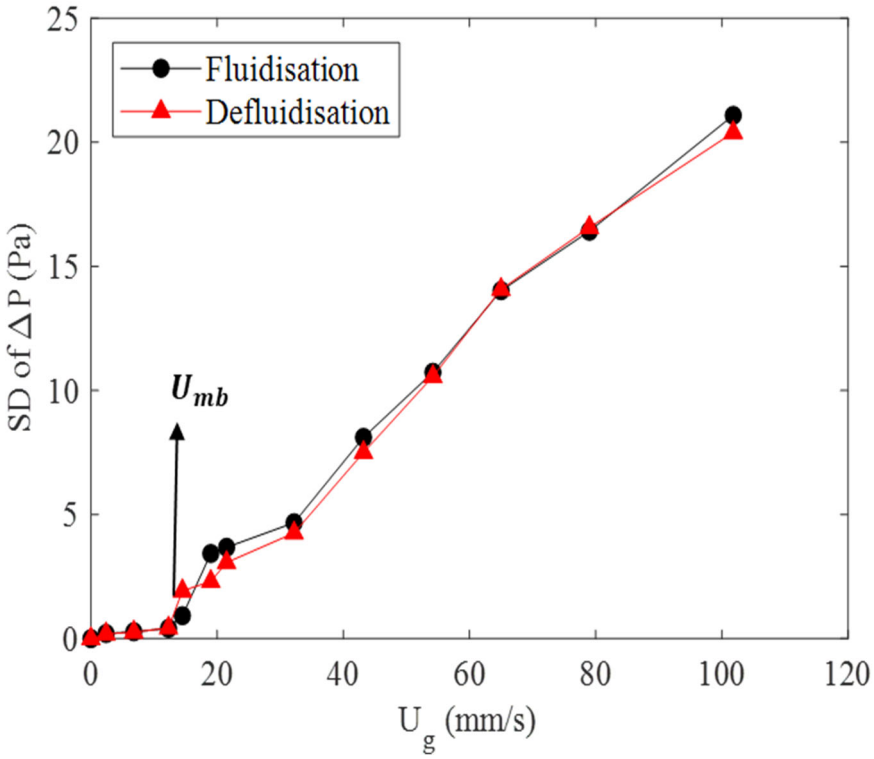

Figure 3.6. Standard deviations of the pressure drop fluctuations as functions of gas superficial velocity in static bed heights (H_s/D_t= 2).

c. Minimum Slugging Velocity

The slugging regime occurs at higher gas velocities; when the gas flowrate increases, gas bubbles become bigger due to the coalescence of smaller bubbles, eventually reaching the size of the MFB's cross-sectional area (D. G. Dimattia, 1997; Kong *et al.*, 2017; McDonough *et al.*, 2019) , leading to larger bubbles or slugs that rise sporadically through the bed at intermittent intervals, and are not equally distributed. Larger bubbles generally move faster than smaller bubbles, which leads to reduced resident time and mass/heat transfer between gas and solid which leads to poor CO_2 capture (Jaiboon *et al.*, 2013). However, it is difficult to differentiate between the desirable bubbling regime and undesirable slugging regime because there is usually no obvious threshold in the time-series pressure drop data signal.

The frequency analysis approach was used to identify the slugging velocity, U_{ms}, which is proposed in a previous study (McDonough *et al.*, 2019). Figure 3.7 plots the frequency spectra of the pressure drop signal in the time domain for each gas flow rate are plotted. To enhance the visual clarity, a cubic interpolation approach was employed to complete the frequency spectrum map. Additionally, the colour intensity was normalised within the range of 0 to 1: deep blue is indicative of a lower probability intensity, while yellow signifies a higher value. Specifically, observations of dominant frequencies are associated with the colour yellow. The lack of gas bubbles or other structures in the packed bed regime is a distinguishing characteristic of all bed designs. This is evident in the frequency domain, which appears uniformly blue in the maps depicted in Figure 3.7. Oscillations can be noted in the time domain pressure drop signal, corresponding to the broad frequency spectrum in Figure 3.7, in accordance with the lowest bubbling velocity. As stated by D.Geldart (1974), slugging is initiated at the moment when the predominant frequency reaches a plateau. McDonough *et al.* (2019) subsequently employed this concept in conjunction with frequency spectrum maps, as illustrated in Figure 3.7, to explicitly ascertain the minimum slugging velocity (U_{ms}). The same approach was utilised in this investigation. For every bed diameter, there is a point at which the dominant frequency (the dominant binary yellow colour) reaches a stable state, which can be defined as U_{ms}. It should be noted that the inclusion of black lines serves the purpose of facilitating the visualisation of the progression of the dominant frequency with the increase in gas flow

rate. This phenomenon is likely indicative of the threshold at which the expansion of bubbles becomes constrained by the dimensions of the channel.

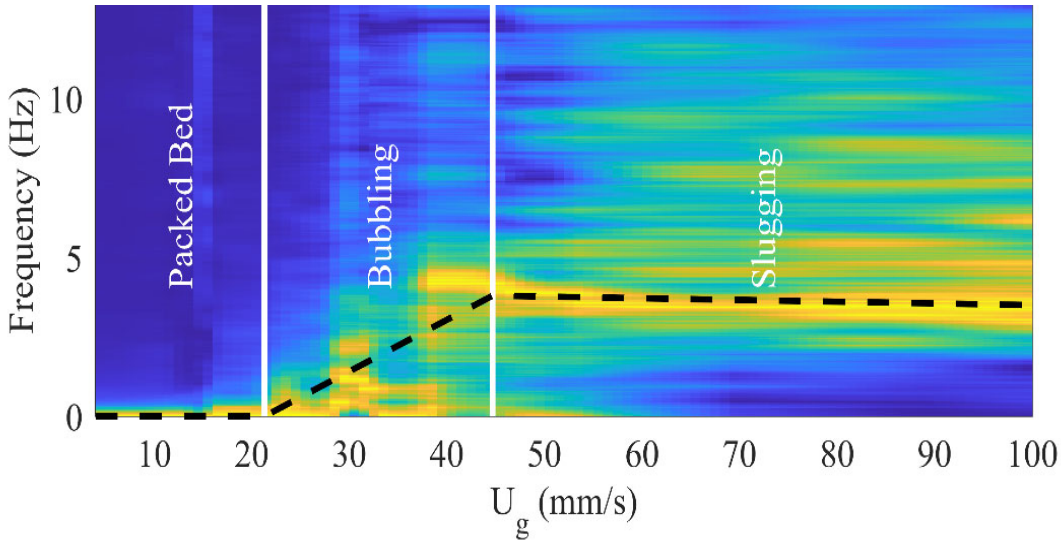

Figure 3.7. Progression of the frequency spectra of the pressure drop signal as gas velocity increases.

3.3.4.2 Pressure Overshoot Analysis

Liu *et al.* (2008) proposed the parameter $\Delta P_W/V_B$ in order to describe wall effects in MFBRs in terms of pressure overshoot; it characterises the excess pressure drop / unit of volume. Equation 5 illustrates how to determine this parameter: H_B is the height of the bed throughout fluidisation. ΔP_B is the pressure drop of the bed through fluidisation. P_E is the excess pressure drop. D_t is the bed (column) diameter. This parameter is plotted against the ratio of bed diameter to particle diameter(D_t/D_p), by McDonough *et al.* (2019) to determine the transition from micro to macro fluidisation, whereas Liu *et al.* (2008) plotted this parameter against the bed diameter. Han *et al.* (2021) determined from these results that when D_t/D_p exceeds approximately 150, the pressure overshoot disappears; this is considered the boundary between micro- and macro-fluidisation behaviour.

$$\frac{\Delta P_W}{V_B} = \frac{\Delta P_B - \Delta P_E}{\frac{\pi}{4} D_t^2 H_B} = \frac{4\left(\frac{\Delta P_B}{H_B} - \frac{\Delta P_E}{H_B}\right)}{\pi D_t^2} \quad (5)$$

However, Han *et al.* (2021) findings cannot inform the current investigation because they were not based on Geldart C powder data. So, Equation 6 is applied to describe the overshoot by adding a new element. Figure 3.4 shows the names of the parameters.

$$\frac{\Delta P_{os}}{\Delta P_{bed}} = \frac{A_1 - A_2}{\Delta P_{bed}} \quad (6)$$

The difference between points A_1 and A_2, indicating the magnitude of the hysteresis between the fluidisation and defluidisation experiments, could characterise the pressure drop overshoot (ΔP_{os}), which can be estimated as in Figure 3.4. The pressure drop increases linearly through the bed within the packed bed regime based on the Ergun equation, and immediately after reaching the delayed minimum fluidisation point, the pressure declines to point C. Points A_2 and C are generally similar for Geldart group A and B particles, and the pressure drop is typically constant when the bed's total mass is supported. In this investigation, however, due to the Geldart C characteristics of the hydrotalcite, point C is larger than point A_2. After the minimum fluidisation point, additional attractive forces lead to a slight increase in ΔP_{bed} even though the bed appears fully fluidised.

3.4 Kinetics Screening (Adsorption)

3.4.1 Materials & Equipment

Figure 3.8 shows a complete diagram of the experimental process for studying CO_2 adsorption into the hydrotalcite in the MFBR, including the gas feeding system, micro-fluidised bed and controlling and measurement system. A 3D-printed MFB with a 10 mm diameter was used among the three-bed diameters tested to test the kinetics of adsorption in batch mode under the conditions found in hydrodynamic studies. This diameter was chosen to reduce the sorbent used because hydrodynamic studies showed that the fluidisation behaviour did not vary much across the three-bed diameters tested. This experiment investigated the impact of CO_2 concentration, temperature, and superficial gas velocity on the adsorption kinetics of the adsorbent (hydrotalcite) in the MFB. The process began by utilising a vacuum oven (OV-11) to remove

any remaining CO_2 and moisture from the solid sorbent particles before introducing them into the MFB.

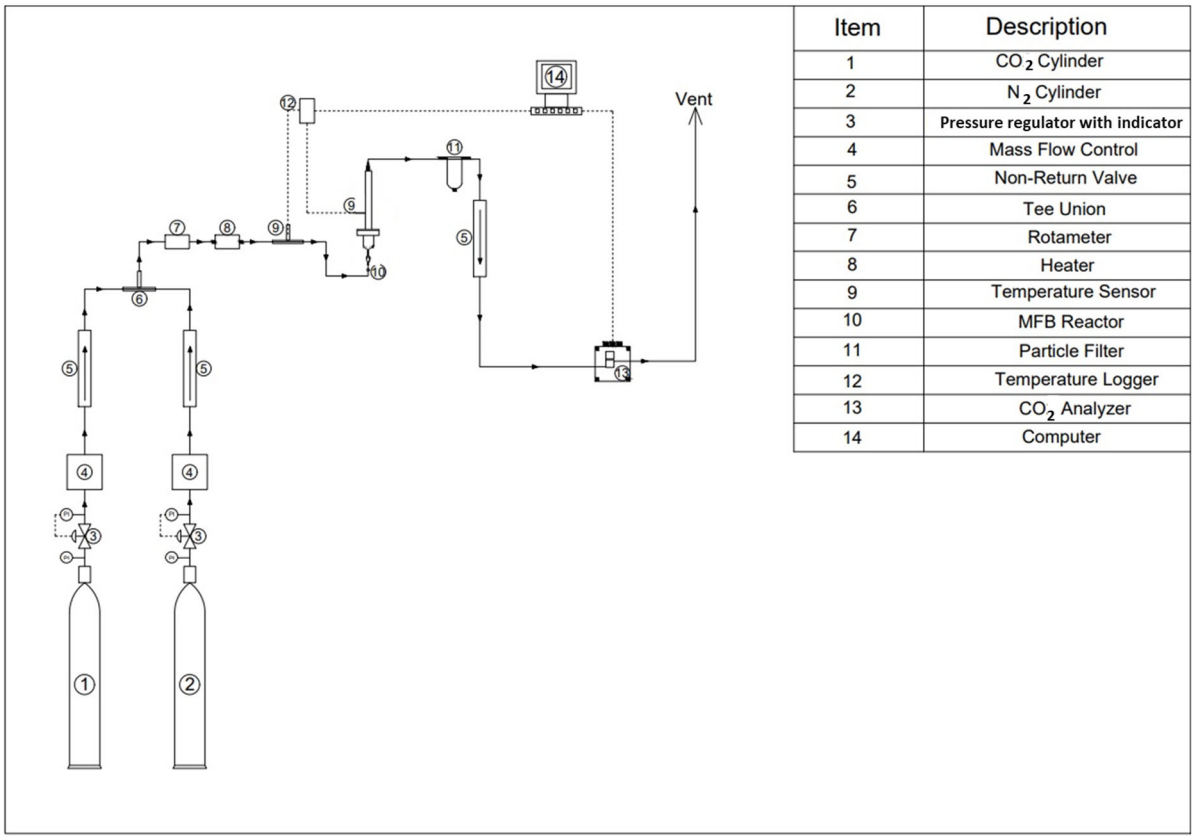

Item	Description
1	CO_2 Cylinder
2	N_2 Cylinder
3	Pressure regulator with indicator
4	Mass Flow Control
5	Non-Return Valve
6	Tee Union
7	Rotameter
8	Heater
9	Temperature Sensor
10	MFB Reactor
11	Particle Filter
12	Temperature Logger
13	CO_2 Analyzer
14	Computer

Figure 3.8. Simplified diagram of the kinetics experiment rig.

An artificial flue gas comprising 8–16 vol% CO_2 in N_2 was produced by mixing pure nitrogen (99.9%) and CO_2 (99.8%) and from standard 9.8 m^3 and 34 kg cylinders respectively. Whilst the flue gas composition from typical industrial applications includes CO_2, N_2, H_2O, CO, SO_x, NO_x, etc., the gas inlet of this experiment contained only CO_2 and N_2. According to Prajapati *et al.* (2016), experiments that use either air or N_2 as an inert gas to dilute CO_2 provided similar results but with the obvious benefit of ease of preparation.

The desired concentration/gas flow rate was achieved using two mass flow controllers. An EL-FLOW (F-201CV-5K0-AAD-22-V) device was used for N_2 whilst a Cole Parmer model (32907-63) was used for CO_2 (0.05–0.5 ln/min). Non-return valves (Swagelok) prevented gas back mixing into the cylinder. An in-line rotameter -Brooks (MR3000) measured the total flow

rate after the mixing point in the range of 0.1–1.2 L/min. A subsequent in-line heater (RS PRO Trace Heating Thermostat) was then used to set the desired operating temperature. Thermocouples were positioned before and within the MFB at 75 mm heights to measure the temperature during the reaction and to avoid any effect on the hydrodynamic behaviour of particles. A filter was used to remove any dust or small particles after the reactor to protect the downstream CO_2 sensor. Finally, the concentration of carbon dioxide (CO_2) was recorded by a CO_2 analyser (GSS, SprintIR) at a sampling rate of 20 Hz throughout the duration of the experiments, which was sufficient to capture phenomena at the time-scales associated with adsorption and the MFB hydrodynamics. This overcomes the challenges of handling small amounts of quantities in the MFB platform compared to alternative approaches.

3.4.2 Breakthrough Procedures

Prior to the adsorption process, the desired amount of adsorbents was introduced into a vacuum oven (OV-11) and subjected to a temperature of 90 °C, in order to remove any remaining CO_2 and moisture. Then, the investigation was conducted as follows. Initially, Hydrotalcite particles with a diameter ranging from 53 to 90 μm were placed inside the 10 mm diameter MFB at a height corresponding to H_s/D_t = 2. Pure N_2 was then used to purge the particles to ensure that all moisture would be removed and the interparticle force would be reduced. This is in accordance with the comprehensive hydrodynamic study results, which are discussed in more detail in the next chapter. Next the N_2 flow rate and gas temperature were set, and the bed was left to stabilise for several minutes at the target conditions. Finally, the CO_2 flow that gave the desired total gas flow rate and CO_2 concentration was initiated simultaneously with the start of data logging. The same procedure was then repeated using the glass particles (≈ 70 μm). This resulted in two sets of data.

All experimental data were analysed in MATLAB. Figure 3.9 shows an example of a breakthrough curve recorded at 40°C, 16 vol% CO_2 and $U_g = 4U_{mf}$. Here the Y axis is $\mathrm{C}/\mathrm{C_O}$, where C, $\mathrm{C_O}$ corresponds to the CO_2 in the inlet and outlet respectively. Two breakthrough curves were recorded for inert glass particles and for the hydrotalcite sample at each condition.

The curve for the glass particles contained information about the CO_2 diffusion through the rig, whilst the curve for the hydrotalcite samples contained information about the kinetics and the CO_2 diffusion characteristics. This was achieved by subtraction of the inert signal from

the hydrotalcite signal enabled recovery of the CO_2 uptake response, as shown in Figure 3.9. A breakthrough time could also be defined: $\Delta_\tau = (\tau_{95} - \tau_{05})$, where $\tau_{95}$is the time needed for the measured outlet concentration to reach 95% of the final value, and τ_{05} is the time needed for the measured outlet concentration to reach 5% of the final value (Jamei *et al.*, 2023). The dead time is the initial period stage in a breakthrough adsorption curve where there is no notable adsorption. This period is frequently caused by variables, including the column void volume or the time required for the adsorbate to reach a sensor. Because it does not offer any information about the adsorption process, it is excluded from the study to concentrate on significant variables, such as breakthrough time and capacity. Assessing adsorption kinetics is more accurate when dead time is excluded (Patel, 2019).

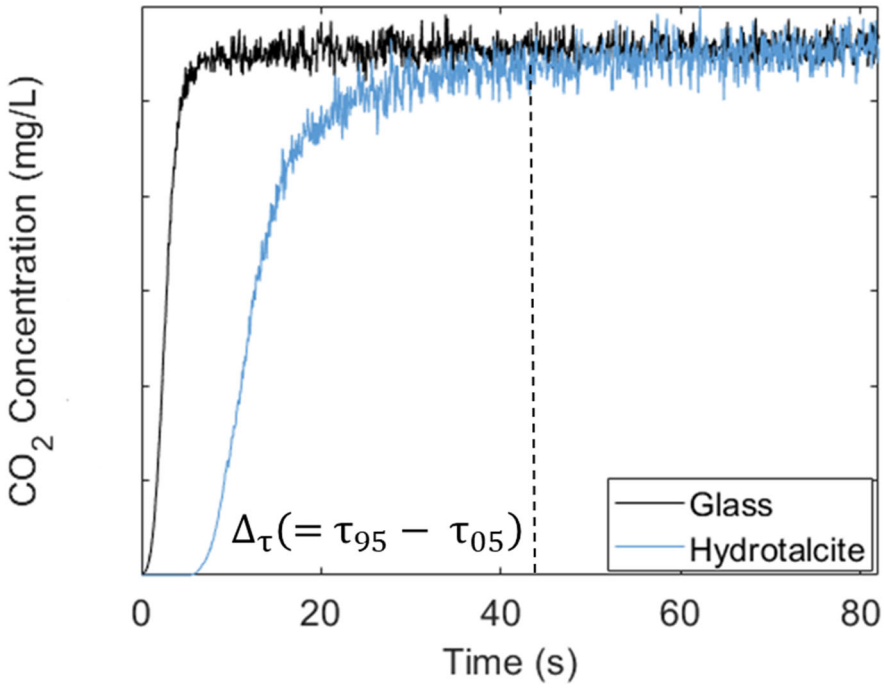

Figure 3.9. The breakthrough curves without dead time (16 % CO_2 4 U_{mf} and 40 °C).

Three kinetic models were compared to the experimental uptake curves: pseudo first and second orders as well as fractional order according to equations 7, 8 and 9, respectively (Serna-Guerrero and Sayari, 2010; Raganati *et al.*, 2019; Jamei *et al.*, 2023). Because of their ability to offer beneficial insights into different aspects of adsorption mechanisms and behaviour, these models are frequently utilised to characterise adsorption phenomena. The pseudo-second-order model is best for describing processes that consist solely of chemisorption, *e.g.,* those marked

by strong chemical interactions between CO_2 molecules and the sorbent surface, while the pseudo-first-order model is suitable for characterising simple physical adsorption mechanisms with relatively low surface covers. That is, it can reasonably define adsorption without taking into account the possibility of bonding or chemical interactions between the two. In contrast, the fractional order model incorporates characteristics of both mechanisms. Fractional-order models are applied to represent adsorption phenomena with diffusional limits or many reaction paths, mainly when procedures for adsorption display non-classical behaviours or mechanisms.

By applying multiple kinetic models, investigators can improve their understanding of the fundamental adsorption processes, examine the accuracy of their predictions about reaction orders, and customise their modelling techniques to the specific characteristics of the adsorption system. The process of matching empirical data with available mathematical models facilitates the determination of the most suitable model and improves the understanding of adsorption kinetics (Serna-Guerrero and Sayari, 2010; Asenjo *et al.*, 2011; Raganati *et al.*, 2019). The fit of these kinetics models to the experimental data was assessed using the R^2 value. The coefficient of correlation, R^2 (equation 10), which ranges from 0 to 1, is used to measure how well the kinetic models match up with the experimental data. More specifically, the definition of the term is as follows: The term is defined as the ratio between the experimental adsorption uptake (q_{exp}) and the modelled adsorption uptake (q_{mod}), where n represents the number of experimental data points, and p represents the number of parameters in the equation (Vargas *et al.*, 2011; Revellame *et al.*, 2020; Jamei *et al.*, 2023).

$$q_{t=}\, q_e \left(1 - e^{k_1 t}\right) \tag{7}$$

$$q_{t=} \left(\frac{{q_e}^2 K_2 t}{1 + q_e K_2 t}\right) \tag{8}$$

$$q_t = \quad q_e - \left(\frac{(n-1)K_f}{m_1} \quad t^{m_1} + \left(\frac{1}{{q_e}^{n-1}}\right)^{\frac{1}{n-1}}\right)^{-1} \tag{9}$$

$$R^2 = 1 - \left(\frac{\sum_{i=1}^{n} (q_{t(exp)} - q_{t(exp)})^2}{\sum_{i=1}^{n} (q_{t(model)} - \tilde{q}_{(exp)})^2} \right) \quad (10)$$

In this context, q_t represents the CO_2 uptake at time t (measured in mmol), while q_e signifies the uptake of CO2 once equilibrium is reached (in mmol). K_1 stands for the pseudo first-order rate constant (in s^{-1}), K_2 is the pseudo second-order rate constant (in g. $mmol^{-1}.s^{-1}$), and K_f represents the fractional-order rate constant (in s^{-1}). The variable t denotes time (in seconds), and n and m_1 are empirical coefficients used to refine the shape of the fractional-order model curve. The n coefficient characterises the driving force, while m_1 represents the adsorption time. These models predict the cumulative uptake behaviour of CO_2 as it is adsorbed onto the material's surface (Jamei *et al.*, 2023).

3.5 Kinetics Screening (Desorption)

3.5.1 Materials & Equipment

A batch system frequently serves as an analogy for a fluidised bed. It is recognised that, in a batch process, the desorption process is achieved at high temperatures while the sorption process is done at low temperatures. Desorption is accomplished by heating the sorption material via the temperature swing adsorption approach. The quantity of heat needed for regeneration depends on the type of adsorbent. Gas-solid fluidisation is a process of contact between the two phases in which the solid phase achieves a fluid-like state under fluidisation conditions. The same equipment for the adsorption process was used during the desorption process. The adsorption and desorption experiments were performed employing an MFB unit at two desorption temperatures which are 40 °C, and 90 °C. In general, experiments were performed in various steps to explore the desorption process, involving pre-treatment, experimental condition adjusting, adsorption, preheating phase when required, and then desorption step.

Figure 3.11 displays schematics of the experimental procedure for investigation CO_2 desorption into the hydrotalcite using the 10 mm 3D printing MFB. The desorption including the gas feeding system, micro-fluidised bed, and measurement system. A 3D-printed MFB (10 mm diameter) was employed for the desorption screening in batch mode under the operation conditions identified during adsorption experiments. These experiments investigated the impact of temperature on the desorption kinetics of the adsorbent (hydrotalcite) in the MFB. The equipment had been used in adsorption experiment was employed in desorption process with placing of an additional inline heater around the MFB. Another heater was placed around the inlet piping prior to the MFB; the temperature could be controlled via adjusting the electric heater's output power. K-type thermocouples were used for recording the temperature profile of the tested adsorbent particles as well as the inlet and outlet air temperatures. The thermocouples were set up at the inlet of the MFB section and at the 75 mm height of the MFB.

3.5.2 The Experimental Procedure

Figure 3.10 summarises the breakthrough curve desorption experiment. The breakthrough curve desorption experiment is a technique applied in a lab to investigate the desorption kinetics of CO_2 from a solid phase. One of the standard desorption techniques is the TSA (Temperature Swing Adsorption) technique, which is achieved by subjecting the sorption material to high temperatures. This leads to the release of CO_2 from hydrotalcite and is recorded at the bed outlet with an increasing temperature over time. Here is an overview of the experiment process for the desorption curve breakthrough. Desorption experiments typically involve pre-treatment, experimental condition adjustment, adsorption, and preheating. Desorption was achieved in the last stage. Initially, before the adsorption procedure, the desired volume of adsorbents was placed in a vacuum oven (OV-11), and the temperature was adjusted to (90 °C) (for 15 min) to eliminate residual CO_2 and moisture. Then, hydrotalcite (53–90 µm diameter) was placed inside MFB (10 mm diameter) at the height of $H_s/D_t = 2$; Hydrotalcite was prepared to be utilised in the desorption experiment before every desorption test by performing adsorption to ensure that the Hydrotalcite particles were entirely saturated with CO_2. The experiment was extended by two more minutes after reaching saturation to ensure complete saturation of the particles. The aforementioned procedure played a vital role in the preparation for the desorption stage.

This was accomplished under the suitable operational conditions for adsorption: 16 vol% CO_2, 40 °C, and $U_g = 4\ U_{mf}$, for the CO_2 concentration, temperature, and superficial gas velocity, respectively. Then, the flow passed via the MFB desorption reactor at a high temperature. The gas supply was set up by utilising cylinders of high-purity N_2 and CO_2, with a volume concentration of 99.995 vol%. The flow rates of the gases were regulated and monitored via two mass flow controllers, an EL-FLOW (F-201CV-5K0-AAD-22-V) and a Cole Parmer model (32907-63), respectively.

Then, after the bed was saturated with CO_2 (adsorption stage), the heating step was next. Two heaters were used to get the target temperature: the first was positioned around the inlet stainless steel tube, and the second was placed around the 3D-printed MFB. Two ways were applied: the first was when only the second heater, which was placed around the MFB, was used, with both N_2 and CO_2 flow rates stopping, which was challenging to reach the target temperature. The second approach entails applying heat while maintaining the nitrogen (N_2) and carbon dioxide (CO_2) flow rates. The desorption temperatures of 40°C and 90°C were selected due to

the limitations which were the limited flow rate of the micro-fluidised bed. In addition, the micro fluidised bed was constructed using a high-temperature polymer material. Moreover, surpassing particular temperature thresholds presented a potential risk for bed damage. The first method was used to obtain 90 °C, heating the bed with only a heater placed around the MFB without injecting a fluidising gas to spread the heat. However, this was difficult because of the limited thermal conductivity of the MFB material, which consists of a high-temperature polymer. The MFB was damaged before reaching the desorption temperature because the polymer material begins to degrade and cannot tolerate high temperatures. Moreover, there is an uneven heat distribution when heat is delivered using only a wrapped heater cable around the MFB, resulting in localised hotspots and temperature changes. The desorption target temperature was achieved using the second way in these experiments by using two thermal cables positioned around the stainless-steel input pipe and the MFB. Therefore, injecting a fluidising gas at a suitable flow rate inside the MFB system throughout the heating process is necessary to avoid these constraints and help spread the heat more uniformly and effectively. The flow rate of the fluidising gas enhances convective heat transfer, improving the MFB's thermal homogeneity and reducing the possibility of localised hotspots. The temperature was measured at the intake and within the MFB. CO_2 levels are recorded throughout the pre-heating step to identify if any CO_2 loss might happen. After getting the desired temperature, the flow rate was converted to only N_2, and the released CO_2 from the Hydrotalcite was recorded through time. The breakthrough curve records the outlet CO_2 concentration profile over time. Analysing the breakthrough curve allows for the provision of information on the CO_2 desorption properties of the solid sorbent. To validate the results, the experiments were conducted three times under each condition to ascertain the mean values and their associated errors.

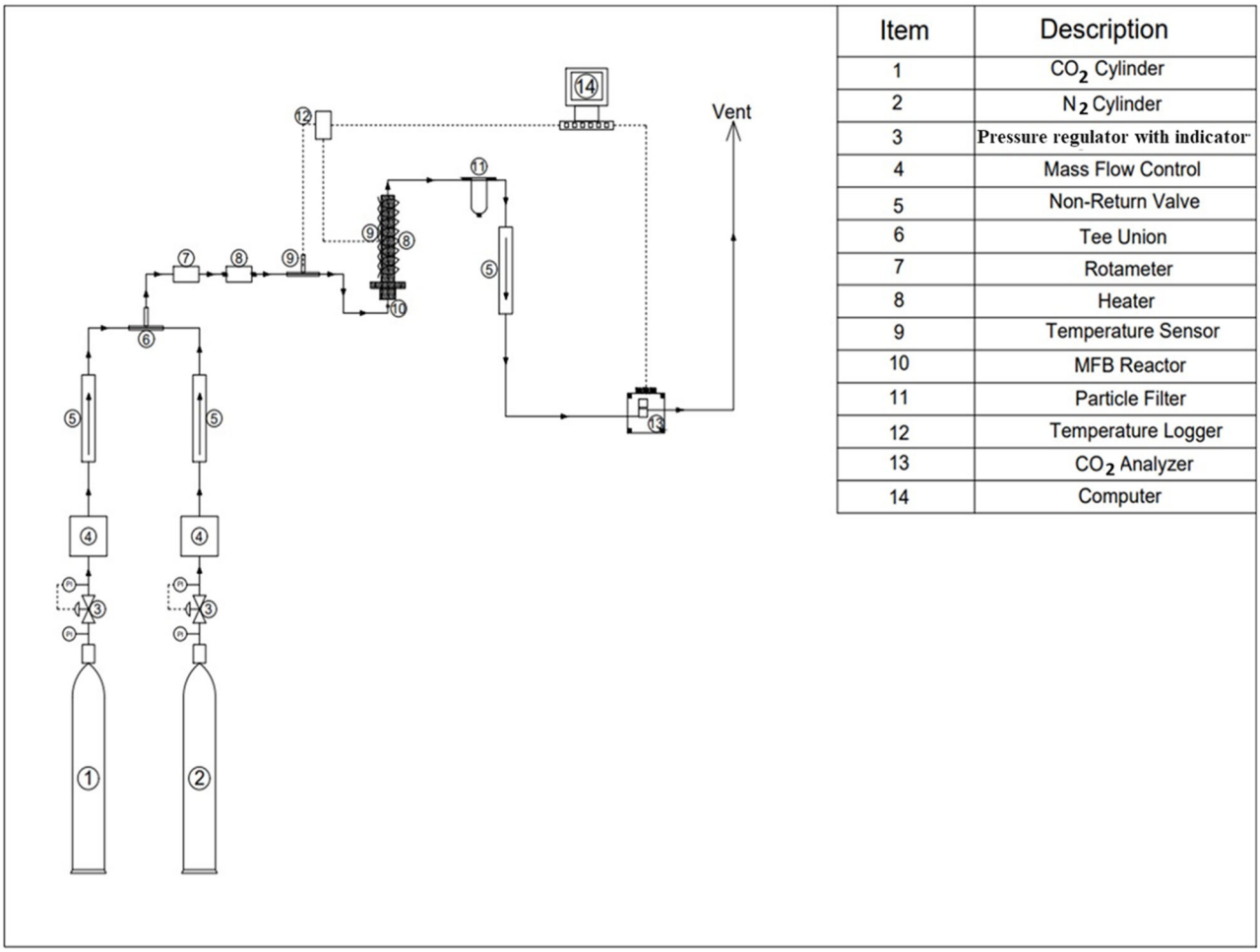

Item	Description
1	CO_2 Cylinder
2	N_2 Cylinder
3	Pressure regulator with indicator
4	Mass Flow Control
5	Non-Return Valve
6	Tee Union
7	Rotameter
8	Heater
9	Temperature Sensor
10	MFB Reactor
11	Particle Filter
12	Temperature Logger
13	CO_2 Analyzer
14	Computer

Figure 3.10. Simplified schematic of the kinetics experiment rig.

Figure 3.11 shows the variation C/C_O, over time where C_O and C represent the amount of CO_2 at the inlet and outlet respectively. It is necessary to subtract the inert signal from the hydrotalcite signal to ascertain the recovery of the CO_2 uptake response. Interpreting these results leads to conclusions about the desorption behaviour of CO_2 from the solid material.

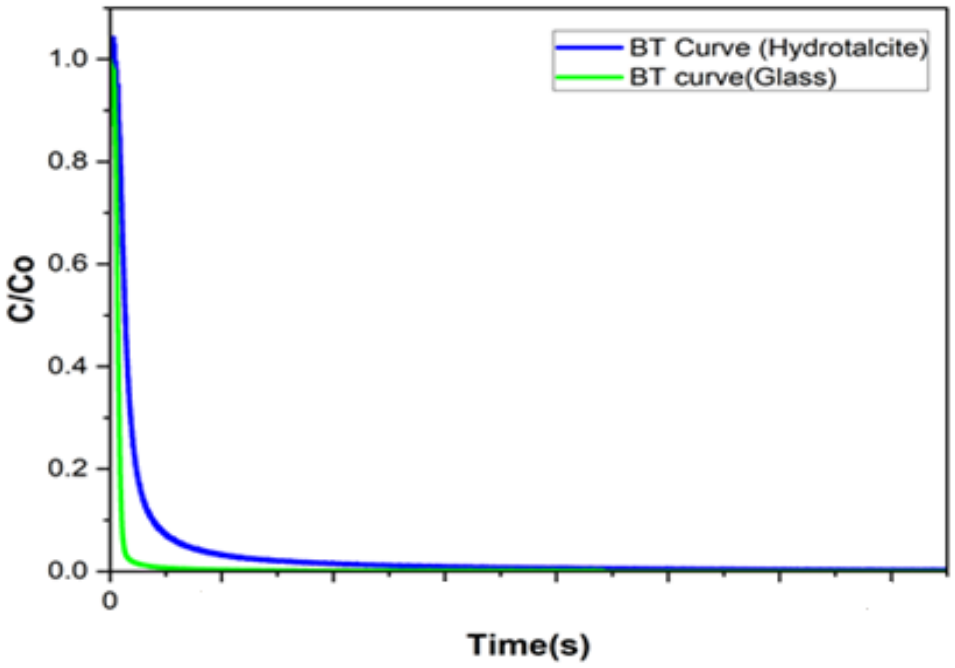

Figure 3.11. The breakthrough curves of desorption process.

Chapter 4. Hydrodynamic Experiments

4.1 Introduction

Hydrotalcites are a promising candidate for capturing CO_2, but their strong inter-particle forces produce significant agglomeration and poor fluidisation quality in micro-fluidised bed technology. Further, in developing a small-scale screening platform there are two competing considerations: minimising the volume or mass of solid particles needed for screening (since usually on small amounts of material are available during the early stages of materials development) and the need for larger quantities of particles to minimise noise levels in detected signals. Therefore, detailed hydrodynamic experiments were conducted utilising the pressure drop characterisation technique to identify viable MFBR designs and operating conditions for these Geldart C particles. Pressure drop analysis is an effective tool for examining hydrodynamic experiments in a micro fluidised bed, with various benefits over other approaches such as high-speed cameras. The advantages of using pressure drop analysis include, offering quantitative data regarding the bed's fluidisation behaviour and the pressure drop across the bed as a function of fluid velocity, such as identifying the minimum fluidisation velocity (Sau *et al.*, 2007; Dang *et al.*, 2014; Shi *et al.*, 2021). High-speed cameras, on the other hand, are beneficial for visualising the fluidisation behaviour of the bed but may not offer quantitative data regarding the fluidisation behaviour. Furthermore, high-speed cameras may not catch all the features of fluidisation behaviour, such as pressure overshooting throughout the bed. As a result, pressure drop analysis is a useful instrument for examining hydrodynamic experiments in a fluidised bed, and it may give vital insights into the fluidisation behaviour of the bed (Bizhaem and Tabrizi, 2013; Dang *et al.*, 2014; McDonough *et al.*, 2019).

It is essential for understanding the hydrodynamic behaviour of the cohesive particles in the micro-fluidised bed prior to performing kinetics screening research to identify optimal fluidisation conditions and understand where regime transitions occur. However, hydrotalcites present another challenge: their Geldart C classification (Aschenbrenner *et al.*, 2011; J.M. Valverde a, 2012; McDonough *et al.*, 2018; Raganati *et al.*, 2018; Coenen *et al.*, 2019). Geldart C powders possess strong inter-particle forces that cause significant particle agglomeration and therefore poor fluidisation quality (Coenen *et al.*, 2019; Jae-Rang Leea b and Kim, 2020). This could limit the usefulness of the screened kinetic data for industrial applications. Gas-solid fluidisation quality generally relies on the interaction between particle density and size (Dietrich

et al., 2018; Hsu *et al.*, 2018). Therefore, to control and fluidise fine powders interventions such as vibration, mechanical stirring, sound waves, or mixing with secondary larger particles have been considered (Wang *et al.*, 2007b; Raganati *et al.*, 2018). In this thesis, for the kinetics study of hydrotalcite in suitable conditions, several affordable treatments were investigated to overcome the cohesive forces of a commercial hydrotalcite powder inside 3D-printed MFBRs. The fluidisation characteristics were studied as a function of gas velocity, static bed height, particle diameter, and bed diameter. The fluidisation quality was defined based on metrics such as pressure overshoot, wall friction, and flow regime transition. Standard pressure drop data was applied to characterise the behaviour of the hydrotalcite powder.

4.2 Results and Discussions

4.2.1 Fluidisation of Hydrotalcite Powder using Different Treatments

Hydrodynamics testing was performed in three different 3D-printed MFBRs with bed diameters of 10 mm, 12.5 mm, and 15 mm. These were selected based on the need to compromise between minimising the amount of material to fill the bed to reduce waste, whilst ensuring enough material was present to eventually observe meaningful reaction kinetics in the future CO_2 breakthrough experiments (to maximise the signal to noise ratio). The standard pressure drop data was analysed to characterise the behaviour of the hydrotalcite powder. Prior to the experiment, the MFBR was filled with either pure hydrotalcite or pure silica (with static bed heights of H_s/D_t = 1, 2 or 3), or a mixture of the two in ratios of 1:2 or 2:1 (with a static bed height of H_s/D_t = 2). Here, the bed height (H_s) corresponded to the 'tapped' height; the height when the bed is lightly vibrated/tapped to settle the particles.

Figure 4.1a-d shows the pressure drop profiles obtained from fluidisation and defluidisation experiments for the raw hydrotalcite powder, pre-sieved hydrotalcite powder, pre-sieved and pre-fluidised hydrotalcite powder, and hydrotalcite-silica mixture. Note, here the x-axis was plotted as the gas velocity U_g only rather than the ratio of U_g/U_{mf} because it was not possible to define U_{mf} for the raw hydrotalcite. The fluidisation quality of the raw as-supplied hydrotalcite powder was clearly poor as shown in Figure 4.1a, exhibiting a clear pressure drop overshoot, large deviation between fluidisation and defluidisation experiments, and no flatlining of the pressure drop following the minimum fluidisation point (Zhang *et al.*, 2021a). The latter feature indicates that not all of the bed was in a fluidised state. This poor fluidisation

quality was the result of the small particle sizes and large inter-particle attractive forces. This enabled the gas to form channels inside the bed rather than gas bubbles, matching similar observations in the literature (Aschenbrenner *et al.*, 2011; J.M. Valverde a, 2012; Lee *et al.*, 2020). The hysteresis between fluidisation and defluidisation experiments was likely a result of some of the fines being driven through the mesh filter at the bed outlet at high gas flow rates, resulting in a lower pressure drop during the defluidisation process because less material was present.

In the next set of experiments (Zhang *et al.*, 2021b), the hydrotalcite powder was pre-sieved to remove the fines so that only particle diameters of >53 μm were retained. This produced a clear improvement of the fluidisation quality indicated by the pressure drop matching the buoyant weight (implying that the whole bed was eventually fluidised), and a closer agreement between fluidisation and defluidisation runs (Figure 4.1b). Finer particles have a higher surface area to volume ratio that increases the relative strength of interparticle forces compared to the drag induced by the fluidising gas. Removing the fines therefore alleviates the strongest interparticle interactions. However, the hydrotalcite is still a 'sticky' powder, and the fluidisation quality is not perfect, indicated by a small increase of the pressure drop after the minimum fluidisation point, whereas usually the pressure drop remains constant.

Pre-sieving and pre-fluidising the bed seemed to further improve the quality by reducing the magnitude of the pressure overshoot (Figure 4,1c). The net interparticle force emerges from the combination of liquid bridges, electrostatics, Van der Waals interactions, etc. Their combined effect can be significant, prolonging the packed state until these forces are eventually overcome. Pre-fluidising the bed for just 2 minutes (at a velocity of 40 mm/s) breaks the capillary-bridges that can form from atmospheric humidity over time (LaMarche *et al.*, 2016). However, effects of this treatment typically diminished over time, meaning pre-fluidisation should be run immediately prior to experiments.

Finally, Figure 4.1d shows that mixing the sieved hydrotalcite powder with an inert Geldart A powder produces a similar improvement to the fluidisation quality as pre-fluidisation. Mixing the hydrotalcite with a slightly larger particle decreases friction and cohesion, where the secondary particle acts as a lubricant and spacer (Ajbar *et al.*, 2011). Consequently, this mixture disintegrates the cohesive structure of the hydrotalcite which reduces agglomeration as well as the particle-particle and particle-wall adhesion forces (Ajbar *et al.*, 2011). Reduced

agglomeration also helps to ensure good surface area contact between the hydrotalcite and fluidising gas for adsorption kinetic screening.

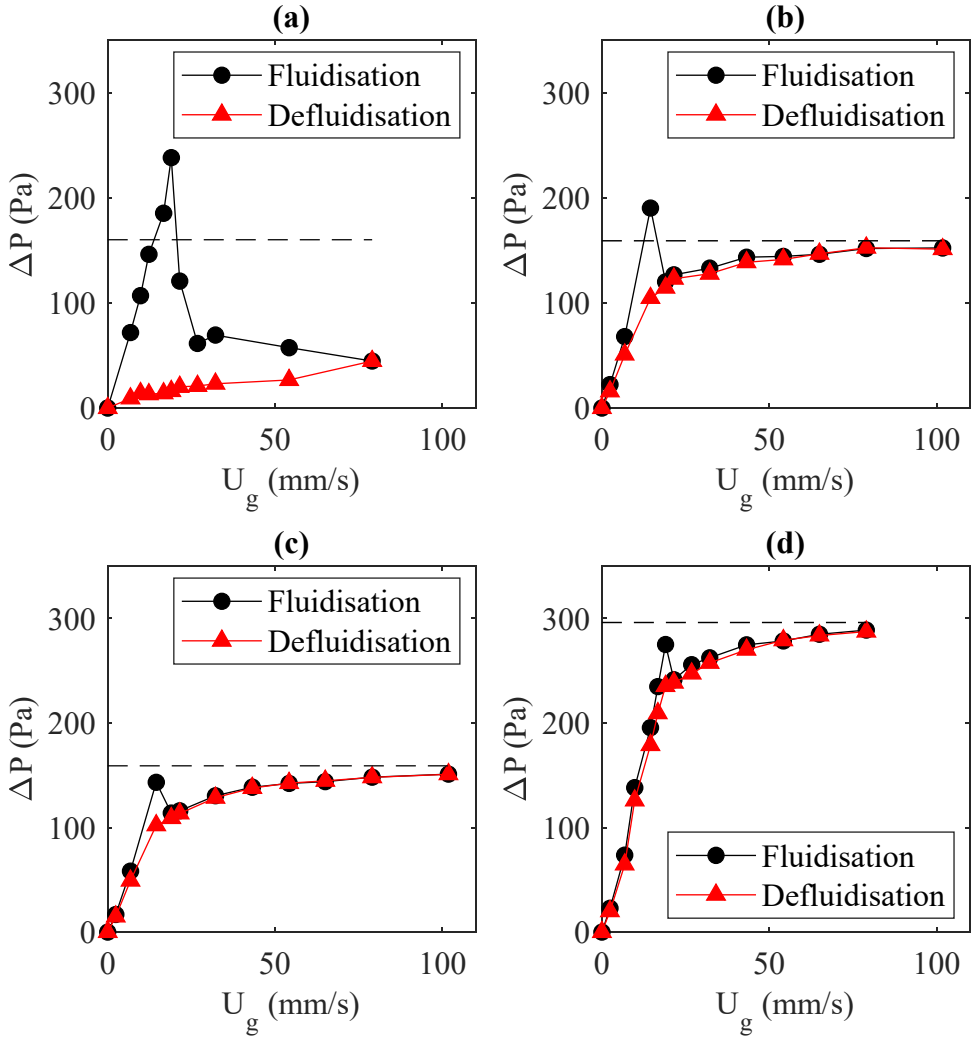

Figure 4.1. Pressure drop profiles for the raw and treated hydrotalcite powder; D_t = 12.5 mm, H_s/D_t = 2; dotted lines correspond to the buoyant weight of the bed; (a) raw as-supplied hydrotalcite powder; (b) pre-sieved hydrotalcite powder (particles diameters of 53–90µm); c) pre-sieved and pre-fluidised hydrotalcite powder (d) pre-sieved hydrotalcite powder mixed with silica in 1:2 ratio.

Geldart C powders have been fluidised in the literature using a variety of methods such as vibration, additional energy fields (acoustic, magnetic, and electric), and mechanical stirring (Zhou and Zhu, 2021). In contrast, similar improvements were achieved by simply sieving, pre-fluidising, and mixing the particles with a secondary material but with clear advantages: easy implementation, low-cost, no need to modify the reactor design, and no need for additional instruments/tools (Bahramian and Olazar, 2021; Zhou and Zhu, 2021). These simple treatments produce fluidisation characteristics resembling Geldart A particles.

4.2.2 Pressure Overshoot and Wall Effects

4.2.2.1 Effect of Pre-Fluidisation

There was a clear pressure overshoot prior to fluidisation in many of the experiments (*e.g.,* Figure 4.1), which resulted in a strong hysteresis between the fluidisation and defluidisation experiments. The pressure overshoot during fluidisation is a consequence of two complementary effects, one inherent to the MFBR technology and the other inherent to the hydrotalcite material. On the technology side, the inherently high surface area to volume ratios of the MFBR increases the relative importance of friction compared to larger scale fluidised beds that produces a stabilising effect (often referred to as wall effects in the literature). This wall friction acts to oppose motion during fluidisation and support the bed during defluidisation. Guo *et al.* (2009) identified that the generation of friction between the particle bed and the wall is attributed to adhesive forces, surface tension effects, and static cohesive effects. This friction serves to stabilize the bed, resulting in a delayed onset of fluidisation and contributing to the support of the particles. However, it can occasionally lead to an increased deviation between the measured and theoretical pressure drop. Furthermore, the investigation by Sánchez-Delgado *et al.* (2011) noted that gas bubbles tend to selectively percolate through the central region of the bed due to bubble coalescence, causing non-uniform voidage throughout the bed. This observation suggests that the wall regions may receive additional support through wall friction and/or additional electrostatic cohesion forces.

When the bed is filled, the static height (H_s) is defined by the tapped density. Here the particles pack together more closely compared to when they are allowed to settle ‘naturally’. This tighter packing combined with the downward acting wall friction during fluidisation increases internal friction in the bed, providing a significant resistance to motion. In contrast, during the

defluidisation process the voidage is larger since the particles are already in a suspended state. Wall friction in this case actually helps to partially support the bed (by supporting some of the buoyant weight). Vanni *et al.* (2015), Peter N. Loezos (2002), and Guo *et al.* (2009) all report similar observations. On the material side, the Geldart C classification of the hydrotalcite powder itself produces strong cohesive forces (particle-particle) and additional adhesive forces (particle-wall) that also stabilise the bed against motion (Hsu *et al.*, 2018; Han *et al.*, 2021).

$$\frac{\Delta P_{os}}{\Delta P_{bed}} = \frac{A_1 - A_2}{\Delta P_{bed}} \tag{1}$$

To gain a more detailed understanding of the combined MFBR wall effects and Geldart C characteristics, the pressure overshoot was investigated using the ratio of $\Delta P_{os}/\Delta P_{bed}$ (Equation 1). Figure 4.2 summarises this normalised pressure overshoot for the pre-sieved powder with and without the pre-fluidisation treatment.

For a fresh particle bed, increasing the bed diameter expectedly reduces the magnitude of the pressure overshoot by reducing the wall effect component of the stabilising force. This is because the surface area and volume of the bed scale with D_t^2 and D_t^3 respectively; a larger value of D_t will reduce the relative importance of friction between the bed and the wall. The overshoot also increases as the static bed height increases. This can again be explained by an enhancement of the friction between the particles and sidewalls, since a taller bed will have a larger surface area.

Also, some insight into the cohesive and adhesive forces can be gained by comparing them (Zhang *et al.*, 2021a; Zhang *et al.*, 2021b). Here it can be seen that the overshoot pressure clearly also depended on whether the bed was 'fresh' or pre-fluidised. Interparticle forces are a sum of electrostatic effects, liquid bridges, Van der Waals interactions, and other physical/chemical interactions (Wang *et al.*, 2017; Hsu *et al.*, 2018). These individual effects are difficult to isolate in practice since the particle assembly usually comprises a range of particle sizes and physical/chemical properties on the surface of the particles Nevertheless, it can be inferred from Figure 4.2 that the liquid bridge must play an important role in contributing to the 'stickiness' of the hydrotalcite. These capillary-bridges can form over time due to atmospheric humidity, which then intensifies the interparticle forces (LaMarche *et al.*, 2016). These in turn increase the pseudo-tensile strength of the bed, increase particle-wall interactions, and increase powder cohesion, all of which lead to poor fluidisation quality overall (Wormsbecker and Pugsley,

2008). Pre-fluidising likely only effects the liquid bridges, since the other interactions will be inherent to the material. This pre-fluidisation effect then weakens over time as the bed absorbs atmospheric moisture. This result suggests that pre-fluidisation in a dry gas should be applied immediately before kinetic screening experiments. This could be coupled with a pre-conditioning treatment of the sorbent (such as establishing the desired temperature and driving off any CO_2 already adsorbed). Further insight into the relative importance of particle-particle and particle-wall interactive effects can still be gained. It is clear that wall effects have a significant impact on the pressure overshoot for the fresh material (not pre-fluidised), which increases as the bed diameter decreases and/or as the static bed height increases (Figure 4.2a). As explained, this is due to the frictional resistance created across the contact area between the particles and wall. However, in Figure 4.2b, the pressure overshoot is hardly affected by the diameter static bed height when the bed is pre-fluidised. This suggests that the cohesive forces inherent to the particle (mainly capillary-bridges) rather than particle-sidewall friction is the dominant factor.

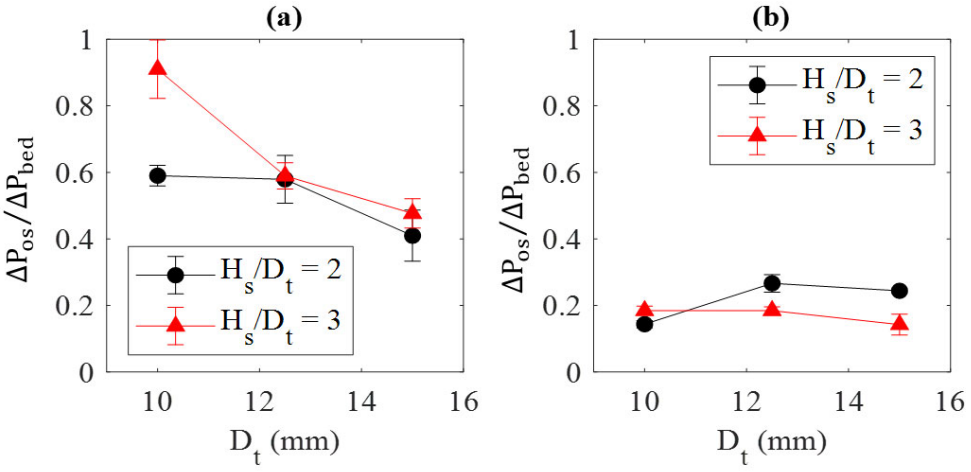

Figure 4.2. Normalised pressure drop overshoot for pre-sieved hydrotalcite as a function of different treatments; (a) pre-sieved particles were fluidised without any prior conditioning, (b) pre-sieved particles were pre-fluidised for 2 minutes at a gas velocity of 40 mm/s.

4.2.2.2 Effect of Adding Secondary Particle

Next, the effects of adding a secondary particle to the hydrotalcite were examined. Figure 4.3 shows the pressure drop profiles recorded for (a) raw as-supplied hydrotalcite powder mixed

with silica (in 1:1 ratio), (b) pure pre-sieved hydrotalcite, (c, d) mixture of pre-sieved hydrotalcite and silica (in ratios of 2:1 and 1:2), and (e) pure silica. Figure 4.4 then shows the normalised pressure overshoot $\Delta P_{os}/\Delta P_{bed}$ parameter plotted against the fraction of hydrotalcite in the mixture.

Figure 4.3a shows a slight improvement in the fluidisation quality compared to the raw hydrotalcite (Zhang *et al.*, 2021a). However, the pressure drop being lower than the predicted buoyant weight still implies that portions of the bed remained unfluidised. In contrast, Figure 4.3b–d show that the mixtures of pre-sieved hydrotalcite and silica did reach the buoyant weight and were thus entirely fluidised. Comparing Figure 4.3b–d, the pressure drop in the fluidised bed regime increased as the amount of silica in the mixture increased. Here the pressure drop increased by 125% from 150 Pa for the pure hydrotalcite to 337 Pa for the pure silica. The silica has a density of 2.65 g/cm^3 compared to the hydrotalcite's density of 2 g/cm^3. Additionally, both sets of particles produce different void fractions. The voidage of the pure pre-sieved hydrotalcite and pure silica can be calculated using Equation 1 (McDonough *et al.*, 2019). Where V_p, V_t , m, A and H are particle volume, total volume of the bed (including voids), total mass of the particle bed, cross-sectional area of the column and static bed height respectively. The measured void fractions for the hydrotalcite and silica were ε = 0.68 and ε = 0.44 respectively. By using these densities and void fractions, Equation 2 predicts a pressure drop increase of 132% when switching from pure hydrotalcite to pure silica, slightly higher than the experimental measurement.

$$\varepsilon = \frac{V_t - V_p}{V_t} = \frac{HA - \frac{m}{\rho_p}}{HA} \tag{2}$$

Differences between theoretical and experimental pressure drop have been observed when changing the bed material. For instance,. Vanni *et al.* (2015) report a larger difference for glass walls than for stainless steel walls. Additionally, particle properties (such as density, diameter, voidage, and cohesiveness) and wall effects are known to influence the pressure drop. In this study, the slight increase of experimental pressure drop is likely caused by the 'stickiness' of the hydrotalcite; the hydrotalcite was more prone to sticking to the walls than the silica, reducing the amount of material being suspended by the fluidising gas. Future studies could address this by refining or optimising the design of the 3D-printed MFBRs, since the pressure

drop is influenced by a combination of wall-effects (combination of particle properties and small bed diameter) and manufacturing method (Guo *et al.*, 2009; Vanni *et al.*, 2015).

Figure 4.3 shows that increasing the amount of silica in the mixture decreases the magnitude of the pressure overshoot for both the raw and pre-sieved hydrotalcite. Similar to the pre-fluidisation experiments, Figure 4.4 implies that the Geldart C characteristics dominate the fluidisation quality. This is because the bed diameter and static bed height were kept constant in these experiments, meaning the same surface area and, therefore, the same magnitude of wall effects are to be expected for each set of mixtures. The cohesive nature of the hydrotalcite leads to enhanced friction within the particles and between the particles and the sidewalls (Landi *et al.*, 2011). The incorporation of the larger secondary particle reduces the strength of the particle-particle and particle-wall interactions (Zhou and Zhu, 2021). Similar findings are reported for a fine Geldart A alumina powder, where an increasing proportion of fines in the bed led to increased importance of the interparticle forces compared to hydrodynamic forces (Bruni *et al.*, 2007). Thus, the more pronounced change of pressure overshoot for the raw hydrotalcite is likely a consequence of the stronger interparticle forces due to the presence of more fines.

Two different mechanisms have been proposed in the literature that could explain the mixing characteristics of the Geldart C hydrotalcite powder with the Geldart A silica particles. In case 1, the larger Geldart A particles act as spacers, which reduces the magnitude of the cohesive forces between the hydrotalcite particles (Visser, 1989). In case 2, the smaller Geldart C particles adhere to the larger Geldart A particles acting as bridges that then increases cohesion of the silica (Visser, 1989). Based on the results in Figure 4.3and 4.4, Case 1 is the likely scenario for experiment's hydrotalcite-silica mixture, since the effects of cohesion appear to diminish as the fraction of silica increases. Thus, for kinetic screening experiments the use of a secondary particle may be beneficial to disrupt particle-particle interactions, which will minimise the micro-fluidisation behaviour and promote more scalable macro-fluidisation behaviour.

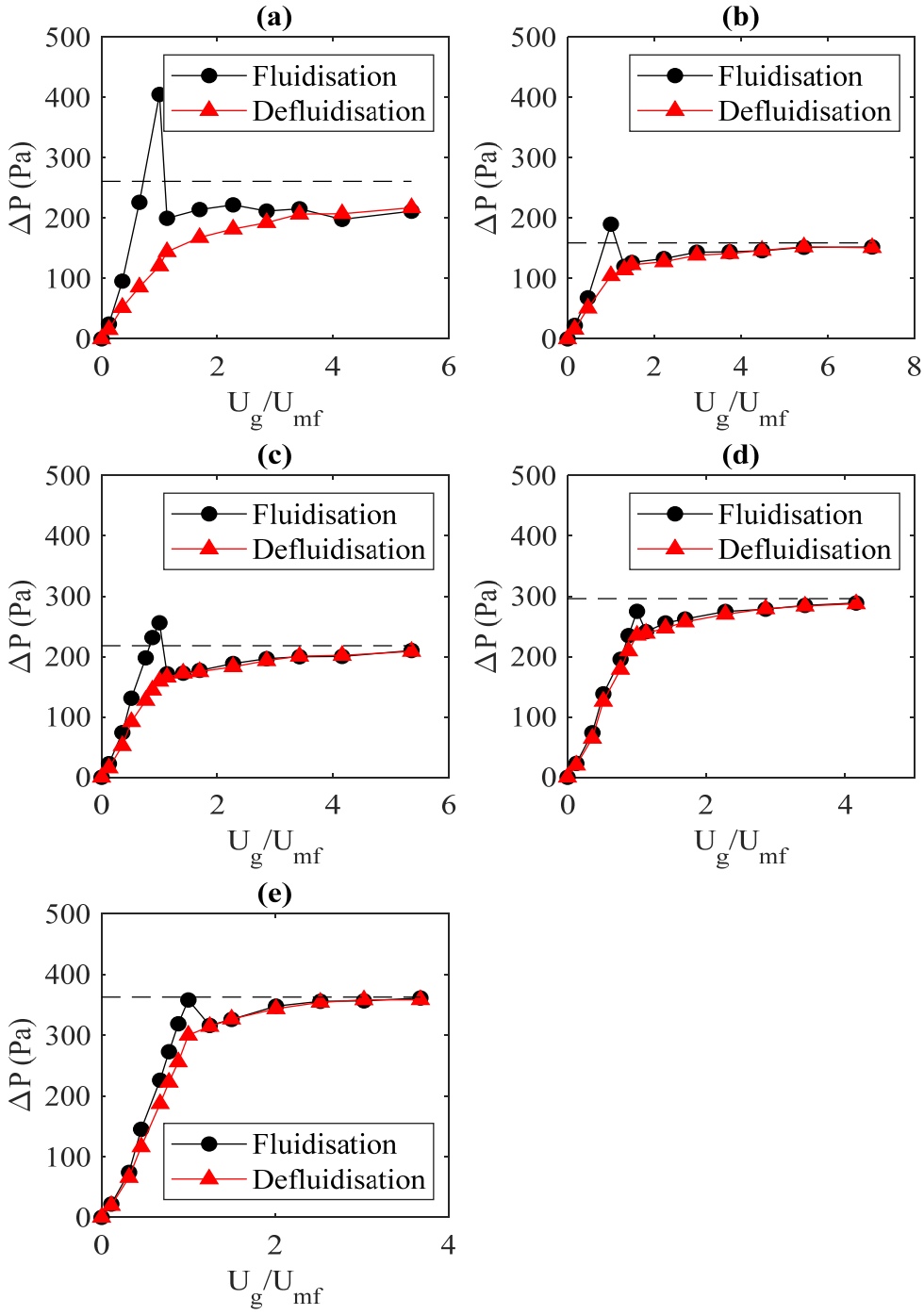

Figure 4.3. Pressure drop profiles during fluidisation and defluidisation experiments, D_t=12.5 mm, H_s/D_t = 2; (a) raw as-supplied hydrotalcite powder mixed with silica in 1:1 ratio, (b) 100% hydrotalcite (pre-sieved), (c) 67% hydrotalcite and 33% silica, (d) 33% hydrotalcite and 67% silica, and (e) 100% silica.

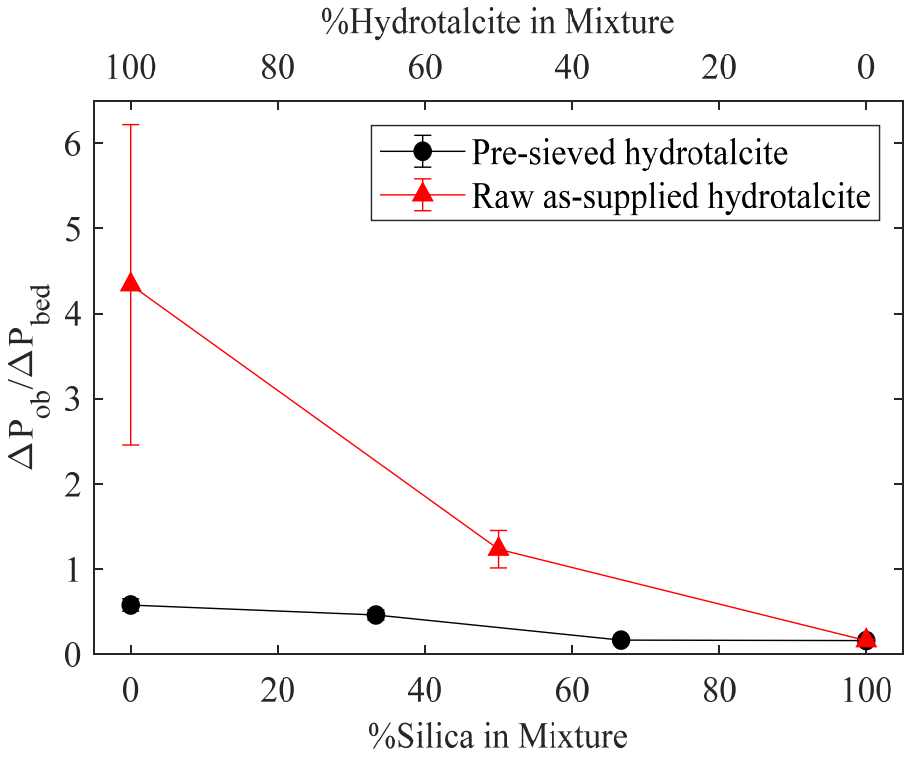

Figure 4.4. Normalised pressure overshoot as a function of % hydrotalcite in the mixture (D_t=12.5 mm, H_s/D_t = 2.

Table 4.1 demonstrates the variation in pressure overshoot and pressure drop after using different methods of treatment. The raw powder clearly demonstrated poor fluidisation quality since the experimental pressure drop (exp) was significantly lower than the predicted buoyant weight (theory) by approximately two thirds. This indicates that portions of the bed remain unfluidised owing to dominant particle-particle cohesive forces. Pre-sieving improves the fluidisation quality, where the measured pressure drop is close to the buoyant weight of the particles (96%), indicating nearly all of the bed is fluidised. The pressure overshoot is significantly reduced after the combination of pre-sieving and pre-treatment (either pre-fluidisation or mixing with larger particles), which is attributable to reducing wall effects and cohesive/adhesive forces. Pre-fluidisation significantly enhanced the fluidisation quality overall. This may be relevant to removing liquid bridges. Furthermore, it is clear that mixing pre-sieved hydrotalcite powder with a secondary *Geldart A* particle leads to reduced pressure overshoot and increased pressure drop that indicates fluidisation is improved overall.

Table 4.1. Pressure drop overshoot and drop for pure and pre-sieved hydrotalcite as a function of different treatments.

Pre-treatment	$\frac{\Delta P_{os}}{\Delta P_{bed}}$	$\frac{\Delta P_{bed\ exp}}{\Delta P_{bed\ ther}}$
Raw materials, as supplied	4.34	0.35
Raw as-supplied hydrotalcite powder mixed with silica in 1:1 ratio	1.23	0.79
Pre-sieved particles were fluidised without any prior conditioning	0.59	0.94
Pre-sieved particles were pre-fluidised for 2 minutes at a gas velocity of 40 mm/s	0.26	0.95
Pre-sieved hydrotalcite powder mixed with silica in 2:1 ratio	0.46	0.95
Pre-sieved hydrotalcite powder mixed with silica in 1:2 ratio	0.16	0.96

Whilst the additional use of a secondary material might improve the macro-fluidisation behaviour, ultimately the goal of this research is kinetic screening. It is probable that this secondary material will not be entirely inert to the screening reactions of interest, and therefore will contaminate the kinetics results, making predictions more difficult. Therefore, to fluidise the Geldart C hydrotalcite sorbent (and similar Geldart C powders), pre-sieving and pre-fluidisation were recommended.

4.2.3 Flow Regimes

4.2.3.1 Minimum Fluidisation Velocity

Table 4.2 summarises the experimentally observed minimum fluidisation velocities for the sieved hydrotalcite powder. It can be seen that U_{mf} increases as the static bed height increases and as the bed diameter decreases. This is attributed to aforementioned wall effects, since the same material was fluidised at each condition. Wall effects become more significant at smaller diameters because of the increased surface area to volume ratio; a greater proportion of the bed

is in close proximity to the wall, enhancing the significance of friction relative to the fluidising gas energy (Liu *et al.*, 2008; Han *et al.*, 2021; Shen *et al.*, 2021). Table 4.2 shows a good agreement between the experimental values of U_{mf} obtained in this work and the predictions of the correlation in Equation3 (Guo *et al.*, 2009; Zhipeng Qie 2022). This implies that the minimum fluidisation velocity was influenced by the particle properties, bed geometry, and voidage (Wang *et al.*, 2017; Shi *et al.*, 2021), which is consistent with previous studies (Chladek *et al.*, 2018; Bérard *et al.*, 2021; Shen *et al.*, 2021).

$$U_{mf} = \left[\frac{H_s}{d_p} exp\left(-6.312 + \frac{242.272}{D_t/d_p}\right) + 1\right] \frac{(7.169 \times 10^{-4}) {d_p}^{1.82} \left(\rho_p - \rho_g\right)^{0.94} g}{{\rho_g}^{0.06}\, {\mu_g}^{0.88}} \quad (3)$$

$$\frac{\Delta P}{H} = 150 \frac{\mu_g U_g (1-\varepsilon)^2}{d_p^2 \varepsilon^3} + 1.75 \frac{(1-\varepsilon)}{\varepsilon^3} \frac{\rho_g U_g^2}{d_p} \quad (Ergun\ Equation) (4)$$

$$\Delta P = (1-\varepsilon)\left(\rho_p - \rho_g\right) g H \quad (5)$$

Table 4.2. Experimental vs predicted minimum fluidisation velocities, $U_{mf,}$, of pure sieved hydrotalcite powder (53–90 µm).

D_t (mm)	H_s/D_t	$U_{mf,exp}$ (mm/s)	$U_{mf,Eq.3}$ (mm/s)	$\frac{U_{mf,Eq.3}}{U_{mf,exp}}$	$U_{mf,Ergun}$ (mm/s)
10	1	12.9	13.8	1.07	4.5
	2	15.3	16.2	1.06	4.5
	3	21.3	22.2	1.04	4.5
12.5	1	9.8	9.3	0.95	4.5
	2	14.5	14.6	1.01	4.5
	3	18.2	19.9	1.09	4.5
15	1	10.1	9.0	0.89	4.5
	2	14.9	14.0	0.94	4.5
	3	16.8	17.7	1.06	4.5

Additionally, it is also possible to predict the minimum fluidisation velocity using the Ergun equation (Equation 4) by equating it to the pressure drop associated with the buoyant particle weight (Equation 5) and solving for U_g. The resulting equation is independent of the bed geometry (D_t and H_s), and instead only depends on the particle and gas properties (d_p, ρ_p, ρ_g, ε). However, Table 4.2 shows that the experimental values of U_{mf} are significantly larger (2 to 4 times) than the value predicted from the Ergun equation. This is again a sign that wall effects and cohesion were influencing the hydrodynamics.

4.2.3.2 Bubbling Velocity

The standard deviation of the pressure signal is commonly used to distinguish flow regimes in gas-solid fluidised beds. The standard deviation is typically zero in the packed bed regime because the particles are fixed. Then as bubbles begin to form, small corresponding pressure fluctuations appear that grow in intensity as the gas velocity (and bubble size) increase (McDonough *et al.*, 2019). Numerous dynamic effects occur in the bubbling regime, such as bubble collisions, bubble coalescence, and bubble splitting. As the gas velocity increases, bubble coalescence tends to dominate leading to the transition from bubbling to slugging fluidisation. This is an undesirable state since significant gas bypassing occurs. With further increases in the gas velocity, eventually bubble splitting starts to dominate since coalescence is eventually restricted by the diameter of the bed. At this point, the mean bubble size begins to decrease with rising superficial gas velocity, which is defined as the onset of turbulent fluidisation.

Figure 4.5 shows an example of the standard deviation of the pressure drop, $\sigma_{\Delta P}$, for the sieved hydrotalcite powder as a function of superficial gas velocity. It can be seen that $\sigma_{\Delta P}$ initially remained approximately zero at small gas velocities. Thereafter, $\sigma_{\Delta P}$ increased as bubbles started to emerge from the distributor plate and rise upwards, indicating that the regime transitioned from fixed bed to bubbling. As mentioned above, bubbling eventually transitions to slugging due to bubble coalescence. However, it is difficult to define slugging using the $\sigma_{\Delta P}$ criteria alone since there is usually no definitive threshold for distinguishing bubbling from slugging (McDonough *et al.*, 2019). In the present study, it was also not possible to observe a peak/maximum in the $\sigma_{\Delta P}$ data, indicating that the turbulent regime was not reached in any of the experiments.

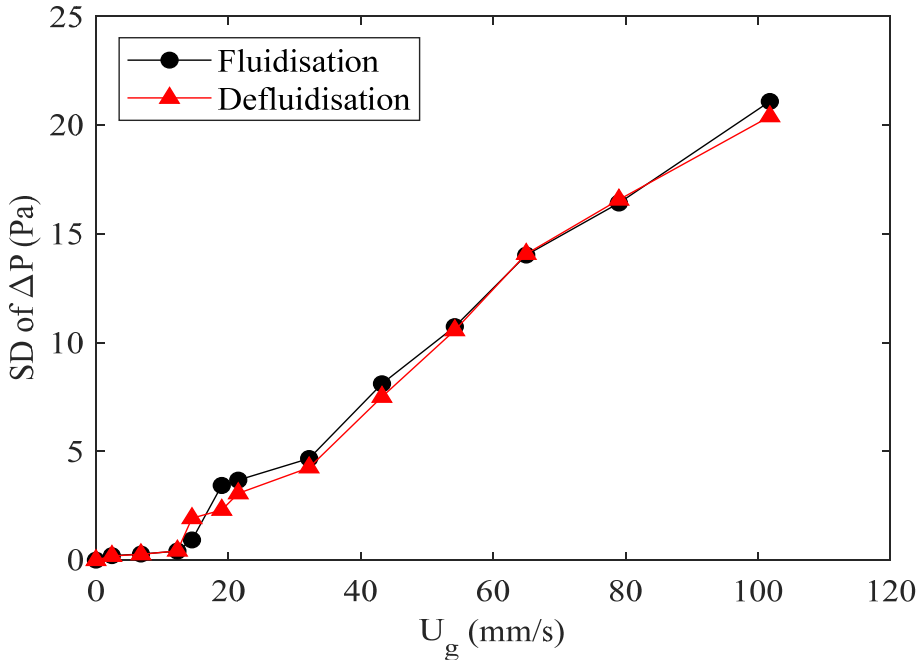

Figure 4.5. Standard deviation of the pressure drop vs superficial gas velocity using sieved hydrotalcite powder (particles diameters of 53–90µm); D_t = 12.5 mm, H_s/D_t= 2.

Table 4.3 summarises the experimentally observed minimum bubbling velocities for the sieved hydrotalcite powder (obtained by considering the standard deviation of the pressure drop as discussed above). The minimum bubbling velocity can also be predicted from the minimum fluidisation velocity using the empirical correlation shown in Equation 6 (Han *et al.*, 2021). As shown in Table 3, the predicted values are again in close agreement with the experimental values across all bed diameters and bed heights considered. Moreover, the final column in Table 4.3 shows that U_{mb} was approximately the same as U_{mf} for the smallest bed diameter, but u_{mb} was slightly larger than U_{mf} for bed diameters of D_t = 12.5 and 15 mm. This suggests the presence of a narrow particulate regime when the bed height is small (H_s/D_t = 1).

$$\frac{U_{mb}}{U_{mf}} = 1.099 - 5.21\frac{H_s}{D_t}\left[exp\left(\frac{0.7}{D_t/d_p}\right) - 1\right] \quad (6)$$

Table 4.3. Experimental vs predicted minimum bubbling velocities, U_{mb}, of pure sieved hydrotalcite powder (53–90 µm).

D_t (mm)	H_s/D_t	$U_{mb,exp}$ (mm/s)	$U_{mb,Eq.4}$ (mm/s)	$U_{mf,exp}$ (mm/s)	$\frac{U_{mb,exp}}{U_{mf,exp}}$
10	1	12.9	13.8	12.9	1.00
	2	15.3	16.0	15.3	1.00
	3	22.1	22.6	21.3	1.03
12.5	1	11.7	12.6	9.8	1.19
	2	14.5	15.3	14.5	1.00
	3	18.9	18.9	18.2	1.00
15	1	11.6	12.5	10.1	1.15
	2	14.9	15.9	14.9	1.00
	3	18.6	19.5	18.6	1.00

4.2.3.3 Slugging Fluidisation

Increasing the gas velocity causes gas bubbles to grow because coalescence processes tend to dominate bubble splitting ones. Eventually, the gas bubbles will be large enough that they completely fill the cross-section of the bed. This is sometimes considered to be the onset of slugging (Kong *et al.*, 2017). This regime corresponds to reduced gas-solid contact, decreased gas residence time, and reduced heat and mass transfer rate. Together these all contribute to poor CO_2 capture performance (Jaiboon *et al.*, 2013), and would be detrimental for material development studies in MFBRs. Generally, bed heights of at least $H_s/D_t \geq 2$ are needed for slugs to fully develop (Cornelius Emeka Agu, 2017). However, it is often difficult to formally identify the onset of slugging, since there is no obvious threshold between what constitutes a bubble and what constitutes a slug.

A common method to determine the minimum slugging velocity in the literature is simple visual observation, typically involving subjective judgement. For example, slugging has been identified as the point where bubbles emerge from the top of the particle bed with a diameter of $D_b \approx 0.6D_t$ (D.Geldart, 1974). Alternatively, according to Leva (1951) slugging corresponds to where the pressure variations are approximately 5–10 % of the average pressure drop Kong *et al.* (2017) used the same definition. However, more sophisticated methods have since been proposed. For example, Geldart defined slugging as the point where the bubbling frequency becomes independent of the gas flow rate (D.Geldart, 1974). This is based on the hypothesis that once the bubble diameter reaches the size of the column, it can no longer continue to grow, and therefore the rise velocity of the bubble depends only on the column size. Alternatively, frequency domain analysis can also be used to analyse slugging behaviour by identifying dominant frequencies relating to bubble coalescence and break-up processes. McDonough *et al.* (2019) combined the frequency spectra methods of Mehrani *et al.* (2005) and Jaiboon *et al.* (2013), together with the stagnating bubbling frequencies of D.Geldart (1974) and D. G. Dimattia (1997) to identify the onset of slugging. This method has the advantage of removing all subjectivity, this approach was adopted in the present investigation. Figure 4.6 plots the frequency spectra of the time-domain pressure drop signal for each gas flow rate recorded. A cubic interpolation was used to fill in the full frequency spectra map whilst the colour intensity was normalised between 0 and 1 to aid visual clarity. Here, deep blue indicates low probability intensity and yellow represents high probability intensity; that is to say, yellow corresponds to where dominant frequencies were observed. The three frequency spectra map in Figure 4.6 correspond to the 10 mm, 12.5 mm, and 15 mm diameter MFBR containing pre-sieved hydrotalcite (D_p= 53–90 m) with H_s/D_t = 3.

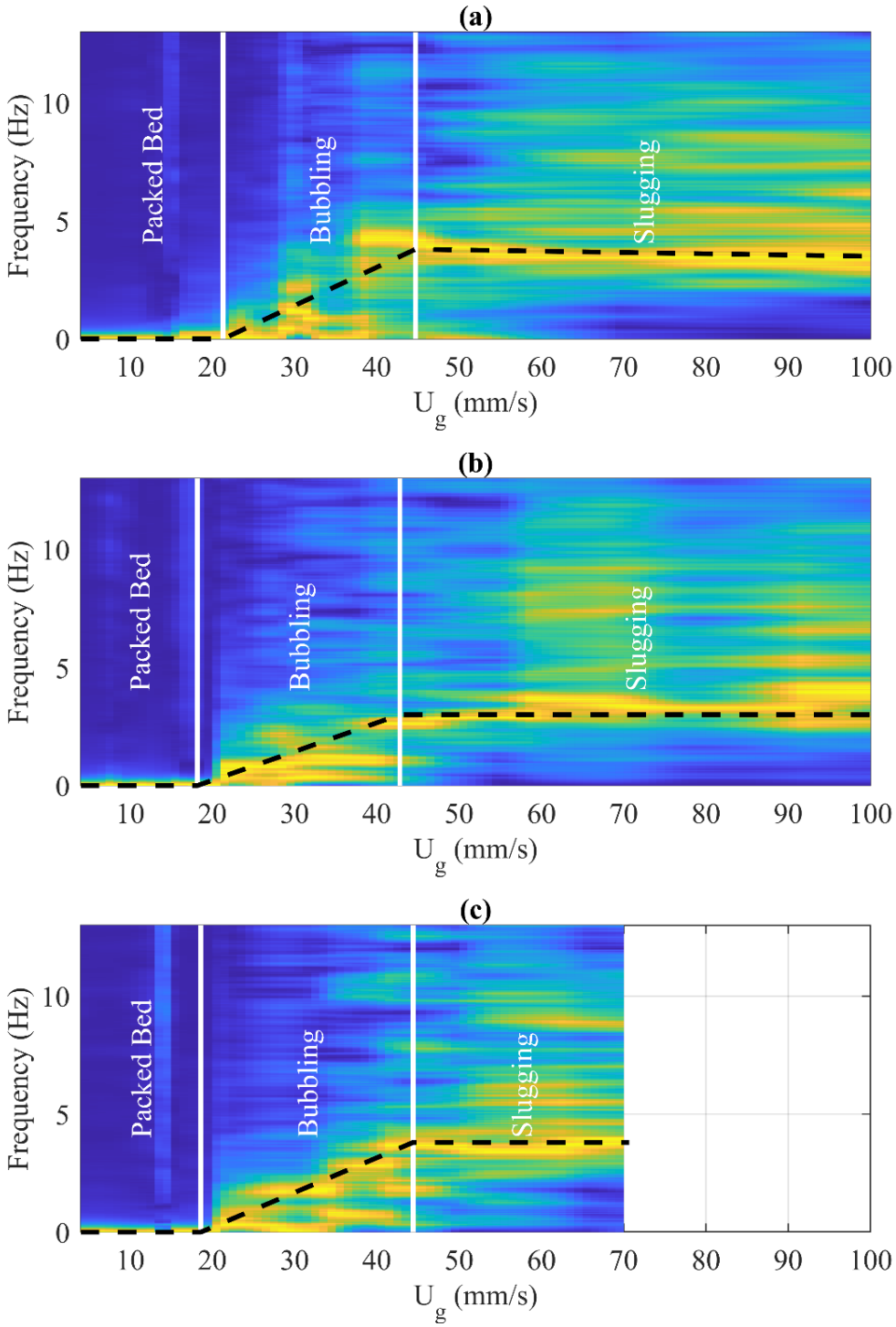

Figure 4.6. Progression of the frequency spectra of the pressure drop signal as gas velocity increases; pre-sieved hydrotalcite powder (particles diameters of 53–90µm), H_s / D_t= 3; (a) D_t = 10 mm, (b) D_t = 12.5 mm, (c) D_t= 15 mm.

Due to a lack of any gas bubbles or other structures, the packed bed regime was characterised in all bed designs by a featureless frequency domain, as indicated by the constant deep blue colour in the maps shown in Figure 4.6. Following the minimum bubbling velocity (superimposed on Figure 4.6 for clarity), oscillations were observed in the time-domain pressure drop signal that manifested as a broad frequency spectrum in Figure 4.6. According to Baeyens and Geldart (1974), the onset of slugging can be defined as the point at which the dominant frequency flatlines. McDonough *et al.* (2019) subsequently used this definition with the frequency spectra maps of the type shown above to formally identify the minimum slugging velocity U_{ms}. The same technique was applied in this study. A point can be clearly identified for all bed diameters where the dominant frequency (intense yellow colour) reaches a steady state, which can be defined as U_{ms}. Note, the dashed lines have been added to aid visualisation of the development of the dominant frequency as the gas flow rate increased.

Using these values of U_{ms}, it is then possible to define the following simple flow regime maps for the MFBR containing cohesive hydrotalcite powder (Figure 4.7). However. this flow regime map is only applicable for the specific adsorbent and bed combinations used in this study, which will likely differ in other cases. To normalise the x-axis, the average particle diameter for the hydrotalcite was used ($\overline{d_p}$ = 71.5 μm). The transition velocities are almost unaffected as the ratio of D_t/d_p increases. This behaviour differs to that of larger scale fluidised beds where U_{ms} normally increases as the bed diameter increases (Wang and Fan, 2011). This is also attributable to the wall effects produced in MFBRs. Overall, each bed diameter offers a broader range of bubble regimes when H_s/D_t = 2, which may be beneficial for kinetics screening experiments. For H_s/D_t = 3, the range of gas velocities for bubbling becomes narrower, suggesting there might be an upper limit for the amount of material that can be screened in these particular 3D-printed beds. Adding too much material compresses the bubble regime, restricting the assessment of the underlying kinetics to a narrow range.

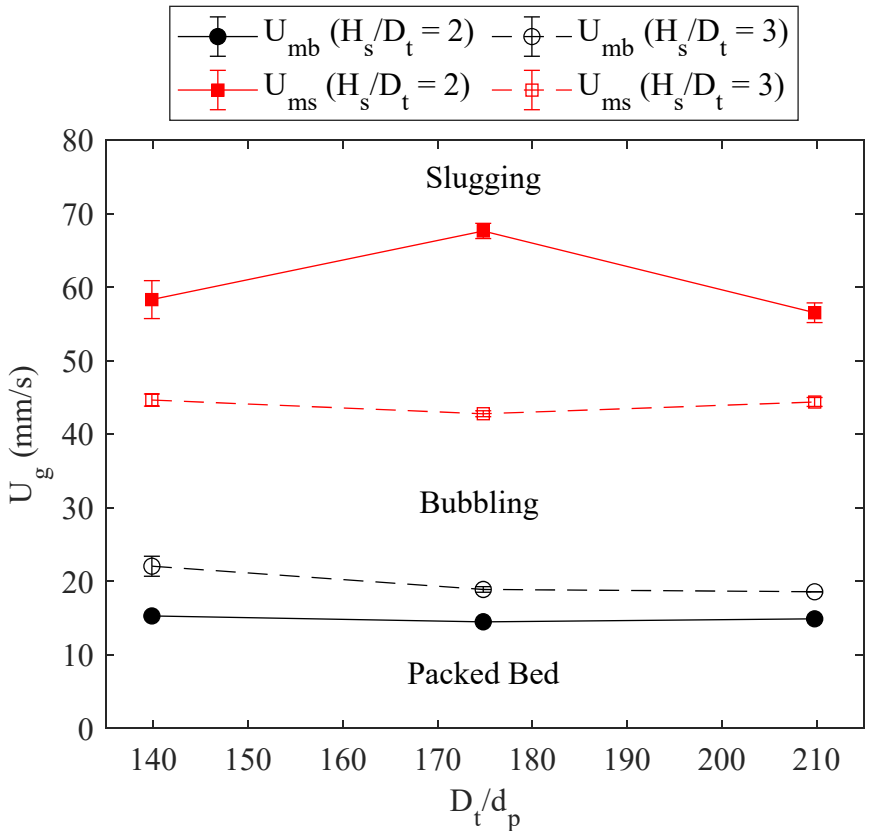

Figure 4.7. Effect of bed diameter to particle diameter ratio (D_t / d_p) and static bed height to diameter ratio (H_s / D_t) on the flow regimes in 3D-printed MFBRs containing cohesive hydrotalcite powder.

4.3 Summary

Hydrodynamic characteristics of gas-solid fluidisation were investigated in 3D-printed MFBRs containing Geldart C hydrotalcite powder to find suitable conditions for kinetic screening experiments. Initially, the observation, the raw powder exhibited poor fluidisation quality, where parts of the bed remained unfluidised due to dominant particle-particle cohesive forces. The most straightforward remedy was to sieve the particles to remove the fines (retaining sizes of >53 µm; density of 2 g/cm^3), drastically improving the fluidisation quality. Another observation was that wall effects and cohesive/adhesive forces significantly impact the hydrodynamic performance of the MFBR, including delayed onset of fluidisation, the appearance of a large pressure drop overshoot prior to fluidisation, and delayed onset of bubbling. Analysis of the pressure overshoot provided insight into the hysteresis behaviour that

is commonly observed in micro-fluidisation experiments. The belief here was that liquid bridges form in the bed by absorbing humidity from the atmosphere over time. This suggests that particle-particle forces rather than wall effects are the dominant factor influencing fluidisation quality. Through subsequent analysis of wall effects by considering the ratio of pressure overshoot to buoyant weight, pre-fluidisation was identified as drastically improving the fluidisation quality, which may remove liquid bridges. Alternatively, a secondary Geldart A particle may be added to the hydrotalcite powder to create a mixture that reduces the micro-fluidisation characteristics. However, the acknowledgment here is that this would be potentially problematic for using the screened kinetic models for design purposes (especially if the secondary particle is not truly inert to the reaction of interest).

In general, the bubbling regime is favoured for its advantages, including uniform fluidisation, stability, enhanced mass transfer, and optimal mixing. These characteristics make it suitable for various industrial processes, ensuring effective mass transfer and efficient mixing. In these experiments, the bubbling regime $\leq 4\ U_{mf}$ for $H_s/D_t = 2$, and $\leq 3\ U_{mf}$ for $H_s/D_t = 3$, respectively. When the bed is in a bubbling regime, gas bubbles rise through the particles and make excellent contact with the solid sorbent, facilitating efficient mixing and improving carbon capture efficiency. This can be accomplished by controlling the gas velocity, bed height, and particulate size. This can be accomplished by controlling the particle size, gas velocity, bed diameter, and bed height.

Chapter 5. Adsorption Kinetics

5.1 Introduction

In the previous chapter, the hydrodynamic properties of gas–solid fluidisation in 3D-printed MFBRs including Geldart C hydrotalcite powder were investigated to determine appropriate conditions for carbon capture kinetic screening tests. In this chapter, adsorption kinetics screening experiments were performed in batch mode (with respect to the hydrotalcite) within a micro-fluidised bed at suitable conditions identified in the hydrodynamic investigations. This ensures that the basic adsorption kinetics were studied under optimal conditions, namely, the bubbling regime (efficient gas/ particles mixing). Identifying this fluidisation regime relied on different parameters, including the bed diameter, bed height, and particle size. The breakthrough experiments aim to determine how the CO_2 concentration, temperature, and gas flow rate (and/or gas velocity) affect the adsorption kinetics and material capacity.

5.2 Breakthrough and Adsorption Experiments

Breakthrough experiments used the best possible operation conditions (bubbling regime) determined by the hydrodynamic experiments. For example, superficial gas velocities less than the U_{mf} were not investigated because these correspond to a packed bed where mixing is the rate determining step. Whereas high gas velocities where the slugging regime occurs were considered to evaluate the effect on adsorption process performance. Under the slugging condition, it is expected that the majority of the CO_2 will bypass the solid phase leading to degradation in adsorption performance. The full set of operating conditions considered are summarised in Table 5.1. Each condition was repeated three times to calculate a mean value and corresponding error range to provide validation of the trends.

Based on observations made during the hydrodynamic study, N_2 gas was initially used as a purge gas for several minutes at a rate of 2.5 U_{mf} to pre-fluidise and condition the bed. This ensured the removal of any moisture/ humidity from the bed to reduce inter-particle cohesion forces, as mentioned in the previous chapter. This approach has been combined with a sorbent pre-conditioning step, which involves subjecting the desired quantity of sorbent to high temperatures (90 °C) in a vacuum oven for several minutes to remove any residual carbon dioxide (CO_2) and moisture and prepare the sorbent.

Table 5.1. The operation conditions of the experiments.

ID	Bed loading (H_s/D_t)	Temp.(°C)	CO_2 conc. (% vol)	U_g/U_{mf}
1	2	25 °C	8%	1.5
2				2
3				3
4				4
5				5
6				6
7			12%	1.5
8				2
9				3
10				4
11				5
12				6
13			16%	1.5
14				2
15				3
16				4
17				5
18				6
19		40 °C	8%	1.5
20				2
21				3
22				4
23				5
24				6
25			16%	1.5
26				2
27				3
28				4
29				5
30				6
31		60 °C	8%	1.5
32				2
33				3
34				4
35				5
36				6
37			16%	1.5
38				2
39				3
40				4
41				5
42				6
43	3	25 °C	8%	1.5
44				2
45				3
46				4

Figure 5.1 shows an example of a breakthrough curve recorded at 40°C, 16 vol% CO_2 and $U_g = 4U_{mf}$. Here the Y-axis is represented as non-dimensional concentration C/C_0, where C_0 corresponds to the CO_2 in the feed. Two breakthrough curves were recorded for inert glass particles and for the hydrotalcite sample at each condition. The curve for the glass particles contained information about the CO_2 diffusion through the rig, whilst the curve for the hydrotalcite samples contained information about the kinetics and the CO_2 diffusion characteristics. Subtraction of the inert signal from the hydrotalcite signal enabled recovery of the CO_2 uptake response, as shown in Figure 5.2. The study of this curve, as described in more detail in the methods chapter, enabled the measurement of the physisorption and chemisorption characteristics and interactions. A breakthrough time could also be defined: $\Delta\tau = (\tau_{95} - \tau_{05})$, where τ_{95} is the time needed for the measured outlet concentration to reach 95% of the final value, and τ_{05} is the time needed for the measured outlet concentration to reach 5% of the final value (Jamei *et al.*, 2023).

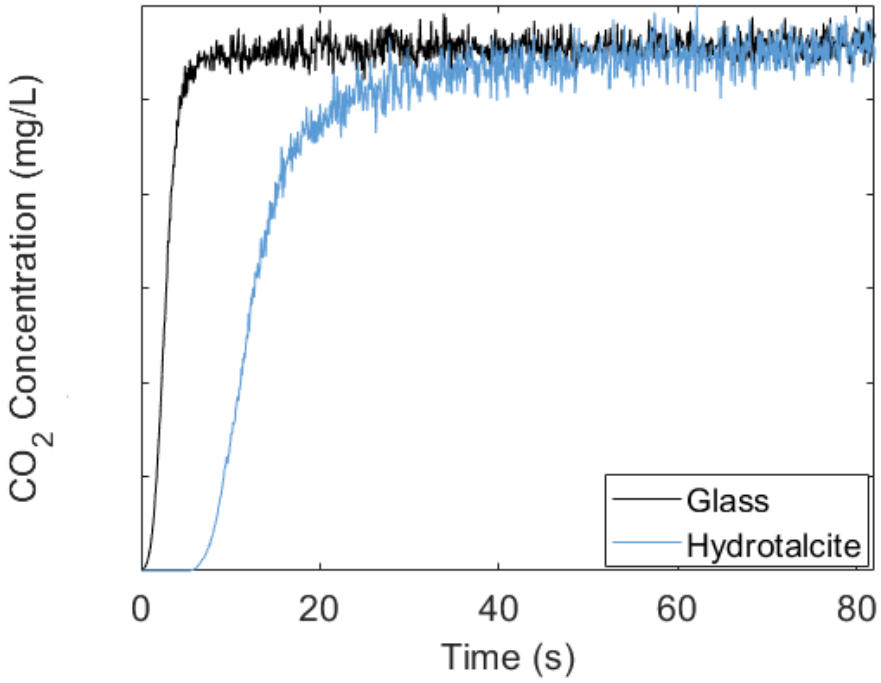

Figure 5.1. The breakthrough curves for the hydrotalcite adsorbent and inert (glass) without dead time for the feed concentration of 16 % CO_2 performed at the fluidising velocity of 4 U_{mf} and 40°C.

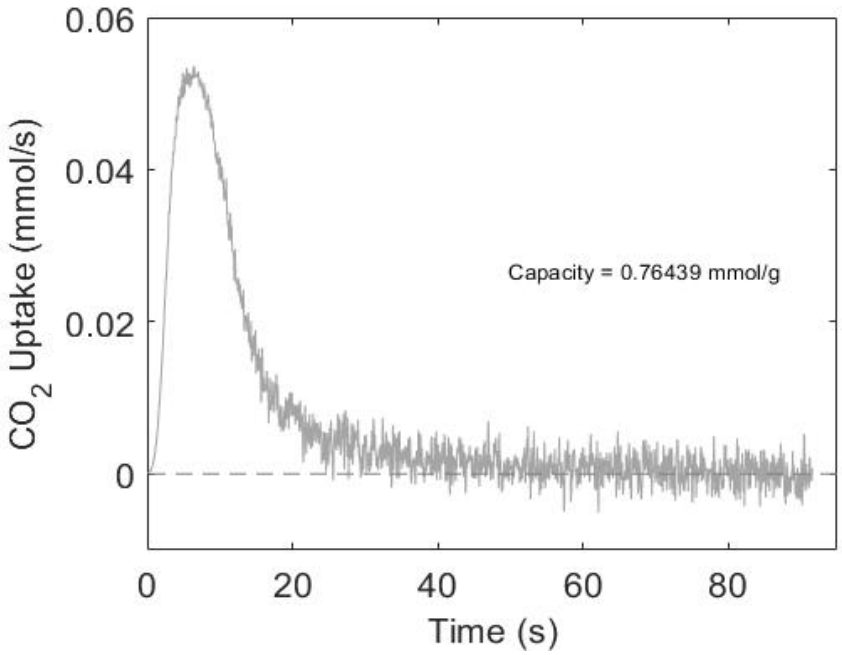

Figure 5.2. The CO_2 uptake curve for the feed concentration of 16 % CO_2 performed in the MFB at the velocity of 4 U_{mf} and temperature of 40 °C.

The shape of the BT curve changes due to a combination of kinetic effects (*e.g.* limited resistance to mass transfer may include mass transfer inside the sorbent, mass transfer across the boundary layer around the sorbent, and mass transfer in the bed itself) and hydrodynamic effects (*e.g.* axial dispersion) (Wilkins *et al.*, 2021; Girimonte *et al.*, 2022). The breakthrough time and curve are also influenced by the CO_2 concentration, superficial gas velocity, adsorption temperature, and bed loading. A rapid adsorption rate is preferable because it allows for more efficient use of the adsorbent and reduces the amount of energy needed for regeneration (Knox *et al.*, 2016b). Changes in operational conditions, such as the CO_2 feed concentration, are needed to understand how CO_2 moves through the adsorbent from the gas to the adsorbed phase. These mechanisms include surface diffusion and mass-transfer resistance (both micro- and macro-pore resistances). In analysing the mass transfer properties of CO_2 capture Sabouni *et al.* (2013); Girimonte *et al.* (2017) observed that the configuration of the breakthrough curve was influenced by the mass transfer coefficient, a parameter controlled by several factors, such as the gas concentration and flow rate.

Their investigations provide evidence that kinetic phenomena, such as limitations in mass transport, may influence the form of the breakthrough curve within fluidised bed systems. This investigation relied on the optimal factors and conditions found in the hydrodynamic study chapter, particularly the superficial gas velocity.

5.3 CO_2 Breakthrough Results

The hydrotalcite adsorption capacity has been examined as a function of various superficial gas velocities (1.5–6 U_{mf}), temperatures (25 °C, 40 °C and 60 °C), and feed CO_2 concentration (8 vol%–16 vol%). The results show that the CO_2 adsorption capacity increases as the gas velocity increases in the bubbling regime before, decreasing again in the slugging regime. According to Figure 5.5, the maximum adsorption capacity occurs at a gas velocity of 4 U_{mf} in all experiments where H_s/D_t = 2. This result highlights the importance of screening the hydrodynamic behaviour before evaluating the adsorption kinetics; the bed must be operated away from a mass transfer limited state.

Table 5.2 shows the capacities measured using TGA at the same conditions as obtained at 4 U_{mf}, performed by the Research Centre for Carbon Solutions, Heriot-Watt University, Edinburgh (UK). In Figure 5.5a–b, the adsorption capacity peaks at 40 °C (at both 8 vol% and 16 vol% CO_2), and this same pattern is present in the TGA results. It will be discussed in more detail in the subsequent sections**.**

Table 5.2. Adsorption capacities measured using TGA performed by the Research Centre for Carbon Solutions.

CO_2 Conc. (vol%)	Capacity at 25 °C (mmol/g)	Capacity at 40 °C (mmol/g)	Capacity at 60 °C (mmol/g)
16	0.551	0.752	0.672
12	0.564	0.732	0.659
8	0.450	0.710	0.642

5.3.1 Effect of Feed CO_2 Concentration

Changing the CO_2 feed concentration was necessary to elucidate the transport behaviour of the adsorbate from the gas to the solid phase. This enabled comparing the relative importance of mass-transfer resistances (both micropore and macropore) and surface diffusion, which are critical in determining the appropriate concentration range for a certain sorbent and its suitability for carbon capture from different real-world sources. Three feed CO_2 concentrations of $8\ vol\%$, $12\ vol\%$, and $16\ vol\%$ were subsequently used to investigate the influence of CO_2 concentration on the adsorption process. These concentrations were used to comprehend the sorbent material's efficiency and technology through real-world scenarios, assuring applicability to various emissions sources and assessing operational conditions and adsorbent properties.

Here the 10 mm diameter bed was used which was filled with 0.85 g of the hydrotalcite matches with $H_S = 2\ D_t$,This quantity was chosen to minimise the amount of solid sorbent required for screening, as only small amounts are produced during the early stages of sorbent development, while ensuring sufficient material was available for detecting significant reaction kinetics in the CO_2 breakthrough tests. Additionally, the effect of concentration was studied at three operating temperatures (25 °C, 40 °C, and 60 °C) across a range of gas velocities to identify whether there were any interaction effects.

Figure 5.3a, 5.4a, and 5.5c show the impact of changing the CO_2 concentration on the breakthrough curve, breakthrough time ($\Delta\tau$) and adsorption capacity respectively. When the concentration increased from $8\ to\ 16\ vol\%$ CO_2, the hydrotalcite breakthrough quicker indicated by the CO_2 breakthrough point shifting to the left (Figure5.3a) and more rapidly as further indicated by the reduction in $\Delta\tau$ in figure 5.4a–c. This can be largely explained by a higher CO_2 partial pressure creating a higher linear driving force (Zeinali *et al.*, 2012; Raganati *et al.*, 2019; Jamei *et al.*, 2023). At higher concentrations, more CO_2 molecules reach and contact the solid sorbent surface. Therefore, the lower breakthrough time at $16\ vol\%$ compared to 8 and 12 $vol\%$ could be a consequence of the hydrotalcite's adsorption sites saturating more quickly due to increases in the CO_2 adsorption rate. As more CO_2 is adsorbed, the chance of a CO_2 molecule locating an unoccupied active site on the hydrotalcite surface decreases. The adsorption rate is increased when increasing the concentration, but this accelerates the saturation of the sorbent. The observed effect is consistent with the anticipated

results since higher CO_2 concentration levels have been demonstrated to increase the diffusion coefficient, leading to enhanced internal mass transfer within the adsorbent material. (Sabouni *et al.*, 2013; Girimonte *et al.*, 2022).

Higher CO_2 concentrations increase adsorption capacity by providing more molecules for adsorption as shown in Figure 5.5c. However, the availability of binding sites on the solid sorbent is crucial. There is a saturation point where, despite an increased CO_2 concentration, the adsorption capacity may not further increase due to limitations in binding sites (Raganati *et al.*, 2021; Akpasi and Isa, 2022; Jamei *et al.*, 2023). This assertion is substantiated by several investigations on CO_2 adsorption using diverse solid sorbents, as documented in the literature (Abid *et al.*, 2021; Reddy *et al.*, 2021; Gunawardene *et al.*, 2022; Zhang *et al.*, 2023). The rise in CO_2 content increases the driving force for diffusion, thereby enhancing the transportation of CO_2 molecules towards the sorbent surface. Furthermore, the observed increase in adsorption capacity might be attributed to multilayer adsorption. A rise in the concentration of carbon dioxide (CO_2) results in a corresponding increase in the quantity of CO_2 molecules that can be adsorbed onto the surface of the sorbent (Gunawardene *et al.*, 2022).

Since the driving force for mass transfer depends on the variance in CO_2 concentration between the adsorbent surface and the bulk phase, an increase in the driving force with raising CO_2 concentration is typical. In investigating the impact of the CO_2 concentration on the driving force for CO_2 adsorption onto activated carbon. Li et al. (2019) observed a substantial increase in the latter when the CO_2 concentration in the input gas was raised. Thus, an increase in CO_2 may enhance the driving force for the adherence of CO_2 to adsorbents (Knox *et al.*, 2016a). Furthermore, several studies have shown that increasing the CO_2 concentration might increase the adsorption capacity (Wang and LeVan, 2009; Álvarez *et al.*, 2017; Jamei *et al.*, 2023).

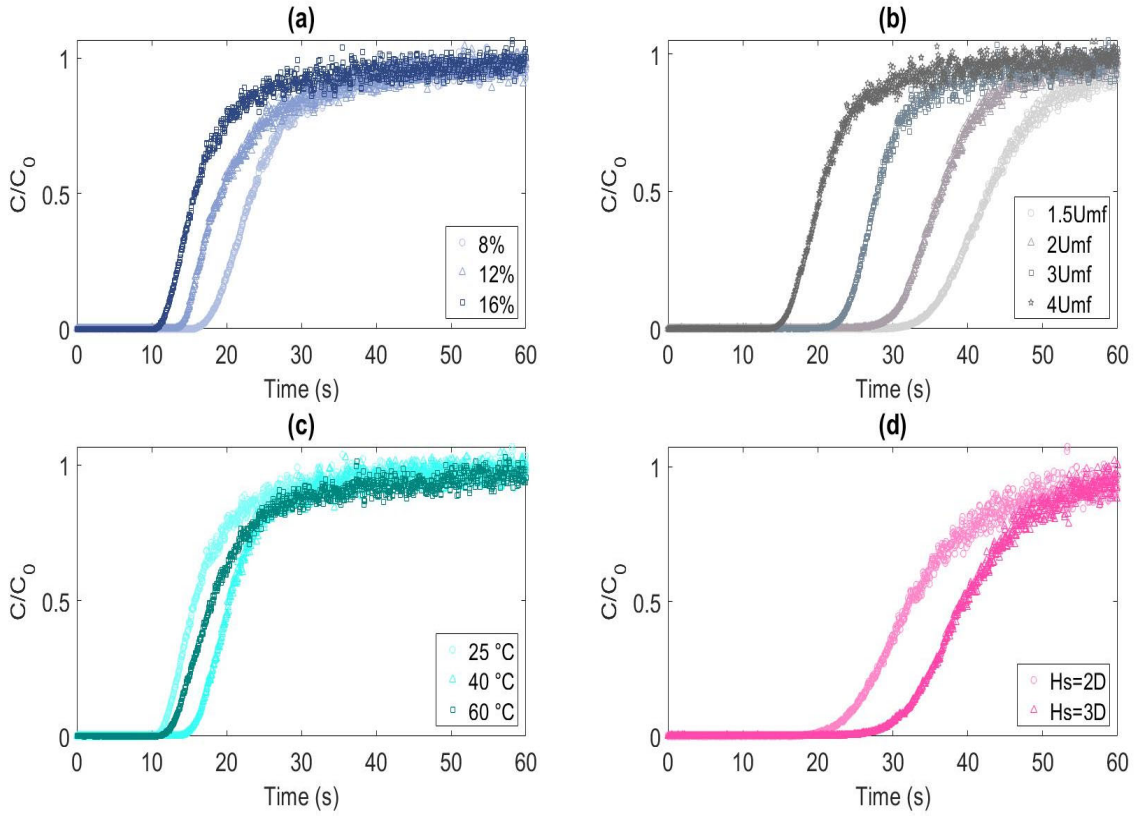

Figure 5.3. Normalised BC as a function of: (a) CO_2 concentration at T = 25 °C, (b) Gas velocity at T = 40 °C, (c) Operating temperature $U_g = 4\ U_{mf}$, , and (d) bed loading at T = 25 °C.

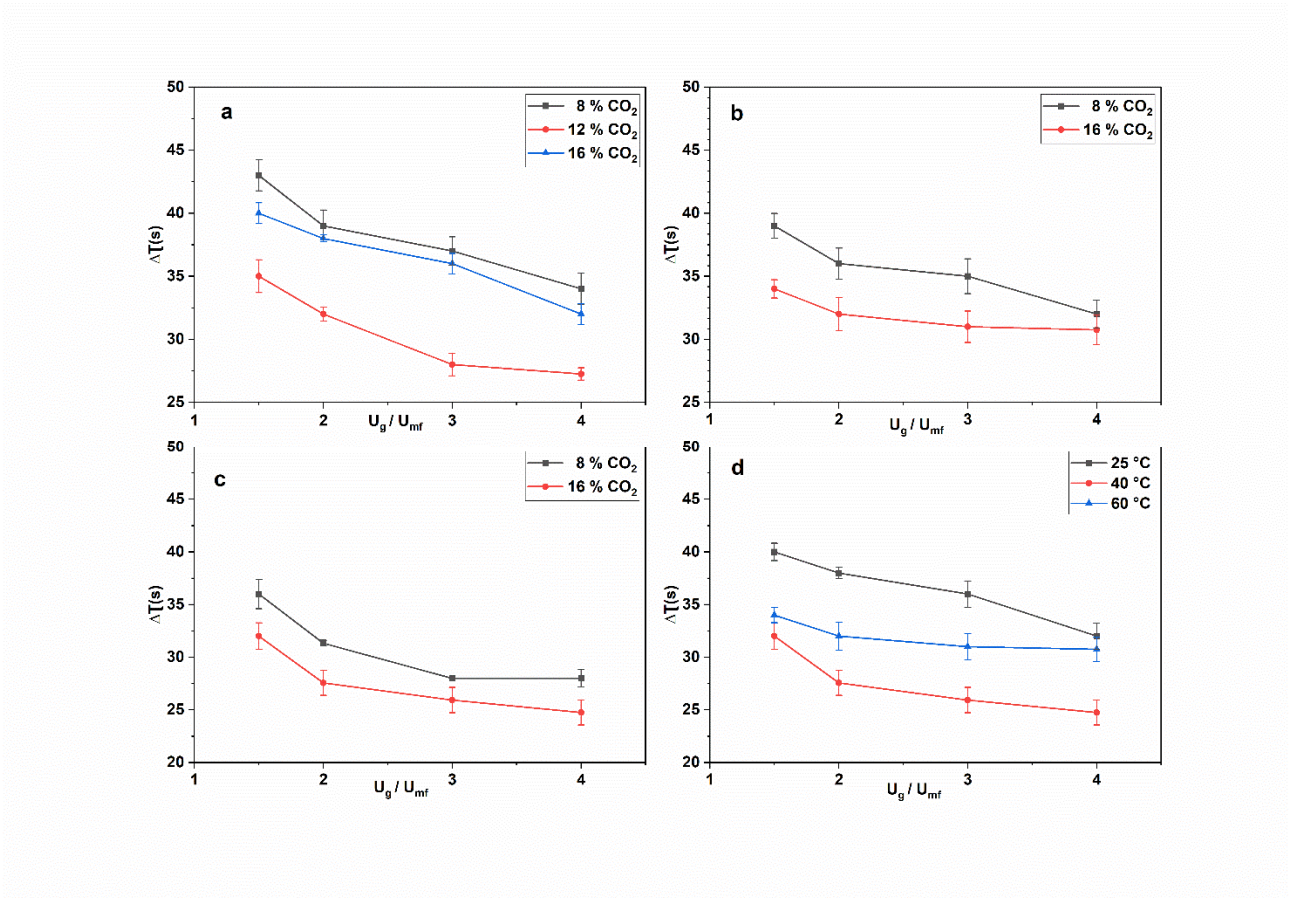

Figure 5.4. Trends of breakthrough time Δτ as a function of superficial gas velocities; (a) varying CO_2 concentration at T = 25 °C, (b) varying CO_2 concentration at T = 40 °C, (c) varying CO_2 concentration at T = 60 °C, and (d) varying temperature at 16 vol% CO_2 concentration.

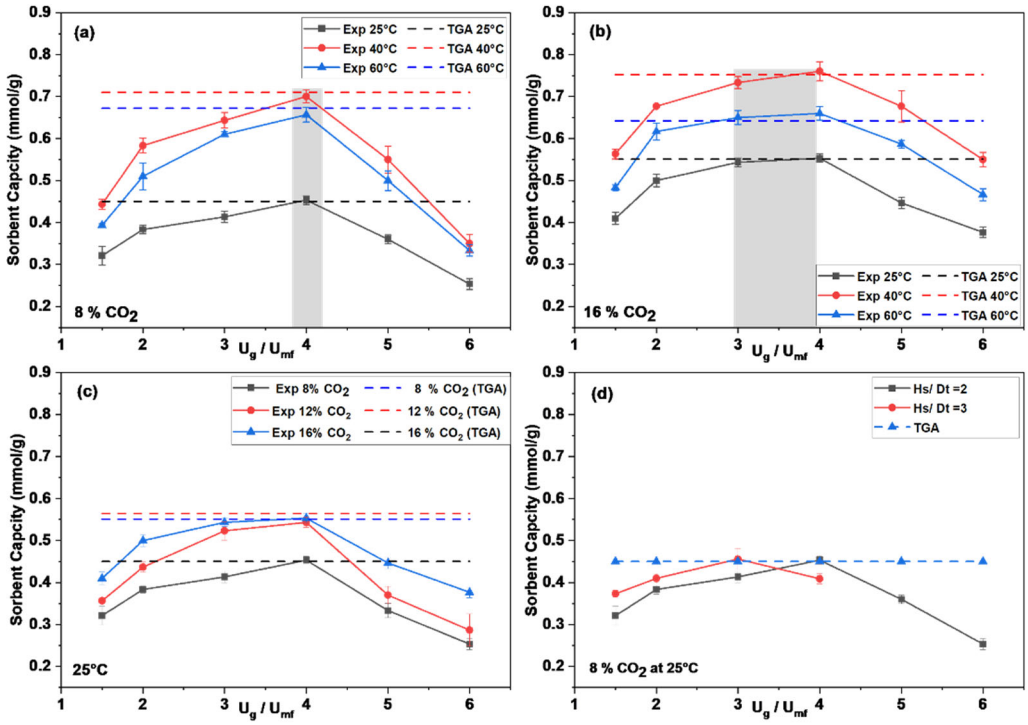

Figure 5.5. Adsorption capacity as a function of superficial gas velocities; (a) varying temperature at 8 vol% CO_2 concentration, (b) varying temperature at 16 vol% CO_2 concentration, (c) varying concentration at T = 25 °C, and (d) varying bed height at 8 vol% CO_2 concentration.

5.3.2 Effect of Gas Flowrate

The gas velocity influences the gas-solid mixing intensity, flow regime, and gas residence time, which all influence the observed adsorption process. To study these effects, a gas velocity range that encompassed a range of regimes from bubbling to slugging was studied based on observations made in the previous chapter. Here, the impact of gas velocity on the shape of the breakthrough curve, breakthrough time, and CO_2 capacity are discussed. Increasing the gas flow rate (superficial gas velocity as the cross-section is fixed) expectedly shifted

the breakthrough curves to the left as shown in Figure 5.3b due to the decrease in residence time. Figure 5.4a–c shows a corresponding reduction in the breakthrough time Δτ as the gas velocity increased. These results indicate that the bed saturated more quickly, which agrees with trends previously reported in the literature (Sabouni *et al.*, 2013; Benmahdi *et al.*, 2019; Abd *et al.*, 2021; Jamei *et al.*, 2023).

Figure 5.5 a-c show that the adsorption capacity went through a maximum as the gas velocity increased, reaching a maximum value at 4 U_{mf}, corresponding to the bubbling regime. Initially the adsorption capacity increases as the gas velocity increases (from 1.5 U_{mf} to 4 U_{mf} . It is speculated that this results from improved gas–solid contact (perhaps due to the increased prevalence of small bubbles), which may correspond with the hydrodynamic study (bubbling regime before the change to a slugging regime). This leads to improvements in the overall observed reaction rate due to higher heat and mass transfer coefficients. The bubbling regime is notably more favourable for the study of CO_2 adsorption as it allows for more homogenous dispersion of the adsorbent and enhanced interactions between the hydrotalcite (solid) and CO_2 (gas) phases (Jaiboon *et al.*, 2013; McDonough *et al.*, 2019). In other words, the increased gas velocity from the bubbling intensifies particulate motion and gas–solid mixing. However, a further increase of gas velocity (> 4 U_{mf}) caused the measured capacity to decrease. This is highly likely to be due to the onset of the slugging regime which leads to gas-bypassing, worse gas-solid mixing (reduction in the contact surface area between adsorbent and adsorbate which corresponds with the hydrodynamic study in the previous chapter that a slugging regime was observed when (> 4 U_{mf}). This is mostly attributed to the slugs separating gas from the solid particles inside the bed. The slugging phenomenon can induce channelling, resulting in non-uniform adsorption in some areas of the bed (localised saturation) and diminished operational efficiency (Jaiboon *et al.*, 2013). Furthermore, the decrease in CO_2 adsorption might also be explained by an insufficient time for CO_2 molecules to diffuse into the pores of the adsorbent before leaving the column (Boonchuay and Worathanakul, 2022). Overall, this results in significant reduction of observed capacity well below TGA results. While the adsorbent would probably reach TGA adsorption capacity in the long runs, the observed effective adsorption capacity would limit the process so obviously slugging regime should be avoided as operational efficiency would be low (Jaiboon *et al.*, 2013).

Figure 5.5 a-c, also shows adsorption capacities at the comparable concentrations and temperatures independently measured using TGA (Gutierrez-Ortega *et al.*, 2022). Highest adsorption capacity corresponds to the TGA; this validates the MFB as a potential platform for CC materials screening. TGA primarily provides information on the adsorption/desorption kinetics and material properties. The micro-fluidised bed approach, on the other hand, offers useful insights into the dynamic behaviour of systems, mass transfer rates, and breakthrough curves under various flow conditions. Consequently, it is beneficial for assessing, optimising, and evaluating a variety of processes.

Figure 5.5 b shows that at a concentration of 16 vol% CO_2, the bubbling regime with the lowest gas velocity of 1.5 U_{mf} exhibits the lowest apparent adsorption capacity, approximately three-quarters of the total value obtained via TGA at the same temperature and concentration. When the superficial gas velocity is increased to 3–4 U_{mf}, this capacity significantly improves to greater than 98% of the TGA-obtained adsorption capacity. Therefore, the optimum operation window occurs at a high gas flow rate (3–4 U_{mf},) in the bubbling regimes, similar to the TGA results. As mentioned earlier, this increase in gas velocity in the bubbling regime increases the bubbling and surface contact within the fluidised bed, thereby improving the gas–solid interaction to enable full utilisation of the adsorption capacity while at lower velocities it seems that the full adsorption capacity is reached in the noise region of saturated part of the breakthrough curve due to lower mixing efficiency, i.e. non-uniform adsorption in some areas of the bed (localised saturation). When the CO_2 concentration is reduced to 8 vol% CO_2 (Figure 5.5a), the operation window narrows to yield an adsorption capacity similar to that obtained via TGA, (only at 4 U_{mf}), however at 3 U_{mf}, the apparent capacity decreases to reach approximately 91% of the TGA-obtained adsorption capacity compared to 98% at a higher concentration (16 vol% CO_2). Consequently, by operating at higher concentrations, a broader range of gas velocities can be used to study kinetics and more importantly in the practical application of micro- and macro-fluidised bed for carbon capture. In the practical case of lower concentration feed, reactors in series might be needed to improve the efficiency as already suggested by other researchers (Dhoke *et al.*, 2021). In this study, kinetic limitations are evident between $3U_{mf}$ and 4 U_{mf} at high concentrations (16%), as shown in Figure 5.5b.

This is likely to be because the 8 vol% condition causes a reduction in mass transfer inside the pores due to a smaller driving force. *I.e.,* as the concentration is reduced, the process becomes

mass transfer-limited rather than kinetically limited. These results can therefore be used to define an operating window of the MFB for screening applications. Operating at higher concentrations means a wider range of gas velocities can be used to study the kinetics. Operating at lower concentrations reduces the size of the screening window, which may increase uncertainty in the measurements. Operating within this window is crucial for observing the true adsorption kinetics rather than mass transfer effects. This means it is highly recommended to make hydrodynamics experiments an integral part of the MFB screening platform, which should form part of the workflow for material and technology development.

5.3.3 Effect of Adsorption Temperature

Effect of Adsorption Temperature

In general, the influence of temperature on the adsorption is complex and dependent on a various factor, such as the adsorbate and adsorbent's properties, the contact force between the adsorbate and adsorbent and, and the heat of adsorption. Both physisorption and chemosorption are influenced by temperature (Gunawardene *et al.*, 2022). The investigation of various temperatures in the adsorption process occurring inside a fluidised bed is important for understanding the implications on thermodynamics, kinetics, material stability, and process optimisation. Therefore, temperatures of 25 °C, 40 °C, and 60 °C were considered. The influence of temperatures on the adsorption capacity and breakthrough time was also studied. Pre-fluidisation in a dry gas is applied as a preliminary step to conducting kinetic screening investigations (based on hydrodynamic studies) to reduce interparticle forces. This approach has been combined with a sorbent pre-conditioning procedure, which involves subjecting the desired quantity of sorbent to high temperatures in a vacuum oven for several minutes to prepare the sorbent through the removal of any residual CO_2 and moisture. After the pre-fluidisation step, the temperature was adjusted to the intended value specific to that run, and the bed was allowed to settle for several more minutes. This was carried out to ensure the complete establishment of the flow regime and reaching the required temperature setpoint. Carbon dioxide (CO2) usually undergoes adsorption through an exothermic process. Consequently, it is expected that the adsorption capacity will decrease with an increase in temperature (Morales-Ospino *et al.*, 2020; Akpasi and Isa, 2022).. However, as shown in Figure 5.5a–b, the adsorption capacity increased with rising temperatures (25 °C to 40 °C). This phenomenon can be attributed to the fact that, under low-temperature conditions, the reactivity of CO_2 is limited to

the CO_2 affinity sites located on the surface of the particles (Xu *et al.*, 2002). Therefore, increasing from 25 °C to 40 °C for this hydrotalcite could be beneficial in overcoming the activation energy for adsorption. As a consequence, there may be a greater number of adsorption sites accessible at the higher temperature. This could be due to an enhancement in the diffusion rate, which is predicted when increased temperature, which could result in a higher apparent adsorption capacity (Xu *et al.*, 2002) . Additionally, the apparent higher adsorption rate could also be a result of increased CO_2 diffusion rates due to improved mass transfer, i.e., molecules diffuse more quickly inside pores due to higher kinetic energy. The adsorption capacity of MCM-41-PEI-50 followed a similar pattern in a previous study (Xu *et al.*, 2002). Moreover, it can be explained by suggesting that at lower temperatures, The channels of the hydrotalcite restrict access of CO_2 to active adsorption sites. Conversely, at higher temperatures, expansion occurs, unveiling more adsorption sites and augmenting the overall adsorption capacity.

Raising the temperature to 60 °C led to a reduce in adsorption capacity as shown in Figure 5.5 a – b. Raising the temperature to 60 °C may destabilise adsorbed CO_2 on the hydrotalcite surface due to rising surface energy and molecular diffusion (Shafeeyan *et al.*, 2015; Raganati *et al.*, 2019). Consequently, the activity of this hydrotalcite for CO_2 removal from the gas stream is decreased as the temperature increases above 40 °C which is consistent with the thermodynamics (Monazam *et al.*, 2013; Raganati *et al.*, 2019).

Peter N. Loezos (2002) investigated the impact of temperature on the adsorption capacity of MCM-41-PEI. Typically, the adsorption capacity increases with rising temperature, peaking at 112 mg/g-adsorbent at 75 °C for MCM-41-PEI-50. However, a slight decrease to 110 mg/g-adsorbent occurs at 100 °C, contrary to the anticipated reduction in adsorption capacity with higher temperatures due to the exothermic nature of CO_2 adsorption into PEI or MCM-41. The initial rise in adsorption capacity is attributed to the expansion of PEI at higher temperatures, exposing more active adsorption sites. (Abdus-Salam and Buhari, 2016)investigated the impact of temperature on fluorescein adsorption within the temperature range of 35 to 70°C, revealing results consistent with my own findings. The observed increase in adsorbed quantity from 35 to 40°C suggests potential chemical interactions between the adsorbate and the adsorbent, accompanied by improved accessibility to more active sites on the solid sorbent. However, the slight decrease in adsorption capacity with further temperature increase is explainable by the

exothermic nature of adsorption, causing a shift in equilibrium towards desorption as the temperature rises.

Adsorption capacity is highly dependent on the physicochemical characteristics and surface chemistry of the solid sorbent. Usually, the adsorption capacity exhibits a decline as temperatures increase. This is because the adsorption process is usually reversible and exothermic. However, in some cases, Increasing the temperature will increase the apparent adsorption rate due to increases in internal diffusion. For this particular hydrotalcite, operating at temperatures of 40 °C will maximise the capacity by decreasing the adsorption activation energy without destabilising the adsorbed CO_2 molecules. This temperature provides the largest number of available active sites yielding a stronger signal for observing/measuring the intrinsic kinetics.

Ultimately, CO_2 adsorption is typically an exothermic reaction. Therefore, the temperature profile of the bed was recorded during the investigation (these results are shown in Table 5.3). The injection of CO_2 into the bed increased the temperature under all conditions due to the heat emitted over adsorption. The temperature then progressively returned to the desired level as the adsorption of CO_2 by the adsorbent was reduced. In addition, a rise was observed in the maximal recorded bed temperature due to a higher CO_2 concentration. This is due to the relationship between the adsorption rate and consequent heat release. Remarkable is that the maximum temperature was reached at the superficial gas velocity at 4 U_{mf} (the best possible fluidisation regime), causing limited gas bypass and achieving higher adsorption capacity.

5.3.4 Effect of Bed Loading

It was observed during the hydrodynamic study (see previous chapter) that the superficial gas velocity where the bed transitioned from bubbling to slugging depended on the bed load (defined by the dimensionless bed height H_s/D_t). Figure 5.5d shows that the same maximum adsorption capacity was measured for both H_s/D_t = 2 and 3 (both matching the TGA value). However, the maximum occurred at a velocity of 3 U_{mf} for H_s/D_t = 3, and 4 U_{mf} for H_s/D_t = 2. This is because the onset of slugging is earlier in the deeper bed; or contrarily, the bubbling regime is wider in shallower beds. For this particular combination of fluidised bed and hydrotalcite adsorbent, the shallower bed height is preferable. Not only does this produce

a potentially wider window for observing the underlying kinetics (where mass transfer is not the rate determining step), but less material is also required.

Though it should be mentioned that when the bed loading increases, the efficacy of CO_2 removal from the artificial flue gas at the target superficial gas velocity may slightly improve because the gas-solid contacting time is increased. Moreover, the amount of adsorbent affects the breakthrough curve shape. When the amount of adsorbent in the bed increases, the breakthrough curves shift to the right, which means the saturation time are increased, as shown in Figure 5.3d. This phenomenon can be attributed to a rise in the number of binding locations, resulting in an increase in the adsorption surface area of the adsorbent. Similar tendencies have been documented in the literature (Zeinali *et al.*, 2012; Monazam *et al.*, 2013; Aguilera and Ortiz, 2016; Benmahdi *et al.*, 2019). *I.e.,* operating with more material might increase the signal-to-noise ratio, so a trade-off might be needed depending on the particular adsorbent.

5.4 Kinetic Modelling

Adsorption occurs when the gas adsorbate binds to the solid active sites via weak physical or strong chemical interactions (Monazam *et al.*, 2013; Raganati *et al.*, 2019). This section carefully examines the experimentally determined CO_2 uptake kinetics using three different kinetic models: pseudo-first-order, pseudo-second-order (Skrip *et al.*, 2013) and fractional order (Serna-Guerrero and Sayari, 2010; Jamei *et al.*, 2023). Note, more details on the method are provided in Chapter 3. Figure 5.6 shows an example of the measured cumulative uptake curve compared to the predicted uptake using all three models, whilst Table 5.3. summarises the fitted kinetic constants and corresponding R^2 values across all conditions. Here, K_1 and K_2 represent the pseudo first and second-order rate constants, respectively, with units in s^{-1} and $g \cdot mmol^{-1} \cdot s^{-1}$. Additionally, K_f stands for the fractional-order rate constant measured in s^{-1}. The variables "n" and "m_1" are empirical coefficients used to refine the shape of the fractional-order model curve. The "n" coefficient characterizes the driving force, while "m_1" represents the adsorption time.

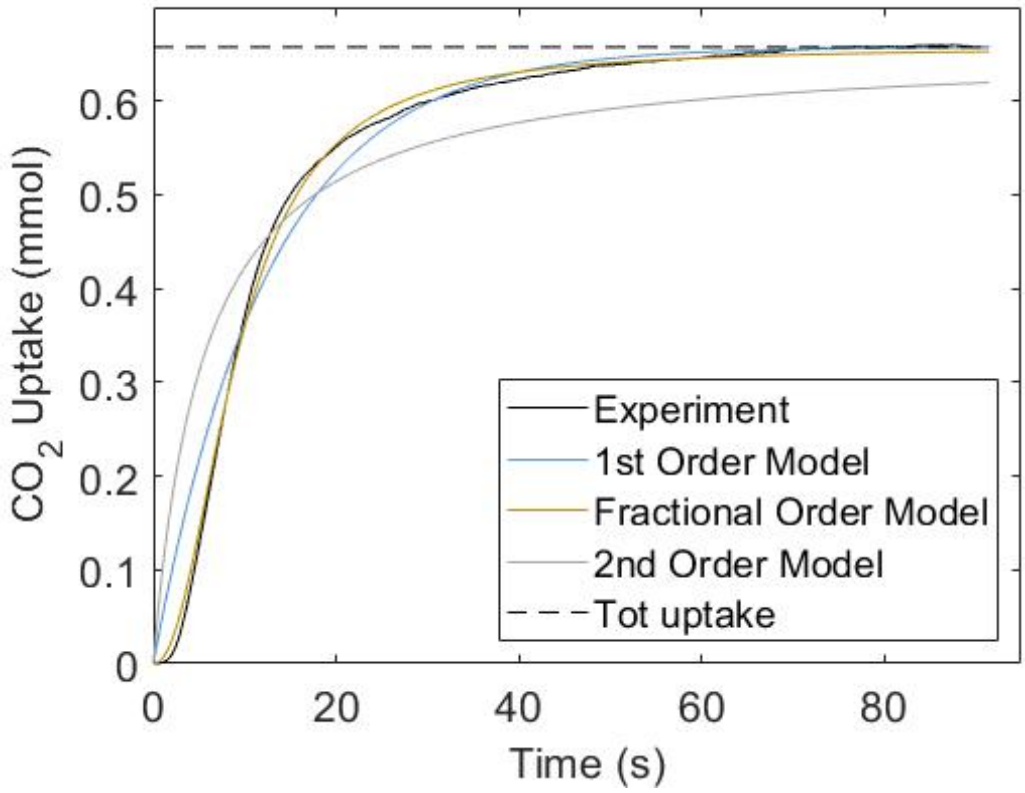

Figure 5.6. Comparison between cumulative CO_2 uptake curve measured experimentally and three different kinetic models (conditions: 16 vol% CO_2, 4 U_{mf}, 40 °C).

Table 5.3. Kinetic data in adsorption breakthrough investigations.

Parameter		$\frac{U_g}{U_{mf}}$	T_{max} (°C)	1st order Model		2nd order Model		Fractional order Model			
T (°C)	[CO_2] (vol%)			R^2	K_1 (s^{-1})	R^2	K_2 ($g.mmol^{-1}s^{-1}$)	R^2	K_f (s^{-1})	n	m_1
25	8	1.5	25.7	0.886	0.027	0.298	0.173	0.990	0.058	1.01	1.96
		2	25.9	0.908	0.031	0.328	0.184	0.991	0.125	1.09	2.13
		3	26.1	0.947	0.053	0.522	0.211	0.996	0.142	1.41	2.15
		4	26.1	0.981	0.057	0.748	0.220	0.995	0.159	1.29	1.95
	12	1.5	25.9	0.871	0.065	0.256	0.319	0.951	0.056	1.01	2.03
		2	25.8	0.945	0.057	0.543	0.329	0.994	0.058	1.76	2.02
		3	26.2	0.940	0.074	0.546	0.367	0.997	0.160	1.88	2.10
		4	26.2	0.986	0.065	0.767	0.317	0.994	0.204	1.26	2.12
	16	1.5	26	0.917	0.056	0.399	0.242	0.983	0.046	1.20	2.03
		2	26.2	0.865	0.052	0.543	0.247	0.972	0.044	1.65	2.09
		3	26.1	0.993	0.084	0.577	0.408	0.99	0.167	1.48	2.16
		4	26.3	0.991	0.080	0.691	0.404	0.99	0.206	1.51	2.26
40	8	1.5	41	0.898	0.027	0.300	0.173	0.963	0.060	1.04	2.10
		2	41.1	0.904	0.044	0.429	0.184	0.974	0.140	1.13	2.27
		3	41.1	0.934	0.057	0.449	0.221	0.984	0.160	1.14	2.11
		4	41.3	0.972	0.063	0.610	0.233	0.997	0.171	1.13	2.20
	16	1.5	41	0.936	0.050	0.457	0.220	0.996	0.090	1.71	2.03
		2	41.1	0.902	0.063	0.367	0.272	0.982	0.106	1.60	2.27
		3	41.4	0.957	0.077	0.592	0.269	0.992	0.160	2.21	2.03
		4	41.4	0.926	0.086	0.549	0.222	0.995	0.161	2.23	2.05
60	8	1.5	60.9	0.856	0.028	0.235	0.213	0.967	0.104	1.08	2.05
		2	60.8	0.918	0.042	0.412	0.257	0.988	0.121	1.08	2.18
		3	61	0.933	0.055	0.454	0.225	0.986	0.107	1.09	2.21
		4	61.1	0.946	0.054	0.521	0.226	0.993	0.139	1.09	2.27
	16	1.5	60.9	0.922	0.050	0.457	0.252	0.990	0.031	1.17	2.09
		2	61.1	0.965	0.057	0.520	0.237	0.997	0.119	1.14	2.15
		3	61.1	0.972	0.085	0.647	0.273	0.996	0.130	1.22	2.08
		4	61.1	0.948	0.084	0.639	0.270	0.991	0.146	1.77	2.18

The R^2 values of the pseudo-first-order model vary from 85% to 99%. This model typically overestimates CO_2 uptake during the initial phase of adsorption before underestimating it at later phases. In accordance with previous studies in the field (Jamei *et al.*, 2023), the pseudo-first-order model is suitable for characterising simple physical adsorption mechanisms with relatively low surface coverage. That is, it can reasonably define adsorption with reversible interactions between the adsorbent surface and the adsorbate without taking into account the probability of bonding or chemical interactions between the two. The pseudo-first-order model exhibits some notable departures from the experimental data, highly probable when the adsorbate surface saturation becomes very high for this particular model. The second-order model performed poorly across most conditions and generally had the lowest R^2-values. The second-order kinetic model is usually used to describe processes that consist solely of chemisorption, where strong chemical interactions occur between the CO_2 molecules and the sorbent surface. As a result, it fails to account for the concurrent incidence of CO_2 physisorption and chemisorption on this hydrotalcite.

It is evident from the above observations that hydrotalcite must undergo a hybrid adsorption method consisting of physisorption and chemisorption. This results in a characteristic 'S' shape in the uptake curve because of complex interactions between the adsorbent and adsorbate. These interactions include several factors such as mass transfer restrictions, heterogeneous surface features, and nonlinear adsorption isotherms. Fractional-order models have been shown to be effective in accurately describing and analysing these phenomena. As shown in Table 5.3, the fractional order model produced the best fit over all conditions to the experimental data, due to its ability to model this 'S' shape (indicated by the higher R^2 values, all above 95%).

The adsorption rate in the fractional order model is a function of the numerical coefficients n and m_1, and a rate constant K_f . The n coefficient represents a driving force factor that can further be considered as an indicator/proxy of the number of active sites in the core of the adsorbent, which is additionally linked to the reaction order, the diffusion resistance, or how many adsorbate molecules can adhere to each adsorption site (Heydari-Gorji and Sayari, 2011; Kudahi *et al.*, 2017) . If the adsorption sites are extremely homogeneous, then n may be close to unity, implying that only one adsorbate molecule may adhere to each site at a time. When

the sites for adsorption are not regular, n may be greater than 1, meaning that more active sites are available, more than one adsorbate molecule may adhere to each site, and/or less internal resistance. As shown in Table 5.3, *n* was always greater than one, indicating that adsorption is not uniform, and so the chance of adsorbing CO_2 is not uniform across the sorbent surface. Table 5.3, also shows that *n* increases as gas flow rate and CO_2 concentration increase, meaning a decrease in internal resistance and/or an increase in active sites as a consequence of increased driving forces. The second factor, m_1, measures the rate of adsorption (Kudahi *et al.*, 2017; Wang *et al.*, 2020b). As anticipated, m rose as the gas flow rate and concentration grew. In other words, greater gas flow rates result in faster saturation. As shown in Table 5.3, *m* increases as gas flow rate and CO_2 concentration increase due to the higher driving force because of increased internal diffusion, which produces a greater apparent kinetic rate (the rate that is observed experimentally).

Regardless of the kinetic model, all kinetic constants (k_f, k_1, and k_2) increase as the gas flow rate and concentration increase, indicating the increasing in adsorption rate. This result suggests that increasing gas flowrate and concentration accelerate the adsorption process Moreover, the fractional order rate constant, k_f,, rises when the gas flow rate and concentration are increased. This phenomenon can be linked to the significant increases in the driving force. Notably, the rise in k_f, that plateaus within the superficial gas velocity range of 3–4 U_{mf} at a high concentration (16 vol%) could explain why the apparent adsorption capacity in this region remains the same despite changes in the diffusion velocity. This stability in the values can be attributed to the onset of kinetic limitations, as described in (5.3.2) of this chapter. These kinetic constraints imply that beyond a certain threshold, the adsorption process is no longer solely determined by the availability of reaction sites but rather by the rate at which molecules can diffuse or interact with these sites. This could explain the differences in the k_f values and reveal how mass transport and reaction kinetics function together in the hydrotalcite structure.

Ultimately, the utility and limitations of MFB as a screening tool have implications. The sensitivity of MFB to changes in gas flow rate (bed regime) and concentration indicates that it may be useful as an instrument for quickly screening absorption processes and materials. Nonetheless, it is essential to recognise possible downsides and limitations. As it operates in a controlled and simplified laboratory environment, the MFB may not always accurately depict conditions in the actual world. Furthermore, the observed kinetics could differ based on the

adsorbent, adsorbate, and operation conditions. Consequently, whereas the MFB could serve as a useful screening platform, it ought to be combined with additional techniques and validated against real-world applications to ensure that its results apply to real-world scenarios. In addition, the results highlight the significance of understanding kinetic limitations, as excessive flow rates may not result in proportional increases in adsorption efficiency and may contribute to a decrease in adsorption capacity (slugging). The MFB's ability to study adsorption processes holds great potential for development and research; however, its limitations must be considered for meaningful and reliable outcomes.

5.5 Summary

Rising the superficial gas velocity in a bubbling regime improves the gas-solid mixing, which enables the true adsorption capacity to be measured (where mass transfer is not the rate determining step). Here the adsorption capacities agreed with independent TGA measurements performed by the Research Centre for Carbon Solutions at Heriot-Watt University. Under these conditions, the bed quickly saturates, enabling rapid measurement of the true underlying adsorption kinetics. Operating in the slugging regime (at high gas velocities) reduces the measured capacity because most of the CO_2 will bypass the solid due to poor mixing. The optimal superficial gas velocity was determined to be at 4 and 3 U_{mf} at H_s/D_t = 2 and 3 respectively at a CO_2 concentration of 8 vol%. By increasing the concentration to 16 vol%, the operating window extended to a gas velocity of 3–4 U_{mf} at H_s/D_t = 2 because internal diffusion in the pores increases, ensuring the adsorption process remains kinetically limited rather than diffusion limited. The optimal temperature for this particular hydrotalcite is 40 °C, where the highest adsorption capacities were measured across all other conditions. Below this temperature the adsorption activation energy becomes dominant, while above this temperature, the CO_2 binds weakly to the active sites.

The experimental CO_2 uptake curves were carefully examined using three distinct kinetic models: pseudo-first-order, pseudo-second order, and fractional order. The fractional order model fit the experimental data best, indicated by a higher R^2 value across all conditions. This model captures the ‘S’-shape of the uptake curve, indicating that this hydrotalcite undergoes a hybrid process between physisorption and chemisorption. Here, the adsorption sites are irregular, as n is typically higher than 1, indicating more active sites, which means that more of

the adsorbate molecule may attach to every site and/or have smaller internal resistance. Moreover, n rises as CO_2 concentration and gas flow rate rise, indicating increased active sites and/or reduced internal resistance due to increased driving forces. Also, as expected, m grew as the concentrations and gas flow rate rose. In other words, higher gas flow rates result in a quicker saturation rate due to the higher driving force caused by enhanced internal diffusion, which results in a higher apparent kinetic rate (the rate observed experimentally). Moreover, the fractional order rate constant,k_f, rises as t concentration and the gas flow rate increase. This phenomenon is correlated with significant increases in driving force.

Chapter 6. Desorption Kinetics

6.1 Introduction

Most research efforts have focused on assessing adsorption in novel fluidised bed systems (Wang *et al.*, 2020a; Jamei *et al.*, 2023), while studies investigating desorption kinetics are limited. Owing to its unique properties and advantages, the micro-fluidised bed (MFB) system may provide a stable platform for studying desorption processes. Typically, the desorption phase occurs after adsorption, facilitating the regeneration and reuse of the solid sorbent. The accumulation of non-desorbed particles can adversely impact the sorbent material's operating capacity and overall lifespan. Consequently, it would be advantageous to develop technological solutions that facilitate the effective mixing of gas and solid for enhanced contact while mitigating the occurrence of bypassing and hot spot regions during the desorption process. This chapter presents the development of a small-scale system (micro-fluidised bed) for the study of desorption process of solid sorbents.

The desorption in a fluidised bed can be accomplished via different methods, such as pressure swing adsorption (PSA), temperature swing adsorption (TSA) (Sun *et al.*, 2011; Salazar Duarte *et al.*, 2017; Zhang *et al.*, 2020), microwave desorption (Ania *et al.*, 2005), and vacuum swing adsorption (VSA) (Sun *et al.*, 2011). In TSA, temperature swing refers to the fluctuations or variations in temperature over a certain period (Ammendola *et al.*, 2015; Ben-Mansour and Qasem, 2018). Desorption often occurs at higher temperatures when the binding strength between CO_2 and the adsorbent is relatively weak (Morales-Ospino *et al.*, 2020). The temperature can be raised via several methods, such as steam injection, employing a hot purge/sweep gas, or thermal conduction/convection with the aid of in-line heaters (Ammendola *et al.*, 2015; Ben-Mansour and Qasem, 2018; Morales-Ospino *et al.*, 2020). However, the techniques used in TSA exhibit several limitations, including possible alterations to the physical and chemical characteristics of the adsorbent heat dissipation to the surrounding apparatus and a long regeneration period (Zeng *et al.*, 2022). Nevertheless, the recovery rate of TSA is better than other techniques. It is a straightforward approach that can be effectively used with the MFB reactor platform (Zeng *et al.*, 2022).

Breakthrough curves (BC) obtained from desorption experiments are valuable for analysing the adsorption/desorption properties and efficiency of adsorbent particles (Benmahdi *et al.*, 2019).

This chapter focuses on the possibility of using a 3D-printed MFB reactor to study the dynamics of desorption. Understanding desorption behaviour and optimising its efficiency are essential for developing effective elimination and separation techniques. The concentration of the CO_2 released from saturated sorbent materials is continuously measured to generate desorption BT curves, which provide key data on the adsorption/desorption kinetics and efficiency of the adsorbent material. Several parameters directly impact how effectively desorption proceeds in an MFB, including the characteristics of and contact between the adsorbent and adsorbate, the required temperature, and the superficial gas velocity of the fluidising medium (Ammendola *et al.*, 2015; Selmert *et al.*, 2022). Evaluating the effect of temperature is thus necessary to comprehend and optimise the desorption dynamics. The implications of the temperature used and how they relate to developing and enhancing adsorption techniques will be discussed by analysing the BT curves and desorption process in an MFB.

6.2 Breakthrough Adsorption Experiments

Figure 6.1 displays the process flowchart of the experiments. Cyclic adsorption and desorption BT tests were conducted in the MFB using the best possible parameters determined from previous adsorption kinetics and hydrodynamic experiments (Chapters 4 and 5), establishing the desired gas flow regime and the best possible apparent adsorption capacity. Therefore, the adsorption kinetics and hydrodynamic information helped identify suitable operating conditions for the BT desorption experiments. In this study, the BT curves were obtained from desorption tests using the TSA method (Ammendola *et al.*, 2015). Figure 6.1 summarises the adsorption and desorption tests, which were conducted utilising an MFB unit operating at two different desorption temperatures: (a) 90 °C and (b) 40 °C. Generally, to study desorption processes, it is preferred that the tests be conducted in several steps, including pre-treatment, the adjustment of experimental conditions, adsorption, preheating if necessary, and then actual desorption itself. The flow rates and concentrations were carefully regulated in the desorption tests. To validate the results, the experiments were independently repeated three times under each condition to determine the mean values and their associated error.

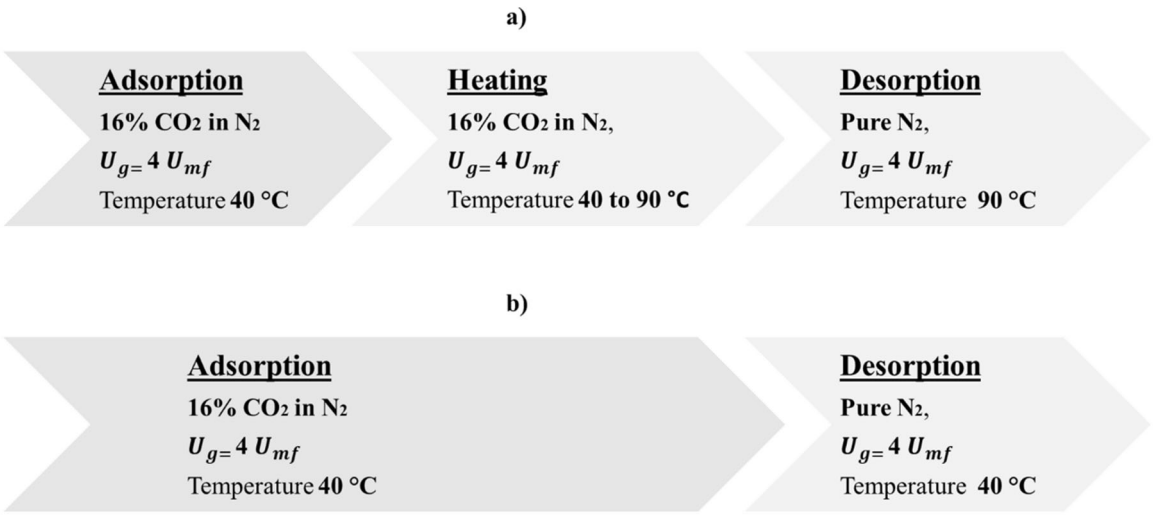

Figure 6.1. Flowchart of the Experimental Procedures at two different desorption temperatures of a) 90°C and b) 40°C.

Prior to the adsorption process, the desired amount of the solid sorbent was placed in a vacuum oven and heated at 90 °C (for 15 min) to eliminate moisture and any remaining CO_2. The solid sorbent particles were then loaded into the MFB, and subsequently, inert gas (N_2) was used to fluidise the particles for several minutes and to adjust to the target adsorption temperature. The adsorption process was then conducted for extended time before the desorption step to ensure that the solid sorbent particles were completely saturated with CO_2. Namely, after reaching saturation, the experiments continued for an additional two minutes to ensure that the particles were completely saturated. This was essential in preparing the bed for subsequent desorption tests. The process was performed at the best possible operating conditions for adsorption, a CO_2 concentration, superficial gas velocity, and temperature of 16 vol% CO_2, U_g= 4 U_{mf}, and 40 °C, respectively, as discussed in the previous chapter (Section 5.3) – to achieve the best possible fluidised regime and apparent adsorption capacity. Then, the preheating phase (for 90°C experiments) starts after the adsorption process (when hydrotalcite is fully saturated with CO_2) until it reaches the target desorption temperature.

Throughout the adsorption and pre-heating stages, a consistent CO_2/N_2 concentration was maintained to address desorption challenges, ensuring accurate recovery measurements and preventing CO_2 desorption, loss, and maintaining the sorbent saturation with CO_2. During

the pre-heating process, the concentration of carbon dioxide (CO_2) is measured in order to detect any CO_2 losses that may occur at this stage. The desorption efficiency was evaluated only at two temperature levels of 40 and 90 °C. Owing to several restrictions and unanticipated obstacles, extra desorption tests became difficult to carry out. Initially, the lab flooding led to a suspension of laboratory operations. After the subsequent reopening of the laboratory, desorption investigations were initiated; however, difficulties occurred in attempting high-temperature desorption (in excess of 90 °C) employing a 3D-printed micro-fluidised bed (MFB).

In the beginning, pre-heating of the bed was tried only using a heater placed around the MFB, without injecting a fluidising gas to spread the heat to minimise possible desorption during pre-heating period. This was difficult because of the limited thermal conductivity of the MFB material, which consists of a high-temperature polymer. However, experiments shown that achieving the desired high desorption temperature is very challenging as the MFB were damaged before reaching the desorption temperature (e.g., 90°C) because the polymer material begins to degrade even though the temperature is below the manufacture specified range. Possible reason might be in uneven heat distribution when heat is delivered using only a wrapped heater cable around the MFB resulting in local hot spots. As illustrated in Figure 6.2, this resulted in deformation and fractures of the MFB structure. Therefore, it is necessary to inject a fluidising gas at a suitable flow rate inside the MFB system throughout the heating process to circumvent these constraints and help spread the heat more uniformly and effectively. However, due to the limited flow rate of the MFB made it challenging to attain higher temperatures (> 90°C). In addition, a heater failure occurred during the following attempts to carry out experiments at lower temperatures (< 90°C). Despite these limitations, the desorption efficiency could be evaluated within a practical temperature range, although considerable time was required to reach the target temperature. Desorption temperatures of 40°C and 90°C were selected as the limited flow rate of the MFB made it challenging to attain higher temperatures. Finally, in the desorption process, a heating and purging regeneration method was used to recover the CO_2 from the saturated sorbent.

Figure 6.2. An example photo of a 3D-printed MFB that has deformed and cracked during packed-bed regime heating only due to possible localised high-temperature spots.

Temperature plays a crucial role during the desorption process. BT curves were acquired for the inert glass particles and the hydrotalcite sample under each condition. The glass-particle BT curve contained information regarding CO_2 diffusion through the rig, and the hydrotalcite one elucidated the kinetics and CO_2 diffusion properties of the combination of sample material and rig. The desorbed amount of CO_2 was determined by subtracting the inert from the hydrotalcite signal. The BT curves and desorption behaviours presented in this chapter clarify the effects of temperature on CO_2 recovery. The results may help elucidate the problems associated with low desorption temperatures and flow rates and provide insights into designing more efficient CO_2 capture systems.

6.3 CO_2 Desorption Results

6.3.1 Effect of Desorption Temperature

Owing to many parameters, including the specific characteristics of the adsorbate and the strength of the connection between the gas and the solid sorbent, the influence of temperature on the desorption process may be intricate (Morales-Ospino *et al.*, 2020). In the case of

molecules with moderate adsorption, lower temperatures may induce desorption, while molecules with strong adsorption may need much higher temperatures. It can be inferred that an elevation in temperature promotes the progression of an endothermic reaction based on Le Chatelier's principle; therefore, temperature is a crucial control variable in the regeneration process (Liu *et al.*, 1996; Kim *et al.*, 2016a). As the temperature rises, there is a tendency for CO_2 to exhibit less binding affinity towards the adsorbent material. Consequently, a greater amount of CO_2 that was previously trapped inside the sorbent sites is released, leading to an enhanced capacity for CO_2 desorption. In order to investigate the instantaneous adsorption-desorption effect, the desorption process in Figure 6.4b was carried out at the same temperature as the adsorption process (T_{ads} - T_{des} = 40 °C). This approach aimed to eliminate any time delay associated with heating the bed to the desired desorption temperature.

The desorption efficiency was evaluated only at two temperature levels of 40 and 90 °C. At the higher temperature, the experiments passed through three stages: adsorption, preheating, and desorption as shown in Figure 6.3. The CO_2 concentration in the effluent gas was continuously recorded throughout the experiment using a CO_2 analyser. Moreover, plots provide temperature profile during experiments. The adsorption process was conducted under the best possible adsorption conditions ($U_g = 4U_{mf}$,16 $\%vol$, and 40 °C) as discussed in the previous section. The adsorption process was run for around 2 additional minutes after reaching saturation level to make sure that the solid sorbent reached full saturation. Once the sorbent becomes saturated, the bed is then preheated to reach the target temperature.

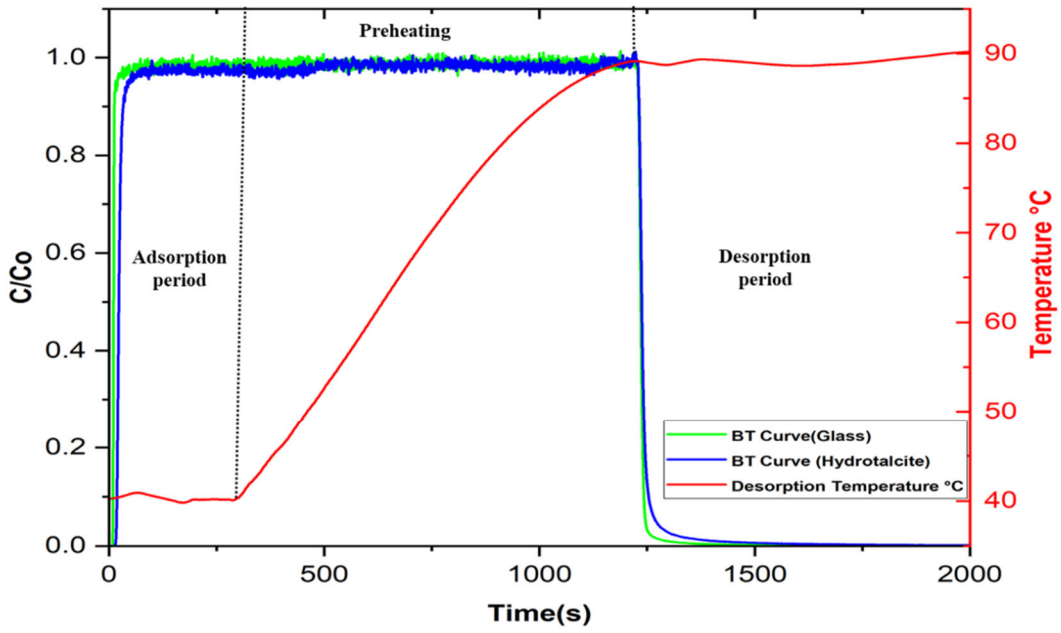

Figure 6.3. An example of CO_2 breakthrough curve as a function of time for the desorption temperature of 90 °C including during preheating step.

The preheating stage took 950 seconds (about 16 minutes) to reach 90°C due to limitations, including a low flow rate. The experimental pre-heating rate was approximately 0.05 °C/s, equating to 950 seconds to heat from 40 °C to 90 °C.

After reaching the target temperature (90 °C), the flow is switched to pure N_2 (without CO_2), and the outlet concentration of the CO_2 due to desorption declines very quickly initially falling, and the observation suggests that a significant portion of the adsorbed CO_2 is rapidly eliminated from the solid sorbent as a result of enhanced thermal energy that break some intermolecular forces. The initial rapid desorption can be attributed to the disruption of the Van der Waals forces and other weak connections existing between CO_2 and the surface of the sorbent material. Then, the curves exhibit an extended tail indicating a decelerated residual CO_2 desorption mechanism, due to the decrease in the driving force (Raganati *et al.*, 2015). This demonstrates that a significant portion of the adsorbed CO_2 is initially released from the samples at a high rate.

Additionally, as shown in Figure 6.4 (a and b) the adsorption and desorption experiments were conducted isothermally at 40 °C (i.e., 40 °C was used in both the adsorption and desorption phases) applying two different methodologies. In order to investigate the instantaneous adsorption-desorption effect, the desorption process in Figure 6.4b was carried out at the same temperature as the adsorption process ($T_{ads} = T_{des} = 40°C$). This approach was designed to eliminate any time delay associated with heating the bed to the desired desorption temperature. The term "neglecting time identical to preheating" underscores the emphasis on minimizing time-related factors linked to temperature adjustments, thereby ensuring a smoother and more immediate transition between the adsorption and desorption phases. It was planned to act as an adsorption/desorption experiment at a high temperature ($T_{ads} = T_{des} = 40°C$) in order to understand the adsorption-desorption behaviour under extreme thermal conditions. As shown in Figure 6.1, the first study neglected the required preheating duration for desorption at a temperature of 90°C. However, the second experiment considered the preheating time (the extra 16 minutes), as shown in Figure 6.5. This experiment was deliberately performed longer to keep it similar to 90 °C experiments, as the bed is saturated rather quickly, and the temperature is back to 40 °C after around 3 minutes in particularly after the initial exotherm. The results of these tests indicated no impact on the desorption capacity and desorption rate when the temperature was maintained at a constant 40°C for a lengthy period, equivalent to the preheating duration of the desorption experiment at 90°C. Two of the experiments showed low recovery (around 7%). However, one significant difference here is that at a low temperature of 40 °C (both experiments), the BT curve is always very close to the inert curve, indicating a negligible amount of CO_2 is desorbed. Therefore, as expected, regeneration is hindered at low temperatures (i.e., 40 °C) because there is insufficient energy to break the adsorbent-adsorbate bonds (Mikhaylov *et al.*, 2018).

In a physical model analogy, envision a molecular-scale barrier representing the activation energy needed for CO2 desorption. At low temperatures, insufficient thermal energy hinders effective barrier crossing, impeding regeneration. Picture the adsorbent-adsorbate bonds as connections between two objects; these bonds become more flexible and easier to break at higher temperatures, facilitating CO2 release. The activation energy argument posits that, at low temperatures, the lack of energy obstructs bond breaking, resulting in observed low recovery rates. This concise model clarifies why regeneration is hindered at low temperatures in a tangible way. A distinct pattern is apparent when examining the BT at 40 °C, including

a rapid release phase. Compared to investigations performed at a higher temperature (90 °C), this phase occurs more rapidly. Moreover, there is a shortage of a "long tail," or what is commonly referred to as a "slow phase,", which appears in high-temperature desorption. The explanation for this behaviour is that in the initial phase at 40 °C, a significant proportion of free CO_2 molecules are released. This might be caused by low thermal energy obtained at low temperatures, not allowing CO_2 molecules to overcome the interaction between the adsorbent and adsorbate (Gunawan *et al.*, 2018).

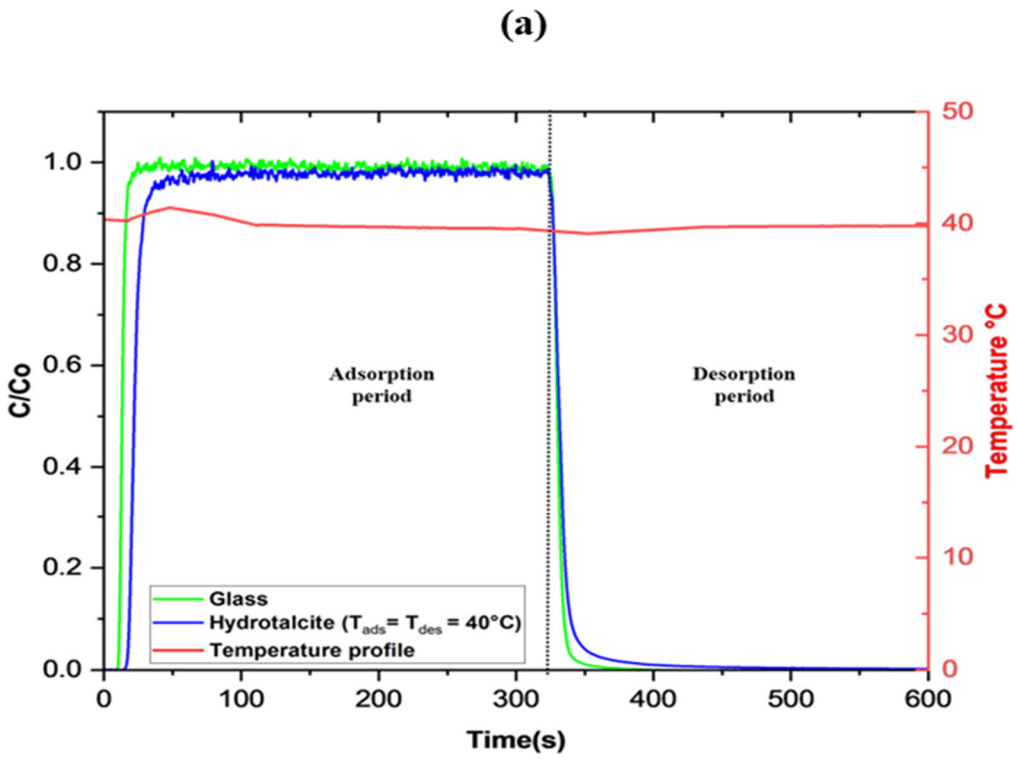

(b)

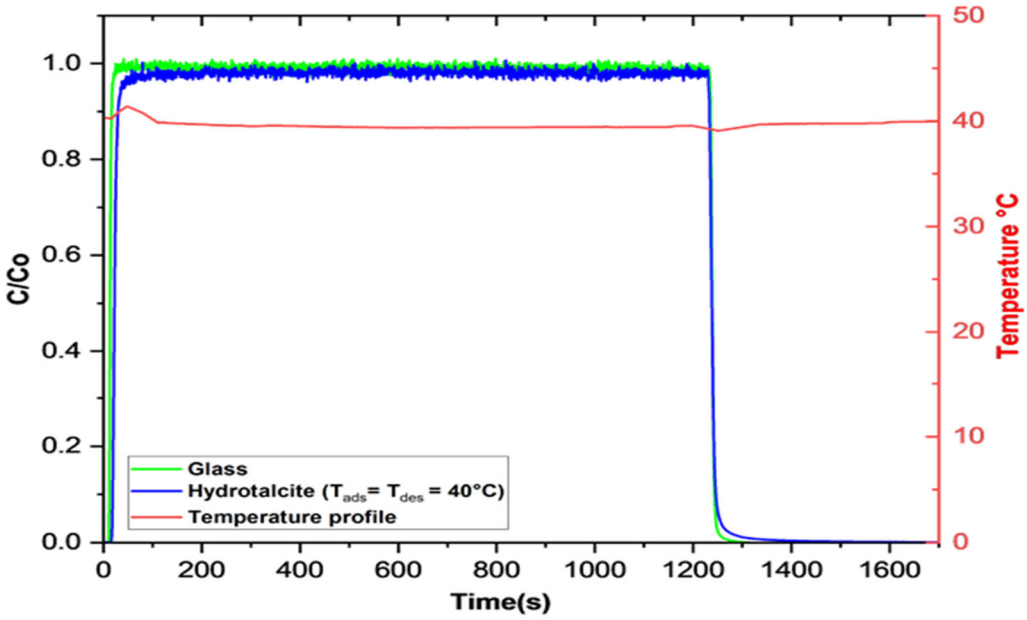

Figure 6.4. Example of CO_2 breakthrough curve as a function of time for isothermal adsorption/desorption temperature of 40 °C: (a) Adding (+16 minutes) the time needed for another experiment's preheating (+16 minutes); (b) Neglecting time identical to preheating.

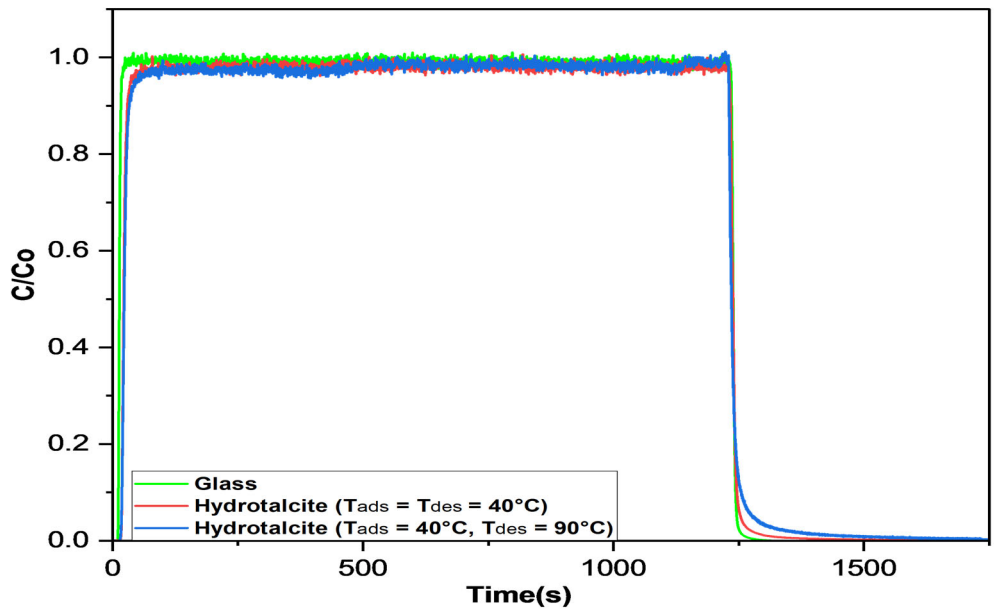

Figure 6.5. The CO_2 breakthrough curve as a function of time at two different desorption temperatures of 40 °C and 90 °C.

Figure 6.5 is showing the curves at these two temperatures to show these differences. One can use thermodynamics to explain the small differences in the desorption curve shapes; the wider the curve, the greater the amount of adsorption that can be produced (Figure 6.5). The rise in temperature from 40°C to 90°C leads to greater width of the desorption breakthrough curve primarily as a result of the elevated thermal energy of molecules. This heightened thermal energy enhances the ability to move of the molecules, hence assisting their desorption form the surface of the solid sorbent. These outcomes are similar to those in the literature (Verougstraete *et al.*, 2020; Wang and Zhu, 2021). Desorption rates are initially high for isothermal desorption experiments, then decline until they ultimately stabilise. However, longer desorption durations lead to extending the regeneration period, which may be adverse in practice.

6.4 Desorption Rate

Figure 6.6, display the average desorption rate and the proportion of CO_2 desorbed at each time point at two different desorption temperatures (40 and 90 °C). In this Figure the adsorption rate during the preheating stage is included to estimate possible undesirable desorption rate in this phase.

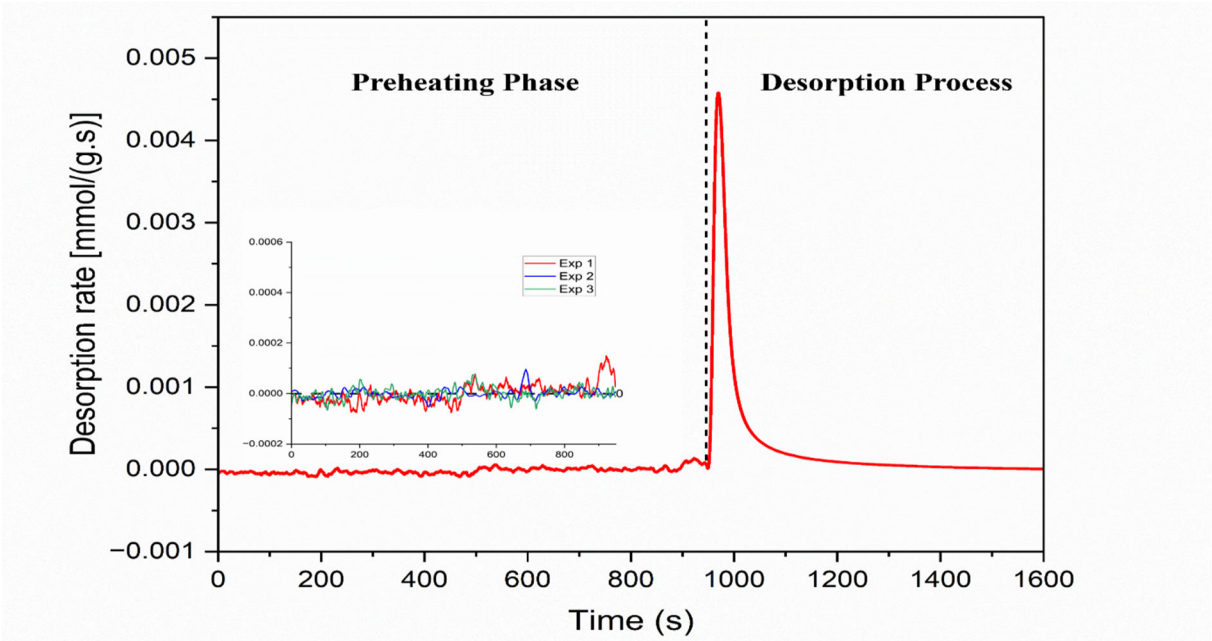

Figure 6.6. The desorption rate of CO_2 as a function of time during the preheating stage (40 to 90°C) and desorption stage (T_{ads}= 90°C).

As shown in Figure 6.6, it is evident that the desorption rate mostly fluctuates around the zero level during preheating phase. Therefore, the maximum desorption detected during this phase (preheating) constitutes about 2% (0.005 mmol/g) of the entire desorption (0.24 mmol/g), which may be considered data background noise. For the objectives of this investigation, disregard this minimal desorption and presume that no desorption occurred during the preheating phase although higher heating rates would be beneficial to eliminate this further.

As shown in Figure 6.7, it is evident that desorption happens quickly at a low temperature of 40 °C, which takes only about 120 seconds compared to 700 seconds at a higher temperature 90 °C (Figure 6.8). As shown in Figure 6.7(a), the desorption rate has a sharper peak (22s) and a reach a peak (0.0024 mmol/ (g.s)), which is lower rate in comparison to the desorption rate at the higher temperature of 90°C (80s) (Figure 6.8(a)). This could be due to a small quantity of carbon dioxide being desorbed at 40 °C. This behaviour may be explained as adsorption tends to occur rather than desorption at lower temperatures (40 °C) (Ben-Mansour and Qasem, 2018; Morales-Ospino *et al.*, 2020), attributed to the thermodynamic principle that favours adsorption over desorption, leading to reduced CO_2 desorption. However, the highest average desorption rate was reached within 40 seconds at high temperature to reach a peak (0.0046 mmol/ (g. s)) and a more extended desorption procedure (700 sec). This is mainly due to increased thermal energy from rising temperatures. Higher thermal energy gives adsorbed carbon dioxide molecules enough kinetic energy to overcome binding forces and detach from the surface. As a result, a greater percentage of carbon dioxide is released from the adsorbent material.

As shown in Figure 6.8a, the desorption rate is initially high due to a large concentration gradient and the thermal energy of the gas molecules, which facilitates the release of CO_2 molecules from the hydrotalcite surface. The experiment showed that 90% of the carbon dioxide (CO_2) desorption occurred within less than 90 seconds. Many CO_2 gas molecules aid the rapid early desorption rate in the adsorbate phase, which generates a significant driving force for desorption. The rate demonstrates an approximately constant rate of change throughout this initial period (there is an almost constant linear decline to about 10% of desorption). This stage requires around 90 seconds for desorption at high temperature. Nevertheless, the concentration gradient decreases with time, and the slope gradually changes, resulting in reduced CO_2 molecules accessible for separation. The diminishing desorption rate after the initial stage may be attributed to the weakened driving force for detachment arising from a decrease in the

number of gas molecules available for desorption. Therefore, following the initial, more rapid stage, the curves exhibit a long tail; the desorption rates decrease with increasing time until they become almost constant after 700 seconds.

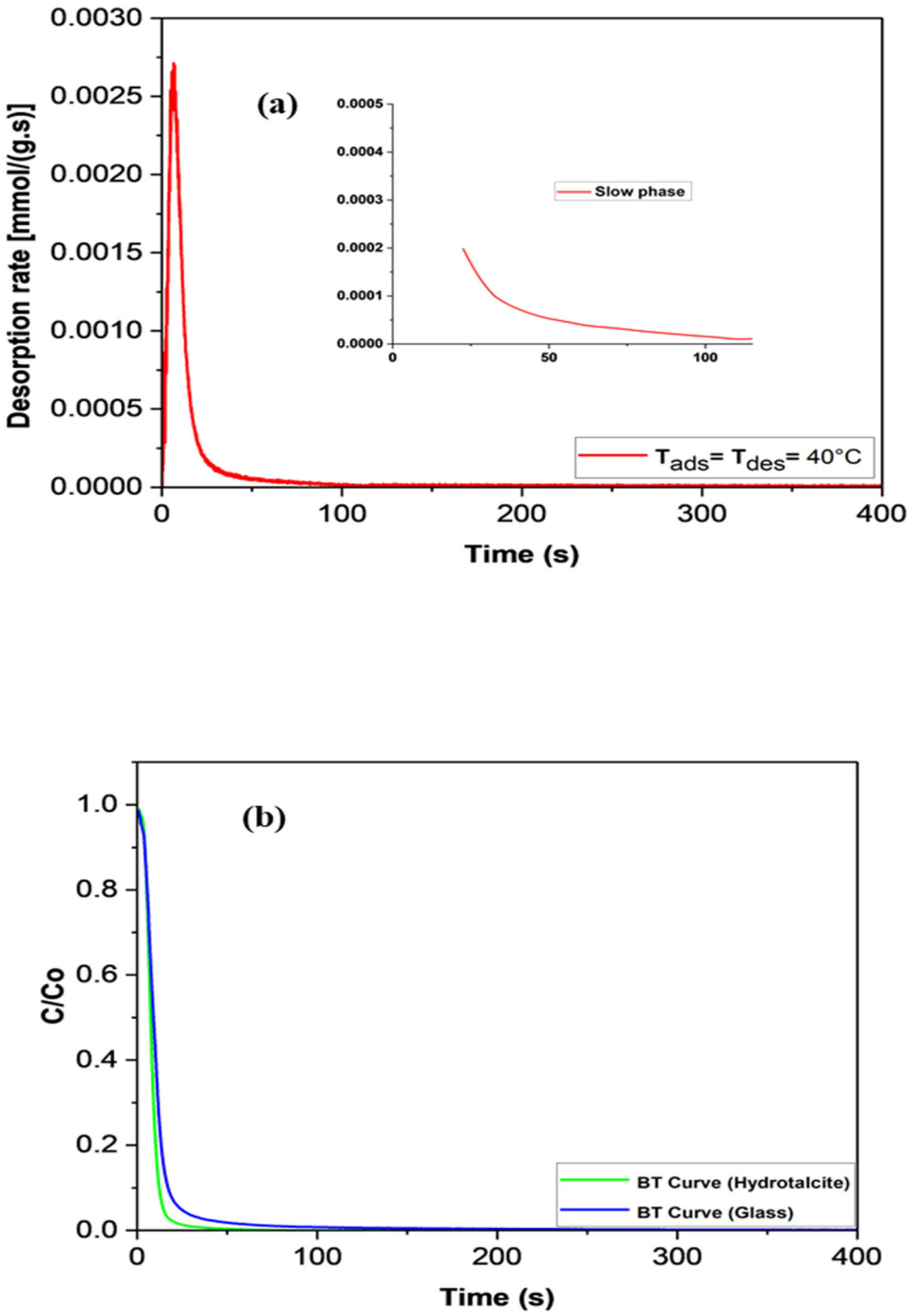

Figure 6.7. (a) The desorption rate of CO_2 as function of time at T_{des} = 40°C, showing slow phase. (b) Concentration profile of CO_2 during desorption step at T_{des}= 40°C.

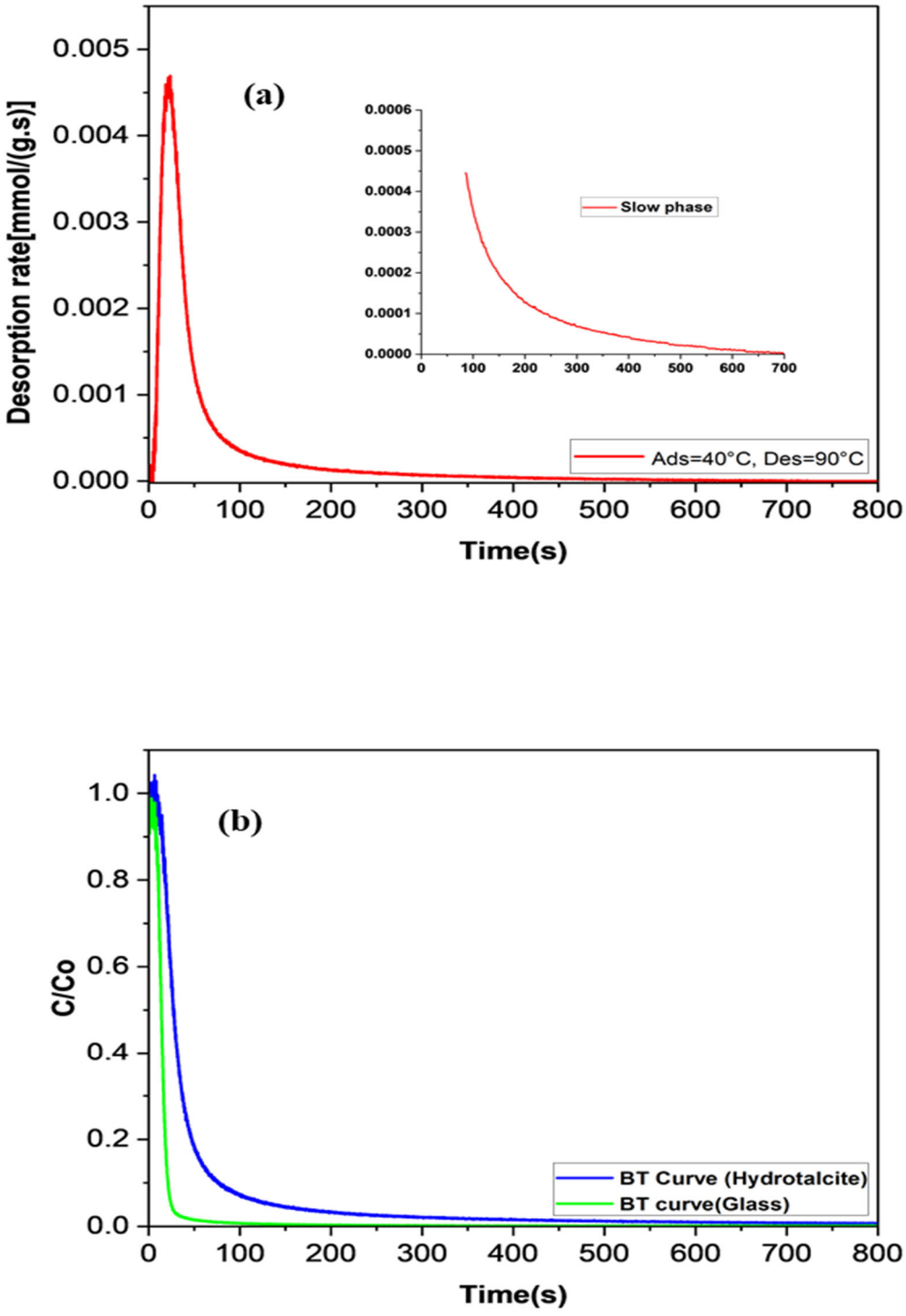

Figure 6.8. (a) The desorption rate of CO_2 as function of time at T_{des} = 90°C, showing slow phase. (b) Concentration profile of CO_2 during desorption step at T_{des} = 90°C.

As shown in Figure 6.9. increasing the temperature is one method for enhancing the desorption process performance. In terms of desorption capacity, removing CO_2 from the adsorbent is more efficient at higher desorption temperatures (Ntiamoah *et al.*, 2016; Verougstraete *et al.*, 2020). This is consistent with the results observed in this study and can be applied to Optimize the regeneration of the hydrotalcite material. The observed CO_2 recovery about 0.05 mmol/g which is less than 7 % at relatively low temperatures (i.e., 40 °C) because it is thermodynamically favourable for the CO_2 to adhere to hydrotalcite pores. Therefore, more CO_2 remains adsorbed and less is desorbed. At 90 °C, the recovery of CO_2 can be increased to approximately 33% of the CO_2 adsorbed, as shown in Figure 4, which is due to the increased thermal energy. With increasing desorption temperatures, the chemical potential difference between adsorbed CO_2 and the gas phase increases, driving more CO_2 release (Wurzbacher *et al.*, 2012; Wijesiri *et al.*, 2019). Moreover, a rising temperature changes the thermodynamic equilibrium, breaking the weaker Van der Waals forces or chemical bonds between CO_2 (Gunawan *et al.*, 2018) with the hydrotalcite surfaces, making it difficult for CO_2 to adhere to hydrotalcite pores. Therefore, more CO_2 is desorbed and less is adsorbed. Although a high recovery of CO_2 is not observed, higher temperatures promote the regeneration of the MFB (Weng *et al.*, 2018).

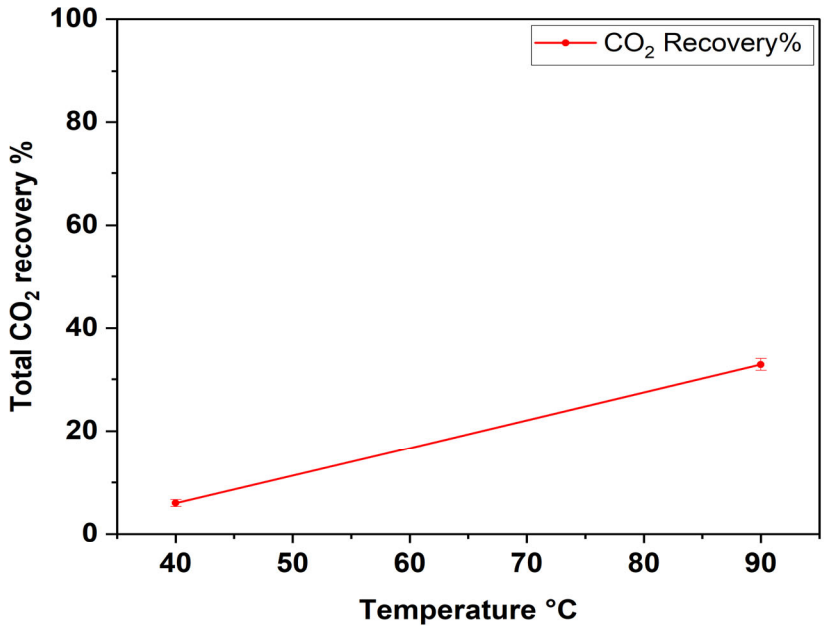

Figure 6.9. CO_2 recovery from Hydrotalcite as a function of desorption temperature.

6.4.1 Temperature Profile

Adsorption is exothermic because of the attractive forces and the creation of bonds between the adsorbent and the adsorbate. These interactions lead to a reduction in potential energy and increased stability. These variables influence the release of energy (heat) throughout adsorption. On the other hand, endothermic desorption entails the disruption of bonds between the surface of the adsorbent and the adsorbate, leading to a rise in potential energy as the atoms or molecules move away. This process reduces stability and increases disorder (entropy), requiring heat to surmount energy barriers and release CO_2 into the gaseous state (Hao *et al.*, 2021; Aumeier *et al.*, 2022).

Figure 6.3 shows the adsorption and desorption occurring at 40 and 90 °C, respectively. Figure 6.4 shows the adsorption and desorption occurring at the same temperature (i.e., 40 °C). In Figure 6.3 and 6.4, after injecting CO_2 into the system (adsorption stage), a positive heat flow (rising signal) appeared during the initial adsorption of CO_2 on hydrotalcite particles (1.4°C), for approximately 2 minutes, indicating an exothermic reaction. This is caused by the adsorption of CO_2 molecules onto the surfaces of hydrotalcite particles, forming Van der Waals forces and chemical bonds. Consequently, thermal energy was discharged into the surroundings (Wurzbacher *et al.*, 2012; Wijesiri *et al.*, 2019). After the adsorption step, the heating phase is initiated to obtain the desorption temperature. After approximately 16 minutes of waiting, the desired temperature of 90 °C was finally reached. Then, at approximately 21 minutes, a negative heat flow (a downward signal) at 90 °C indicated the endothermic reaction (0.6 °C) and release of CO_2 from the hydrotalcite. It appears that there are two temperature drops during desorption, indicating that after an initial period of rapid desorption, the rate of desorption slows over time. The endothermic reaction occurs because the bonds break between the CO_2 molecules and the surfaces of the hydrotalcite particles. Conversely, in Figure 6. 4, for adsorption and desorption at 40 °C, the same pattern occurred during adsorption, exhibiting a positive signal (exothermic reaction (1.4°C)), whereas a negative heat flow (endothermic reaction) was observed as being tiny (0.2 °C) due to very low desorption at that temperature.

6.5 Summary

An MFB combined with the hydrotalcite adsorbent was used in this study to examine the effects of temperature on the adsorption and desorption processes. TSA is used for desorption experiments and obtaining the BT curves. The solid sorbent particles were fully saturated with CO_2 before each desorption test, and 16 vol % CO_2, $U_g = 4U_{mf}$, and 40°C were the optimal conditions for adsorption. Considering the limitations, a desorption temperature range of 40–90 °C was selected. The effect of desorption temperatures on description capacity was studied. Rising temperatures often result in enhanced desorption efficiencies as a consequence of increased movement of molecules and decreased adsorbent-adsorbate interactions. Indeed, it was shown that the hydrotalcite's ability for desorption increased along with the increase in temperature. This is explained by the thermal energy present at high temperatures, which facilitates the desorption process. The thermodynamic equilibrium that causes CO_2 to stick to hydrotalcite pores reduced the CO_2 recovery to 16% at lower temperatures. At 90°C, the CO_2 recovery reached 33% of the adsorbed CO_2. Thus, raising the desorption temperature changes the thermodynamic equilibrium, making it easier to detach CO_2 molecules from hydrotalcite pores and helping CO_2 overcome weaker Van der Waals forces or chemical interactions with the surfaces. Hydrotalcite's heat stability makes regeneration more difficult at 40 °C. The BT curves suggest that raising the temperature to 90°C the mass-transfer higher because the increased temperature may help overcome the activation energy for desorption, improving the desorption capacity. Additionally, the desorption process is endothermic, and a signal drop is observed, whereas the adsorption process is exothermic and releases heat energy. This confirms that heat is produced as a consequence of the adsorption reaction. At the onset, the rate of desorption was high. Over time, the rate of desorption displayed a progressive decline. The diminishing desorption rate may be attributed to the weakened driving force for detachment, arising from a decrease in the number of gas molecules available for desorption. Finally, 3D-printed micro fluidised beds are regarded as promising instruments for desorption research. Nonetheless, a number of essential considerations must be kept in account. One of these factors is the desired temperature, which can be difficult to attain. However, it should be noted that using materials with high thermal conductivity might help attain the desirable temperature for these types of research.

Chapter 7. Conclusion

7.1 Conclusion

Due to the many benefits of micro-fluidised bed reactor (MFBR) technology such as their low sorbent quantity requirements, enhanced safety, low costs, minimal energy consumption, and high mass and heat transfer properties (Jiang *et al.*, 2020; Han *et al.*, 2021; Qie *et al.*, 2022), they have been suggested as an appropriate system to investigate gas/solid reaction kinetics. Consequently, this research aimed to develop an MFBR as a platform for the low-cost, fast screening of CO_2 adsorbents under real-world conditions for decision-making purposes.

In the present investigation, the performance of commercial hydrotalcite was investigated due to several benefits such as high CO_2 selectivity, fast adsorption and desorption kinetics, high CO_2 adsorption capacity, rapid and moderate conditions for regeneration, high cost efficiency and thermal/mechanical stability for circulation between adsorption and desorption processes (Rossi *et al.*, 2016; Dębek *et al.*, 2017; Suescum-Morales *et al.*, 2022). This hydrotalcite product was investigated in 3D-printed micro-fluidised beds with diameters ranging from 10 to 15 mm. These were chosen based on achieving a compromise between reducing the quantity of material required for use in the bed to decrease waste and ensuring that sufficient material existed to detect meaningful reaction kinetics during subsequent CO_2 breakthrough tests (*i.e.* ensuring a good signal to noise ratio).

Although hydrotalcites are a promising candidate for CO_2 capture, their inter-particle solid forces result in considerable agglomeration and poor fluidisation quality when using micro-fluidised bed technology. Therefore, an initial hydrodynamic study aimed to identify suitable low-cost treatments enabling the fluidisation of these cohesive hydrotalcite particles in a micro-fluidised bed (MFB) and, thereafter, to explore the hydrodynamics of these hydrotalcite granules in different 3D-printed MFB configurations by measuring the effects of gas velocity, bed diameter, particle size, and static bed height on the pressure drop. Subsequently, the optimal fluidisation conditions and regime transitions that occurred could be determined.

The hydrodynamic screening work was conducted using the pressure drop characterisation method, with the results indicating that the initial fluidisation quality of the raw powder was poor, with large portions of the bed remaining unfluidised due to the dominance of the particle-

particle cohesive interactions. Sieving was the straightforward approach to remove fine particles (retaining sizes of >53 μm; density of 2 g/cm^3), which substantially improved the fluidisation quality. The results confirm that wall effects and cohesive/adhesive forces significantly impact the hydrodynamic performance of the MFBR, as evidenced by the delayed onset of fluidisation, the emergence of a significant pressure drop overshoot prior to fluidisation, and the delayed onset of bubbling. Pressure overshoot analysis provides information on the hysteresis pattern usually found in micro-fluidisation experiments. The overshoot could have occurred from the formation of liquid bridges in the bed through the absorption of atmospheric humidity over time. This indicates that the primary factor influencing the fluidisation quality could be particle-particle forces rather than wall effects. In addition, further analysis of the pressure overshoot and wall effects reveals that fluidisation substantially improves the fluidisation quality, possibly due to the elimination of liquid bridges. Further, after mixing the hydrotalcite powder with a second Geldart A particle (silica; 93 ± 10 μm; density of 2.65 g/cm^3), the micro-fluidisation properties, such as high-pressure overshoot, were diminished, and fluidisation significantly improves the quality of fluidisation. In these experiments, a silica particle type was chosen due to its cost-effectiveness and availability, adjustable particle size and density, surface properties, and chemical inertness. The addition of silica with cohesive hydrotalcite particles leads to better overall fluidisation performance and more efficient industrial processes. However, this may pose a problem when using a mixture for screening designs for kinetic models, mainly when the secondary particle is not truly inert to the reaction of interest. Therefore, only pre-sieving and pre-fluidisation treatments were used thereafter to identify the optimum fluidisation regime for kinetic screening. The experimental minimum and bubbling fluidisation velocities are similar to those obtained from empirical correlations and enabled the selection of appropriate gas velocities to achieve the desirable bubbling behaviour (corresponding to $U_g = 4U_{mf}$).

After identifying suitable conditions for kinetics screening from the hydrodynamic experiments, the next research objective was addressed: screening the CO_2 adsorption kinetics of hydrotalcite in the 3D-printed MFB utilising breakthrough experiments, including studying the influence of superficial gas velocity (1.5 to 6 U_{mf}), CO_2 concentration (8 to 16 vol%), temperature (25 to 60 °C), and bed loading (bed-height-to-particle-diameter ratio of Hs/Dt = 2–3). The gas velocities encompassed both bubbling and slugging regimes, enabling the examination of the influence of the fluidisation regime on the kinetics. The CO_2

concentration ranged from 8% to 16% vol%, which represented diverse carbon capture sources and ensured that it was applicable in a variety of situations. The temperature range was between 25 °C and 60 °C, which helped to determine the stability, kinetics, and capacity of the adsorbent material under varying operational conditions (the design temperature was 40 °C). Incorporating these conditions into the experiment provided a comprehensive analysis of the behaviour of the material, thereby shedding light on its potential for effective carbon capture in a variety of real-world scenarios.

The results reveal that in a bubbling regime, raising the superficial gas velocity enhances gas–solid mixing and decreases the breakthrough time, allowing for the measurement of the actual adsorption capacity. Increasing the gas velocity during the bubbling fluidisation regime has the potential to enhance the measured adsorption capacity for several reasons. Firstly, the heightened presence of bubbles within the micro-fluidised bed results in an increased interfacial area, creating more contact points between the adsorbent material and the gas. This expanded interfacial area fosters a heightened interaction between gas molecules and the adsorbent material, consequently elevating adsorption rates. Furthermore, the dynamic environment filled with bubbles facilitates more efficient mass transfer between the gas and adsorbent phases. Additionally, higher gas velocities promote increased interaction between solid particles and gas, leading to the accelerated mass transfer of CO_2 to the hydrotalcite sites. In summary, elevating gas velocity within the bubbling regime improves interfacial area, mixing, and mass transfer, collectively resulting in an enhanced apparent adsorption capacity.

The maximum adsorption capacity measured in the fluidised bed was consistent with independent TGA measurements performed by the Research Centre for Carbon Solutions. The results indicate a maximum capacity of 0.74 mmol/g during the bubbling operation regime at 16 vol% CO_2 concentration, gas flow rate of 4 U_{mf}, and bed height of Hs/Dt = 2. The maximum capacity is not achieved at lower gas flow velocities (<3U_{mf}) due to insufficient gas–solid mixing, nor higher gas velocities (>4U_{mf}) due to gas bypassing caused by slugging. Using a CO_2 concentration of 8 vol%, the maximum capacity was obtained at flow rates of 3 and 4 U_{mf} at Hs/Dt = 2 and 3, respectively. After increasing the concentration to 16 vol%, the range of optimum operating conditions expanded to include (3–4U_{mf}) with Hs/Dt = 2. The increase can be attributed to the enhancement of internal diffusion within the pores, which effectively

maintains the adsorption process in a state where the adsorbent is kinetically rather than diffusion limited.

Moreover, the optimal temperature for the investigated adsorption-specific hydrotalcite was 40 °C, at which the highest adsorption capacities were observed under all tested conditions. The adsorption activation energy dominates below this temperature, while at temperatures higher than 40°C, CO_2 binds less strongly to the active sites. In addition, the experimental CO_2 adsorption trajectories were further analysed by applying three distinct kinetic models: pseudo-first-order, pseudo-second order, and fractional order. Among all the tested conditions, the fractional order model provided the best fit to the experimental data, as measured by a higher R^2 value and ability to capture the 'S'-shape of the adsorption curve. This demonstrates the significance of incorporating hydrodynamic screening into the materials development workflow utilizing the MFBR platform.

The last research objective was to study the desorption kinetics via the TSA approach. The final research objective was to investigate desorption kinetics using the TSA approach. The experiments were performed using the temperature swing adsorption (TSA) technique because it typically has a reduced regeneration time and energy consumption compared to pressure swing adsorption and vacuum swing adsorption (Jiang *et al.*, 2020). Desorption temperatures of 40 and 90 °C were selected because the MFB's relies on gas-solid heat transfer to heat the material, which was impacted by the low flow rates used in this study. Initially, heating the bed was performed by placing a heater around the MFB without injecting fluidising gas to distribute the heat. This was challenging due to the low thermal conductivity of the MFB material (a high-temperature polymer); the polymer tended to burn before the particles inside reached the desired setpoint desorption temperature. Moreover, delivering heat using only a heater cable around the MFB leads to an irregular distribution of heat, resulting in localised heated spots and variations in temperature. Therefore, besides the additional external heater cable, injecting a fluidising gas at a suitable flow rate (4 U_{mf}) into the MFB system throughout the heating process is necessary to avoid these limitations and to help distribute the heat more uniformly and efficiently.

The result showed that, due to inadequate thermal mass of the inlet gas, desorption of only approximately 35% of the adsorbed CO_2 gas was possible at 90 °C. At lower temperatures, the intermolecular interactions binding the CO_2 molecules to the adsorbent surface are stronger, thereby limiting the desorption forces. To improve CO_2 recovery in MFBs, increasing the

desorption temperature is required. This is possible when employing alternative MFB materials with a higher thermal conductivity, such as copper or stainless steel, which must be considered in the future to improve heat transfer and prevent material degradation.

In conclusion, the results indicate that the hydrotalcite effectively adsorbed CO_2 and could be partially regenerated within the limitations of the 3D printed polymer material. Based on the results presented in this thesis, it can be concluded that 3D-printed MFBs can be applied to adsorption experiments to develop carbon capture sorbents, thus offering insights for decision-making and design purposes. However, the limited desorption kinetics results in an insufficient understanding of the desorption kinetics and therefore may result in an insufficient assessment of desorption performance given the current capabilities of desktop scale 3D printing.

7.2 Recommendations and Future Work

7.2.1 Circulating Fluidised Beds

Due to the advantages of MFBs, the present research used semi-batch MFB technology for studying cohesive powders for carbon capture where a batch of material was contacted with a continuous gas flow. In the context of encouraging future research directions, future work could focus on developing experimental designs that shift from conventional batch testing to continuous evaluation of adsorption and desorption processes. This shift towards spontaneous and real-time assessment of phenomena could reveal complex behaviours and kinetics that were previously intractable during batch experimental settings. Development of a micro circulating fluidised bed for screening the adsorption and desorption behaviour of CO_2 capture is likely to overcome the disadvantages of a batch MFB, including its poor productivity and regular reloading requirements. The proposed design of the CMFB necessitates the optimization of fluidisation dynamics, the incorporation of a particle interlock (e.g., cyclone), meticulous selection of adsorbents, and the capacity to process continuous data for enhanced insights. This sentence provides additional detail about the purpose and significance of the particle interlock design in the CMFB, emphasizing its role in maintaining stable and efficient fluidisation dynamics.

This type of CMFB platform could help move carbon capture research forward by giving a full picture of how adsorbents behave in conventional circulating fluidised beds. This study would include hydrodynamic analysis to identify a fast fluidisation regime to ensure the particles are fluidised properly. Moreover, the cyclone design and loop seal are essential parts of the circulating micro fluidised bed as well as the heating system design. The effects of different operating conditions (gas flow rate, gas composition, temperature, etc) could be studied to screen the feasibility of solid adsorbents for a CO_2 capture system and regeneration of the sorbent simultaneously.

7.2.2 Direct Air Capture

In the context of future avenues of study for this project, one novel pathway is the use of micro fluidised beds (MFBs) in direct air capture (DAC). The comprehensive examination of catalyst materials and reactions in the MFB, or a CMFB, may provide valuable insights that may be applied to remove pollution gases from the atmosphere. This approach has an opportunity to contribute towards the progression of carbon capture technology and the mitigation of global carbon emissions to help meet the Net Zero goal.

7.2.3 New Methods for Desorption

In order to achieve higher operational temperatures for the desorption process, the application of metal 3D-printing becomes appealing. *E.g.,* the 3D printing of stainless steel would improve the thermal conductance of the reactor, and this material is already extensively used in industry meaning the data would be more transferable. Overall, this modification would enable heat to be transferred quickly through the MFB system to attain higher temperatures that can be maintained for longer periods of time; both of which are necessary in order for CO_2 to be released from the adsorbent. Additionally, the applicability of this method extends beyond carbon capture to other sectors requiring precise temperature management. This trajectory can potentially develop desorption processes, improve overall system performance, and provide helpful insights into the function of temperature on the desorption kinetics. Moreover, vacuum fluidisation and other systems like microwaves could also be used for desorption or a combination of them.

References

Abd, A.A., Othman, M.R. and Helwani, Z. (2021) 'Evaluation of thermal effects on carbon dioxide breakthrough curve for biogas upgrading using pressure swing adsorption', *Energy Conversion and Management*, 247, p. 114752.

Abdus-Salam, N. and Buhari, M. (2016) 'Adsorption of Alizarin and Fluorescein Dyes onto Palm Seeds Activated Carbon: Kinetic and Thermodynamic Studies', *Journal of the Chemical Society of Pakistan*, 38(4).

Abid, H.R., Iglauer, S., Al-Yaseri, A. and Keshavarz, A. (2021) 'Drastic enhancement of CO_2 adsorption capacity by negatively charged sub-bituminous coal', *Energy*, 233, p. 120924.

Abraham, B., Asbury, J., Lynch, E. and Teotia, A.P. (1982) 'Coal-oxygen process provides CO/sub 2/for enhanced recovery', *Oil Gas J.;(United States)*, 80(11).

Adamu, A., Russo-Abegão, F. and Boodhoo, K. (2020) 'Process intensification technologies for CO_2 capture and conversion – a review', *BMC Chemical Engineering*, 2(1), p. 2.

Aguilera, P. and Ortiz, F.G. (2016) 'Prediction of fixed-bed breakthrough curves for H2S adsorption from biogas: Importance of axial dispersion for design', *Chemical Engineering Journal*, 289, pp. 93-98.

Ahn, J.H. and Kim, T.S. (2020) 'Effect of oxygen supply method on the performance of a micro gas turbine-based triple combined cycle with oxy-combustion carbon capture', *Energy*, 211.

Ajbar, A., Bakhbakhi, Y., Ali, S. and Asif, M. (2011) 'Fluidization of nano-powders: Effect of sound vibration and pre-mixing with group A particles', *Powder Technology*, 206(3), pp. 327-337.

Akpasi, S.O. and Isa, Y.M. (2022) 'Effect of operating variables on CO_2 adsorption capacity of activated carbon, kaolinite, and activated carbon–Kaolinite composite adsorbent', *Water-Energy Nexus*, 5, pp. 21-28.

Alamri, A., McDonough, J. and Zivkovic, V. (2023) 'Fluidisation behaviour and wall effects of cohesive hydrotalcite powder in a micro-fluidised bed', *Powder Technology*, 415, p. 118192.

Allangawi, A., Alzaimoor, E.F., Shanaah, H.H., Mohammed, H.A., Saqer, H., El-Fattah, A.A. and Kamel, A.H. (2023) 'Carbon Capture Materials in Post-Combustion: Adsorption and Absorption-Based Processes', *C*, 9(1), p. 17.

Álvarez, N., Gil, M.V., Rubiera, F. and Pevida, C. (2017) 'Kinetics of CO_2 adsorption on cherry stone-based carbons in CO_2/CH_4 separations', *Chemical Engineering Journal*, 307, pp. 249-257.

Amiri, M. and Shahhosseini, S. (2018) 'Optimization of CO_2 capture from simulated flue gas using K_2CO_3/Al_2O_3 in a micro fluidized bed reactor', *Energy & Fuels*, 32(7), pp. 7978-7990.

Ammendola, P., Raganati, F. and Chirone, R. (2015) 'Effect of operating conditions on the CO_2 recovery from a fine activated carbon by means of TSA in a fluidized bed assisted by acoustic fields', *Fuel Processing Technology*, 134, pp. 494-501.

Ammendola, P., Raganati, F. and Chirone, R. (2017) 'CO_2 adsorption on a fine activated carbon in a sound assisted fluidized bed: Thermodynamics and kinetics', *Chemical Engineering Journal*, 322, pp. 302-313.

Ania, C., Parra, J., Menéndez, J. and Pis, J. (2005) 'Effect of microwave and conventional regeneration on the microporous and mesoporous network and on the adsorptive capacity of activated carbons', *Microporous and Mesoporous Materials*, 85(1-2), pp. 7-15.

Anwar, M.N., Fayyaz, A., Sohail, N.F., Khokhar, M.F., Baqar, M., Khan, W.D., Rasool, K., Rehan, M. and Nizami, A.S. (2018) 'CO_2 capture and storage: A way forward for sustainable environment', *J Environ Manage*, 226, pp. 131-144.

Aschenbrenner, O., McGuire, P., Alsamaq, S., Wang, J., Supasitmongkol, S., Al-Duri, B., Styring, P. and Wood, J. (2011) 'Adsorption of carbon dioxide on hydrotalcite-like compounds of different compositions', *Chemical Engineering Research and Design*, 89(9), pp. 1711-1721.

Asenjo, N.G., Álvarez, P., Granda, M., Blanco, C., Santamaría, R. and Menéndez, R. (2011) 'High performance activated carbon for benzene/toluene adsorption from industrial wastewater', *Journal of hazardous materials*, 192(3), pp. 1525-1532.

Aumeier, B.M., Augustin, A., Thönes, M., Sablotny, J., Wintgens, T. and Wessling, M. (2022) 'Linking the effect of temperature on adsorption from aqueous solution with solute dissociation', *Journal of Hazardous Materials*, 429, p. 128291.

Bahramian, A. and Olazar, M. (2021) 'Evaluation of elastic and inelastic contact forces in the flow regimes of Titania nanoparticle agglomerates in a bench-scale conical fluidized bed: A comparative study of CFD-DEM simulation and experimental data', *Chemical Engineering Research and Design*, 176, pp. 34-48.

Bai, Y., Zhao, P., Guo, M., Yan, G., Zhou, C., Sun, Z., Gao, T. and Zhang, B. (2023) 'Apparent viscosity of high-density fluidized bed and synergistic effect of density and apparent viscosity on particle separation', *Energy Sources, Part A: Recovery, Utilization, and Environmental Effects*, 45(2), pp. 4822-4838.

Ben-Mansour, R., Habib, M., Bamidele, O., Basha, M., Qasem, N., Peedikakkal, A., Laoui, T. and Ali, M. (2016) 'Carbon capture by physical adsorption: materials, experimental investigations and numerical modeling and simulations–a review', *Applied Energy*, 161, pp. 225-255.

Ben-Mansour, R. and Qasem, N.A. (2018) 'An efficient temperature swing adsorption (TSA) process for separating CO_2 from CO_2/N_2 mixture using Mg-MOF-74', *Energy Conversion and Management*, 156, pp. 10-24.

Benmahdi, F., Semra, S., Haddad, D., Mandin, P., Kolli, M. and Bouhelassa, M. (2019) 'Breakthrough curves analysis and statistical design of phenol adsorption on activated carbon', *Chemical Engineering & Technology*, 42(2), pp. 355-369.

Bérard, A., Blais, B. and Patience, G.S. (2021) 'Fluidized bed hydrodynamic modeling of CO_2 in syngas: Distorted RTD curves due to adsorption on FCC', *AIChE Journal*.

Bhatta, L.K.G., Subramanyam, S., Chengala, M.D., Olivera, S. and Venkatesh, K. (2015) 'Progress in hydrotalcite like compounds and metal-based oxides for CO_2 capture: a review', *Journal of Cleaner Production*, 103, pp. 171-196.

Bi, H.T. and Grace, J.R. (1995) 'Flow regime diagrams for gas-solid fluidization and upward transport', *International Journal of Multiphase Flow*, 21(6), pp. 1229-1236.

Biniek, K., Henderson, K., Rogers, M. and Santoni, G. (2020) 'Driving CO_2 emissions to zero (and beyond) with carbon capture, use, and storage', *McKinsey Quarterly*.

Bizhaem, H.K. and Tabrizi, H.B. (2013) 'Experimental study on hydrodynamic characteristics of gas–solid pulsed fluidized bed', *Powder technology*, 237, pp. 14-23.

Boonchuay, A. and Worathanakul, P. (2022) 'The diffusion behavior of CO_2 adsorption from a CO_2/N_2 gas mixture on zeolite 5A in a fixed-bed column', *Atmosphere*, 13(4), p. 513.

Bruni, G., Lettieri, P., Newton, D. and Barletta, D. (2007) 'An investigation of the effect of the interparticle forces on the fluidization behaviour of fine powders linked with rheological studies', *Chemical Engineering Science*, 62(1-2), pp. 387-396.

Cann, D., Font-Palma, C. and Willson, P. (2021) 'Moving packed beds for cryogenic CO_2 capture: analysis of packing material and bed precooling', *Carbon Capture Science & Technology*, 1.

Chaiw, Y.N., Ang, K.K., Lee, T. and Lim, X.Y. (2016) 'Investigation of the Coffee Waste-Derived Adsorbent', *J. Eng. Sci. Technol*, (2), p. 16.

Chalermsinsuwan, B., Piumsomboon, P. and Gidaspow, D. (2010) 'A computational fluid dynamics design of a carbon dioxide sorption circulating fluidized bed', *AIChE journal*, 56(11), pp. 2805-2824.

Chao, C., Deng, Y., Dewil, R., Baeyens, J. and Fan, X. (2021) 'Post-combustion carbon capture', *Renewable and Sustainable Energy Reviews*, 138, p. 110490.

Chen, C., Werther, J., Heinrich, S., Qi, H.-Y. and Hartge, E.-U. (2013) 'CPFD simulation of circulating fluidized bed risers', *Powder Technology*, 235, pp. 238-247.

Chladek, J., Jayarathna, C.K., Moldestad, B.M.E. and Tokheim, L.-A. (2018) 'Fluidized bed classification of particles of different size and density', *Chemical Engineering Science*, 177, pp. 151-162.

Choi, J.H., Son, J.E. and Kim, S.D. (1988) 'Bubble size and frequency in gas fluidized beds', *Journal of chemical engineering of Japan*, 21(2), pp. 171-178.

Choi, S., Drese, J.H. and Jones, C.W. (2009) 'Adsorbent materials for carbon dioxide capture from large anthropogenic point sources', *ChemSusChem: Chemistry & Sustainability Energy & Materials*, 2(9), pp. 796-854.

Coenen, K., Gallucci, F., Hensen, E. and van Sint Annaland, M. (2019) 'Kinetic model for adsorption and desorption of H_2O and CO_2 on hydrotalcite-based adsorbents', *Chemical Engineering Journal*, 355, pp. 520-531.

Cornelius Emeka Agu, L.A.T., Marianne Eikeland, Britt M.E. Moldestad (2017) 'Determination of onset of bubbling and slugging in a fluidized bed using a dual-plane electrical capacitance tomography system', *Chemical Emgineering Journal*, 328, p. 12.

Cousins, A., Wardhaugh, L.T. and Feron, P.H.M. (2011) 'A survey of process flow sheet modifications for energy efficient CO_2 capture from flue gases using chemical absorption', *International Journal of Greenhouse Gas Control*, 5(4), pp. 605-619.

D. G. Dimattia, P.R.A., F. Hamdullahpur (1997) 'Slugging characteristics of group d particles in fluidized beds', *Can. J.Chem. Eng.*, 75, p. 8.

D.Geldart, J.B. (1974) 'An investigation into slugging fluidized beds', *Chemical Engineering Science*, 29, p. 11.

Dang, N.T.Y., Gallucci, F. and van Sint Annaland, M. (2014) 'An experimental investigation on the onset from bubbling to turbulent fluidization regime in micro-structured fluidized beds', *Powder Technology*, 256, pp. 166-174.

Daniel, S. and Thomas, S. (2020) 'Layered double hydroxides: fundamentals to applications', in *Layered double hydroxide polymer nanocomposites*. Elsevier, pp. 1-76.

Dantas, T.L.P., Amorim, S.M., Luna, F.M.T., Silva, I.J., de Azevedo, D.C.S., Rodrigues, A.E. and Moreira, R.F.P.M. (2010) 'Adsorption of Carbon Dioxide onto Activated Carbon and Nitrogen-Enriched Activated Carbon: Surface Changes, Equilibrium, and Modeling of Fixed-Bed Adsorption', *Separation Science and Technology*, 45(1), pp. 73-84.

Darde, V., Thomsen, K., van Well, W.J. and Stenby, E.H. (2009) 'Chilled ammonia process for CO_2 capture', *Energy procedia*, 1(1), pp. 1035-1042.

Das, D., Behera, S.K. and Meikap, B. (2019) 'Removal of CO_2 in a multistage fluidized bed reactor by amine impregnated activated carbon: optimization using response surface methodology', *International Journal of Coal Science & Technology*, 6, pp. 445-458.

Dębek, R., Motak, M., Grzybek, T., Galvez, M.E. and Da Costa, P. (2017) 'A short review on the catalytic activity of hydrotalcite-derived materials for dry reforming of methane', *Catalysts*, 7(1), p. 32.

Deen, N., Annaland, M.V.S., Van der Hoef, M.A. and Kuipers, J. (2007) 'Review of discrete particle modeling of fluidized beds', *Chemical engineering science*, 62(1-2), pp. 28-44.

Dhoke, C., Zaabout, A., Cloete, S. and Amini, S. (2021) 'Review on reactor configurations for adsorption-based CO_2 capture', *Industrial & Engineering Chemistry Research*, 60(10), pp. 3779-3798.

Dietrich, F., Schöny, G., Fuchs, J. and Hofbauer, H. (2018) 'Experimental study of the adsorber performance in a multi-stage fluidized bed system for continuous CO_2 capture by means of temperature swing adsorption', *Fuel Processing Technology*, 173, pp. 103-111.

Do Nascimento, O.L., Reay, D.A. and Zivkovic, V. (2016) 'Influence of surface forces and wall effects on the minimum fluidization velocity of liquid-solid micro-fluidized beds', *Powder Technology*, 304, pp. 55-62.

Evans, D.G. and Slade, R.C. (2006) 'Structural aspects of layered double hydroxides', *Layered double hydroxides*, pp. 1-87.

Fanucci, J.B., Ness, N. and Yen, R.-H. (1979) 'On the formation of bubbles in gas-particulate fluidized beds', *Journal of Fluid Mechanics*, 94(2), pp. 353-367.

Font-Palma, C., Cann, D. and Udemu, C. (2021) 'Review of Cryogenic Carbon Capture Innovations and Their Potential Applications', *C*, 7(3), p. 58.

Formisani, B., De Cristofaro, G. and Girimonte, R. (2001) 'A fundamental approach to the phenomenology of fluidization of size segregating binary mixtures of solids', *Chemical Engineering Science*, 56(1), pp. 109-119.

Fuchs, J., Schmid, J.C., Müller, S. and Hofbauer, H. (2019) 'Dual fluidized bed gasification of biomass with selective carbon dioxide removal and limestone as bed material: A review', *Renewable and Sustainable Energy Reviews*, 107, pp. 212-231.

Funazukuri, T., Hudgins, R. and Silveston, P. (1986) 'Product distribution in pyrolysis of cellulose in a microfluidized bed', *Journal of analytical and applied pyrolysis*, 9(2), pp. 139-158.

Geng, S., Han, Z., Yue, J., Li, Y., Zeng, X., Lai, D., Yu, J. and Xu, G. (2018) 'Conditioning micro fluidized bed for maximal approach of gas plug flow', *Chemical Engineering Journal*, 351, pp. 110-118.

Girimonte, R., Formisani, B. and Testa, F. (2017) 'Adsorption of CO_2 on a confined fluidized bed of pelletized 13X zeolite', *Powder Technology*, 311, pp. 9-17.

Girimonte, R., Testa, F., Turano, M., Leone, G., Gallo, M. and Golemme, G. (2022) 'Amine-Functionalized Mesoporous Silica Adsorbent for CO_2 Capture in Confined-Fluidized Bed: Study of the Breakthrough Adsorption Curves as a Function of Several Operating Variables', *Processes*, 10(2), p. 422.

González, G., Herrera, G., Garcı, x, a, M.T. and Peña, M. (2001) 'Biodegradation of phenolic industrial wastewater in a fluidized bed bioreactor with immobilized cells of Pseudomonas putida', *Bioresource Technology*, 80(2), pp. 137-142.

Gopan, A., Kumfer, B.M., Phillips, J., Thimsen, D., Smith, R. and Axelbaum, R.L. (2014) 'Process design and performance analysis of a Staged, Pressurized Oxy-Combustion (SPOC) power plant for carbon capture', *Applied Energy*, 125, pp. 179-188.

Gunawan, T., Wijiyanti, R. and Widiastuti, N. (2018) 'Adsorption–desorption of CO 2 on zeolite-Y-templated carbon at various temperatures', *RSC advances*, 8(72), pp. 41594-41602.

Gunawardene, O.H., Gunathilake, C.A., Vikrant, K. and Amaraweera, S.M. (2022) 'Carbon Dioxide capture through physical and chemical adsorption using porous carbon materials: A review', *Atmosphere*, 13(3), p. 397.

Günther, A. and Jensen, K.F. (2006) 'Multiphase microfluidics: from flow characteristics to chemical and materials synthesis', *Lab on a Chip*, 6(12), pp. 1487-1503.

Guo, Q.j., Xu, Y. and Yue, X. (2009) 'Fluidization Characteristics in Micro-Fluidized Beds of Various Inner Diameters', *Chemical Engineering & Technology*, 32(12), pp. 1992-1999.

Guo, Y., Zhao, Y., Meng, S., Feng, D., Yan, T., Wang, P. and Sun, S. (2016) 'Development of a Multistage in Situ Reaction Analyzer Based on a Micro Fluidized Bed and Its Suitability for Rapid Gas–Solid Reactions', *Energy & Fuels*, 30(7), pp. 6021-6033.

Gutierrez-Ortega, A., Nomen, R., Sempere, J., Parra, J., Montes-Morán, M. and Gonzalez-Olmos, R. (2022) 'A fast methodology to rank adsorbents for CO_2 capture with temperature swing adsorption', *Chemical Engineering Journal*, 435, p. 134703.

Habib, M.A., Badr, H.M., Ahmed, S.F., Ben-Mansour, R., Mezghani, K., Imashuku, S., la O, G.J., Shao-Horn, Y., Mancini, N.D., Mitsos, A., Kirchen, P. and Ghoneim, A.F. (2011) 'A review of recent developments in carbon capture utilizing oxy-fuel combustion in conventional and ion transport membrane systems', *International Journal of Energy Research*, 35(9), pp. 741-764.

Han, Z., Yue, J., Geng, S., Hu, D., Liu, X., Suleiman, S.B., Cui, Y., Bai, D. and Xu, G. (2021) 'State-of-the-art hydrodynamics of gas-solid micro fluidized beds', *Chemical Engineering Science*, 232, p. 116345.

Han, Z., Yue, J., Zeng, X., Yu, J., Wang, F., Sun, S., Yao, H., Luo, G., Liu, X., Sun, Y., Ding, F., Fu, L., Shi, L., Wang, K., Yang, J., Wang, S., Chen, X., Bai, D. and Xu, G. (2020) 'Characteristics of gas-solid micro fluidized beds for thermochemical reaction analysis', *Carbon Resources Conversion*, 3, pp. 203-218.

Hao, J., Liang, B. and Sun, W. (2021) 'Experimental study on the thermal effect during gas adsorption and desorption on the coal surface', *ACS omega*, 6(2), pp. 1603-1611.

He, T., Liu, Z., Son, H., Gundersen, T. and Lin, W. (2023) 'Comparative analysis of cryogenic distillation and chemical absorption for carbon capture in integrated natural gas liquefaction processes', *Journal of Cleaner Production*, 383.

Heydari-Gorji, A. and Sayari, A. (2011) 'CO_2 capture on polyethylenimine-impregnated hydrophobic mesoporous silica: Experimental and kinetic modeling', *Chemical Engineering Journal*, 173(1), pp. 72-79.

Hickman, D.A., Degenstein, J.C. and Ribeiro, F.H. (2016) 'Fundamental principles of laboratory fixed bed reactor design', *Current Opinion in Chemical Engineering*, 13, pp. 1-9.

Hsu, W.-Y., Huang, A.-N. and Kuo, H.-P. (2018) 'Analysis of interparticle forces and particle-wall interactions by powder bed pressure drops at incipient fluidization', *Powder Technology*, 325, pp. 64-68.

Hu, X., Liu, L., Luo, X., Xiao, G., Shiko, E., Zhang, R., Fan, X., Zhou, Y., Liu, Y., Zeng, Z. and Li, C.e. (2020) 'A review of N-functionalized solid adsorbents for post-combustion CO_2 capture', *Applied Energy*, 260.

J.M. Valverde a, F.J.D.a., F. Pontiga b, H. Moreno b (2012) 'CO_2 capture enhancement in a fluidized bed of a modified CrossMark Geldart C powder', *Powder Technology*, 212, p. 6.

Jae-Rang Leea b, K.-S.L.C., Naim Hasollia, Young-Ok Parka, Kwan-Young Lee and Kim, Y.-H. (2020) 'Fluidization and mixing behaviors of Geldart groups A, B and C particles assisted by vertical vibration in fluidized bed', *Chemical Engineering & Processing: Process Intensification* 149(107856), p. 7.

Jaiboon, O.-a., Chalermsinsuwan, B., Mekasut, L. and Piumsomboon, P. (2013) 'Effect of flow patterns/regimes on CO_2 capture using K_2CO_3 solid sorbent in fluidized bed/circulating fluidized bed', *Chemical Engineering Journal*, 219, pp. 262-272.

Jamei, R., McDonough, J., Reay, D. and Zivkovic, V. (2023) 'Rapid and intensified screening of a carbon capture adsorbent using a 3D-printed swirling fluidised bed', *Chemical Engineering Journal*, 451, p. 138405.

Jansen, D., Gazzani, M., Manzolini, G., Dijk, E.v. and Carbo, M. (2015) 'Pre-combustion CO_2 capture', *International Journal of Greenhouse Gas Control*, 40, pp. 167-187.

Jiang, L., Wang, R., Gonzalez-Diaz, A., Smallbone, A., Lamidi, R. and Roskilly, A. (2020) 'Comparative analysis on temperature swing adsorption cycle for carbon capture by using internal heat/mass recovery', *Applied Thermal Engineering*, 169, p. 114973.

Jiang, Z. and Fatah, N. (2022) 'New investigation of Micro-fluidized bed: The effect of wall roughness and particle size on hydrodynamics regimes', *Chemical Engineering Journal*, 430, p. 133075.

Jose, N.A., Zeng, H.C. and Lapkin, A.A. (2018) 'Hydrodynamic assembly of two-dimensional layered double hydroxide nanostructures', *Nature communications*, 9(1), p. 4913.

Jung, W., Park, J. and Lee, K.S. (2018a) 'Kinetic modeling of CO_2 adsorption on an amine-functionalized solid sorbent', *Chemical Engineering Science*, 177, pp. 122-131.

Jung, W., Park, J., Won, W. and Lee, K.S. (2018b) 'Simulated moving bed adsorption process based on a polyethylenimine-silica sorbent for CO_2 capture with sensible heat recovery', *Energy*, 150, pp. 950-964.

Kamranian Marnani, A., Bück, A., Antonyuk, S., van Wachem, B., Thévenin, D. and Tomas, J. (2019) 'The Effect of the Presence of Very Cohesive Geldart C Ultra-Fine Particles on the Fluidization of Geldart A Fine Particle Beds', *Processes*, 7(1).

Kanniche, M., Gros-Bonnivard, R., Jaud, P., Valle-Marcos, J., Amann, J.-M. and Bouallou, C. (2010) 'Pre-combustion, post-combustion and oxy-combustion in thermal power plant for CO_2 capture', *Applied Thermal Engineering*, 30(1), pp. 53-62.

Kárászová, M., Zach, B., Petrusová, Z., Červenka, V., Bobák, M., Šyc, M. and Izák, P. (2020) 'Post-combustion carbon capture by membrane separation, Review', *Separation and Purification Technology*, 238, p. 116448.

Khraisheh, M., Mukherjee, S., Kumar, A., Al Momani, F., Walker, G. and Zaworotko, M.J. (2020) 'An overview on trace CO_2 removal by advanced physisorbent materials', *J Environ Manage*, 255, p. 109874.

Kim, C., Cho, H.S., Chang, S., Cho, S.J. and Choi, M. (2016a) 'An ethylenediamine-grafted Y zeolite: a highly regenerable carbon dioxide adsorbent via temperature swing adsorption without urea formation', *Energy & Environmental Science*, 9(5), pp. 1803-1811.

Kim, K.-Y., Yang, W., Ye, Y., LaBarge, N. and Logan, B.E. (2016b) 'Performance of anaerobic fluidized membrane bioreactors using effluents of microbial fuel cells treating domestic wastewater', *Bioresource Technology*, 208, pp. 58-63.

Kim, K., Son, Y., Lee, W.B. and Lee, K.S. (2013) 'Moving bed adsorption process with internal heat integration for carbon dioxide capture', *International Journal of Greenhouse Gas Control*, 17, pp. 13-24.

Kim, S., Jeon, S.G. and Lee, K.B. (2016c) 'High-Temperature CO_2 Sorption on Hydrotalcite Having a High Mg/Al Molar Ratio', *ACS Appl Mater Interfaces*, 8(9), pp. 5763-7.

Kim, Y., Lim, S.-R. and Park, J.M. (2012) 'The effects of Cu (II) ion as an additive on NH_3 loss and CO_2 absorption in ammonia-based CO_2 capture processes', *Chemical engineering journal*, 211, pp. 327-335.

Knowlton, T.M., Karri, S.B.R. and Issangya, A. (2005) 'Scale-up of fluidized-bed hydrodynamics', *Powder Technology*, 150(2), pp. 72-77.

Knox, J.C., Ebner, A.D., LeVan, M.D., Coker, R.F. and Ritter, J.A. (2016a) 'Limitations of breakthrough curve analysis in fixed-bed adsorption', *Industrial & engineering chemistry research*, 55(16), pp. 4734-4748.

Knox, J.C., Ebner, A.D., LeVan, M.D., Coker, R.F. and Ritter, J.A. (2016b) 'Limitations of Breakthrough Curve Analysis in Fixed-Bed Adsorption', *Ind Eng Chem Res*, 55(16), pp. 4734-4748.

Kong, W., Tan, T., Baeyens, J., Flamant, G. and Zhang, H. (2017) 'Bubbling and Slugging of Geldart Group A Powders in Small Diameter Columns', *Industrial & Engineering Chemistry Research*, 56(14), pp. 4136-4144.

Kongkitisupchai, S. and Gidaspow, D. (2013) 'Carbon dioxide capture using solid sorbents in a fluidized bed with reduced pressure regeneration in a downer', *AIChE Journal*, 59(12), pp. 4519-4537.

Kono, H., Chiba, S., Ells, T. and Suzuki, M. (1986) 'Characterization of the emulsion phase in fine particle fluidized beds', *Powder technology*, 48(1), pp. 51-58.

Krishnamurthy, S., Lind, A., Bouzga, A., Pierchala, J. and Blom, R. (2021) 'Post combustion carbon capture with supported amine sorbents: From adsorbent characterization to process simulation and optimization', *Chemical Engineering Journal*, 406, p. 127121.

Kudahi, S.N., Noorpoor, A.R. and Mahmoodi, N.M. (2017) 'Determination and analysis of CO_2 capture kinetics and mechanisms on the novel graphene-based adsorbents', *Journal of CO_2 Utilization*, 21, pp. 17-29.

Kumar, P., Tokas, J., Kumar, N., Lal, M. and Singal, H. (2018) 'Climate change consequences and its impact on agriculture and food security', *International Journal of chemical studies*, 6(6), pp. 124-133.

LaMarche, C.Q., Miller, A.W., Liu, P. and Hrenya, C.M. (2016) 'Linking micro-scale predictions of capillary forces to macro-scale fluidization experiments in humid environments', *AIChE Journal*, 62(10), pp. 3585-3597.

Lamia, N., Wolff, L., Leflaive, P., Leinekugel-Le-Cocq, D., Sá Gomes, P., Grande, C.A. and Rodrigues, A.E. (2008) 'Equilibrium and Fixed Bed Adsorption of 1-Butene, Propylene and Propane Over 13X Zeolite Pellets', *Separation Science and Technology*, 43(5), pp. 1124-1156.

Landi, G., Barletta, D. and Poletto, M. (2011) 'Modelling and experiments on the effect of air humidity on the flow properties of glass powders', *Powder Technology*, 207(1-3), pp. 437-443.

Lee, D., Shun, D., Bae, D.H., Ryu, H.-J. and Baek, J.-I. (2019) 'Solid Circulation Characteristics of Two Lower Loop Seals with Two Kinds of Particles in a Circulating Fluidized Bed System', *Journal of Chemical Engineering of Japan*, 52(1), pp. 106-110.

Lee, J.-R., Lee, K.-S., Hasolli, N., Park, Y.-O., Lee, K.-Y. and Kim, Y.-H. (2020) 'Fluidization and mixing behaviors of Geldart groups A, B and C particles assisted by vertical vibration in fluidized bed', *Chemical Engineering and Processing - Process Intensification*, 149.

Lee, S.-Y. and Park, S.-J. (2015) 'A review on solid adsorbents for carbon dioxide capture', *Journal of Industrial and Engineering Chemistry*, 23, pp. 1-11.

León, M., Diaz, E., Bennici, S., Vega, A., Ordónez, S. and Auroux, A. (2010) 'Adsorption of CO_2 on hydrotalcite-derived mixed oxides: sorption mechanisms and consequences for adsorption irreversibility', *Industrial & engineering chemistry research*, 49(8), pp. 3663-3671.

Leva, M., Weintraub, M., Grummer, M., Pollchik, M., Storch, H.H. (1951) ' Fluid flow through packed and fluidized systems. ', *US Government Printing Office, Washington, DC, .*

Li, X., Liu, M. and Li, Y. (2018) 'Hydrodynamic behavior of liquid–solid micro-fluidized beds determined from bed expansion', *Particuology*, 38, pp. 103-112.

Li, X., Wang, L., Jia, L. and Cai, W. (2017) 'Numerical and experimental study of a novel compact micro fluidized beds reactor for CO_2 capture in HVAC', *Energy and Buildings*, 135, pp. 128-136.

Li, Y., Li, Z., Wang, H. and Cai, N. (2020) 'CaO carbonation kinetics determined using micro-fluidized bed thermogravimetric analysis', *Fuel*, 264, p. 116823.

Lim, J.-H., Bae, K., Shin, J.-H., Kim, J.-H., Lee, D.-H., Han, J.-H. and Lee, D.H. (2016) 'Effect of particle–particle interaction on the bed pressure drop and bubble flow by computational particle-fluid dynamics simulation of bubbling fluidized beds with shroud nozzle', *Powder Technology*, 288, pp. 315-323.

Liu, X., Xu, G. and Gao, S. (2008) 'Micro fluidized beds: Wall effect and operability', *Chemical Engineering Journal*, 137(2), pp. 302-307.

Liu, Z.-K., Agren, J. and Hillert, M. (1996) 'Application of the Le Chatelier principle on gas reactions', *Fluid phase equilibria*, 121(1-2), pp. 167-177.

Loezos, P.N., Costamagna, P. and Sundaresan, S. (2002) 'The role of contact stresses and wall friction on fluidization', *Chemical Engineering Science*, 57(24), pp. 5123-5141.

Luo, Z., Zhao, Y., Lv, B., Fu, Y., Xu, X. and Chen, C. (2022) 'Dry coal beneficiation technique in the gas–solid fluidized bed: a review', *International Journal of Coal Preparation and Utilization*, 42(4), pp. 986-1014.

Macdonald, N.P., Cabot, J.M., Smejkal, P., Guijt, R.M., Paull, B. and Breadmore, M.C. (2017) 'Comparing Microfluidic Performance of Three-Dimensional (3D) Printing Platforms', *Anal Chem*, 89(7), pp. 3858-3866.

MacDowell, N., Florin, N., Buchard, A., Hallett, J., Galindo, A., Jackson, G., Adjiman, C.S., Williams, C.K., Shah, N. and Fennell, P. (2010) 'An overview of CO_2 capture technologies', *Energy & Environmental Science*, 3(11), pp. 1645-1669.

Madejski, P., Chmiel, K., Subramanian, N. and Kuś, T. (2022) 'Methods and Techniques for CO_2 Capture: Review of Potential Solutions and Applications in Modern Energy Technologies', *Energies*, 15(3), p. 887.

Mallakpour, S., Hatami, M. and Hussain, C.M. (2020) 'Recent innovations in functionalized layered double hydroxides: Fabrication, characterization, and industrial applications', *Advances in Colloid and Interface Science*, 283, p. 102216.

Management, O.o.F.E.a.C. (2023) *Pre-Combustion Carbon Capture Research*.Available at: https://www.energy.gov/fecm/pre-combustion-carbon-capture-research(Accessed: 17/07/2023).

McDonough, J.R., Law, R., Reay, D.A., Groszek, D. and Zivkovic, V. (2020) 'Miniaturisation of the toroidal fluidisation concept using 3D printing', *Chemical Engineering Research and Design*, 160, pp. 129-140.

McDonough, J.R., Law, R., Reay, D.A. and Zivkovic, V. (2018) 'Intensified carbon capture using adsorption: Heat transfer challenges and potential solutions', *Thermal Science and Engineering Progress*, 8, pp. 17-30.

McDonough, J.R., Law, R., Reay, D.A. and Zivkovic, V. (2019) 'Fluidization in small-scale gas-solid 3D-printed fluidized beds', *Chemical Engineering Science*, 200, pp. 294-309.

Mehrani, P., Bi, H.T. and Grace, J.R. (2005) 'Electrostatic charge generation in gas–solid fluidized beds', *Journal of Electrostatics*, 63(2), pp. 165-173.

Mesfer, M.K.A., Danish, M., Khan, M.I., Ali, I.H., Hasan, M. and Jery, A.E. (2020) 'Continuous Fixed Bed CO_2 Adsorption: Breakthrough, Column Efficiency, Mass Transfer Zone', *Processes*, 8(10).

Mikhaylov, R.V., Nikitin, K.V., Glazkova, N.I. and Kuznetsov, V.N. (2018) 'Temperature-programmed desorption of CO_2, formed by CO photooxidation on TiO_2 surface', *Journal of Photochemistry and Photobiology A: Chemistry*, 360, pp. 255-261.

Molerus, O. (1982) 'Interpretation of Geldart's type A, B, C and D powders by taking into account interparticle cohesion forces', *Powder Technology*, 33(1), pp. 81-87.

Monazam, E.R., Spenik, J. and Shadle, L.J. (2013) 'Fluid bed adsorption of carbon dioxide on immobilized polyethylenimine (PEI): Kinetic analysis and breakthrough behavior', *Chemical Engineering Journal*, 223, pp. 795-805.

Mondal, M.K., Balsora, H.K. and Varshney, P. (2012) 'Progress and trends in CO_2 capture/separation technologies: A review', *Energy*, 46(1), pp. 431-441.

Morales-Ospino, R., Santiago, R.G., Siqueira, R.M., de Azevedo, D.C.S. and Bastos-Neto, M. (2020) 'Assessment of CO_2 desorption from 13X zeolite for a prospective TSA process', *Adsorption*, 26, pp. 813-824.

Moreira, R., Soares, J., Casarin, G. and Rodrigues, A. (2006) 'Adsorption of CO_2 on Hydrotalcite-like Compounds in a Fixed Bed', *Separation science and technology*, 41(2), pp. 341-357.

Mukherjee, A., Okolie, J.A., Abdelrasoul, A., Niu, C. and Dalai, A.K. (2019) 'Review of post-combustion carbon dioxide capture technologies using activated carbon', *Journal of Environmental Sciences*, 83, pp. 46-63.

Najmi, B., Bolland, O. and Colombo, K.E. (2016) 'A systematic approach to the modeling and simulation of a Sorption Enhanced Water Gas Shift (SEWGS) process for CO_2 capture', *Separation and Purification Technology*, 157, pp. 80-92.

Nam, H., Won, Y., Kim, J.-Y., Yi, C.-K., Park, Y.C., Woo, J.M., Jung, S.-Y., Jin, G.-T., Jo, S.-H., Lee, S.-Y., Kim, H. and Park, J. (2020) 'Hydrodynamics and heat transfer coefficients during CO_2 carbonation reaction in a circulated fluidized bed reactor using 200 kg potassium-based dry sorbent', *Energy*, 193, p. 116643.

Nemitallah, M.A., Habib, M.A., Badr, H.M., Said, S.A., Jamal, A., Ben-Mansour, R., Mokheimer, E.M.A. and Mezghani, K. (2017) 'Oxy-fuel combustion technology: current status, applications, and trends', *International Journal of Energy Research*, 41(12), pp. 1670-1708.

Nishimura, S., Takagaki, A. and Ebitani, K. (2013) 'Characterization, synthesis and catalysis of hydrotalcite-related materials for highly efficient materials transformations', *Green Chemistry*, 15(8), pp. 2026-2042.

Ntiamoah, A., Ling, J., Xiao, P., Webley, P.A. and Zhai, Y. (2016) 'CO_2 capture by temperature swing adsorption: use of hot CO_2-rich gas for regeneration', *Industrial & Engineering Chemistry Research*, 55(3), pp. 703-713.

Ochedi, F.O., Yu, J., Yu, H., Liu, Y. and Hussain, A. (2020) 'Carbon dioxide capture using liquid absorption methods: a review', *Environmental Chemistry Letters*, 19(1), pp. 77-109.

Oliveira, E.L.G., Grande, C.A. and Rodrigues, A.E. (2008) 'CO_2 sorption on hydrotalcite and alkali-modified (K and Cs) hydrotalcites at high temperatures', *Separation and Purification Technology*, 62(1), pp. 137-147.

Ortrud Aschenbrenner a, P.M.b., Suzanne Alsamaqb, Jiawei Wangb, and Somsak Supasitmongkol a, B.A.-D.b., Peter Styring a, Joseph Woodb, (2011) 'Adsorption of carbon dioxide on hydrotalcite-likecompounds of different compositions', *Chemical Engineering Research and Design*, p. 11.

Pan, S., Ma, J., Liu, D., Chen, X. and Liang, C. (2022) 'Theoretical and experimental insight into the homogeneous expansion of wet particles in a fluidized bed', *Powder Technology*, 397, p. 117016.

Patel, H. (2019) 'Fixed-bed column adsorption study: a comprehensive review', *Applied Water Science*, 9(3), p. 45.

Pell, M. (1990) *Gas fluidization*. (Volume 8).Amsterdam. Elsevier.

Peredo-Mancilla, D., Ghouma, I., Hort, C., Matei Ghimbeu, C., Jeguirim, M. and Bessieres, D. (2018) 'CO_2 and CH4 adsorption behavior of biomass-based activated carbons', *Energies*, 11(11), p. 3136.

Peter N. Loezos, P.C., Sankaran Sundaresan (2002) 'The Role of Contact Stresses and Wall Friction on Fluidization', *Chemical Engineering Science*, 57 p. 19.

Potic, B., Kersten, S.R.A., Ye, M., van der Hoef, M.A., Kuipers, J.A.M. and van Swaaij, W.P.M. (2005) 'Fluidization with hot compressed water in micro-reactors', *Chemical Engineering Science*, 60(22), pp. 5982-5990.

Prajapati, Renganathan and Krishnaiah. (2016) 'Kinetic Studies of CO_2 Capture Using K2CO3/Activated Carbon in Fluidized Bed Reactor', *Energy & Fuels*, 30(12), pp. 10758-10769.

Qie, Z., Alhassawi, H., Sun, F., Gao, J., Zhao, G. and Fan, X. (2022) 'Characteristics and applications of micro fluidized beds (MFBs)', *Chemical Engineering Journal*, 428, p. 131330.

Rabbani, G., Rahman, A. and Mainuddin, K. (2013) 'Salinity-induced loss and damage to farming households in coastal Bangladesh', *International Journal of Global Warming*, 5(4), pp. 400-415.

Raganati, F., Alfe, M., Gargiulo, V., Chirone, R. and Ammendola, P. (2019) 'Kinetic study and breakthrough analysis of the hybrid physical/chemical CO_2 adsorption/desorption behavior of a magnetite-based sorbent', *Chemical Engineering Journal*, 372, pp. 526-535.

Raganati, F., Ammendola, P. and Chirone, R. (2014) 'CO_2 adsorption on fine activated carbon in a sound assisted fluidized bed: Effect of sound intensity and frequency, CO_2 partial pressure and fluidization velocity', *Applied Energy*, 113, pp. 1269-1282.

Raganati, F., Ammendola, P. and Chirone, R. (2015) 'Effect of acoustic field on CO_2 desorption in a fluidized bed of fine activated carbon', *Particuology*, 23, pp. 8-15.

Raganati, F., Chirone, R. and Ammendola, P. (2018) 'Gas–solid fluidization of cohesive powders', *Chemical Engineering Research and Design*, 133, pp. 347-387.

Raganati, F., Miccio, F. and Ammendola, P. (2021) 'Adsorption of Carbon Dioxide for Post-combustion Capture: A Review', *Energy & Fuels*, 35(16), pp. 12845-12868.

Ram, D.K. (2013) 'The Determination of Minimum Bubbling Velocity, Minimum Fluidization Velocity and Fluidization Index of Fine Powders (Hematite) using Gas-Solid Tapered Beds', *International Journal of Science and Research*, 2(2), p. 6.

Rao, A., Curtis, J.S., Hancock, B.C. and Wassgren, C. (2010) 'The effect of column diameter and bed height on minimum fluidization velocity', *AIChE journal*, 56(9), pp. 2304-2311.

Reddy, M.S.B., Ponnamma, D., Sadasivuni, K.K., Kumar, B. and Abdullah, A.M. (2021) 'Carbon dioxide adsorption based on porous materials', *RSC advances*, 11(21), pp. 12658-12681.

Reijers, H.T.J., Valster-Schiermeier, S.E., Cobden, P.D. and Van Den Brink, R.W. (2006) 'Hydrotalcite as CO_2 sorbent for sorption-enhanced steam reforming of methane', *Industrial & engineering chemistry research*, 45(8), pp. 2522-2530.

Ren, H., Zhang, H., Li, W., Tang, Z. and Zhang, D. (2022) 'Simulation of CO_2 capture process in gas-solid bubbling fluidized bed by computational mass transfer', *Journal of Environmental Chemical Engineering*, 10(5), p. 108548.

Revellame, E.D., Fortela, D.L., Sharp, W., Hernandez, R. and Zappi, M.E. (2020) 'Adsorption kinetic modeling using pseudo-first order and pseudo-second order rate laws: A review', *Cleaner Engineering and Technology*, 1, p. 100032.

Rogelj, J., Geden, O., Cowie, A. and Reisinger, A. (2021) 'Net-zero emissions targets are vague: three ways to fix', *Nature*, 591(7850), pp. 365-368.

Røkke, N.A. and Langørgen, Ø. (2009) 'Enabling pre-combustion plants—the DECARBit project', *Energy Procedia*, 1(1), pp. 1435-1442.

Rongtao, F., Junguo, L., Libo, D., Zhenhua, H., Zhongren, B., Haijuan, Z. and Yitian, F. (2019) 'Gas-solid flow behaviors in a multi-stage circulating fluidized bed under elevated pressure', *Chemical Engineering Science*, 196, pp. 1-13.

Rossi, T.M., Campos, J.C. and Souza, M.M. (2016) 'CO_2 capture by Mg–Al and Zn–Al hydrotalcite-like compounds', *Adsorption*, 22, pp. 151-158.

Rüdisüli, M., Schildhauer, T.J., Biollaz, S.M.A. and van Ommen, J.R. (2012) 'Scale-up of bubbling fluidized bed reactors — A review', *Powder Technology*, 217, pp. 21-38.

Sabouni, R., Kazemian, H. and Rohani, S. (2013) 'Mathematical modeling and experimental breakthrough curves of carbon dioxide adsorption on metal organic framework CPM-5', *Environmental science & technology*, 47(16), pp. 9372-80.

Salazar Duarte, G., Schürer, B., Voss, C. and Bathen, D. (2017) 'Adsorptive separation of CO_2 from flue gas by temperature swing adsorption processes', *ChemBioEng Reviews*, 4(5), pp. 277-288.

Samanta, A., Zhao, A., Shimizu, G.K.H., Sarkar, P. and Gupta, R. (2011) 'Post-Combustion CO_2 Capture Using Solid Sorbents: A Review', *Industrial & Engineering Chemistry Research*, 51(4), pp. 1438-1463.

Sánchez-Delgado, S., Almendros-Ibáñez, J.A., García-Hernando, N. and Santana, D. (2011) 'On the minimum fluidization velocity in 2D fluidized beds', *Powder Technology*, 207(1-3), pp. 145-153.

Sande, P. and Ray, S. (2014) 'Mesh size effect on CFD simulation of gas-fluidized Geldart A particles', *Powder technology*, 264, pp. 43-53.

Sau, D.C., Mohanty, S. and Biswal, K.C. (2007) 'Minimum fluidization velocities and maximum bed pressure drops for gas–solid tapered fluidized beds', *Chemical Engineering Journal*, 132(1-3), pp. 151-157.

Scholes, C.A., Smith, K.H., Kentish, S.E. and Stevens, G.W. (2010) 'CO_2 capture from pre-combustion processes—Strategies for membrane gas separation', *International Journal of Greenhouse Gas Control*, 4(5), pp. 739-755.

Scott, D. and Piskorz, J. (1982) 'The flash pyrolysis of aspen-poplar wood', *The Canadian Journal of Chemical Engineering*, 60(5), pp. 666-674.

Selmert, V., Kretzschmar, A., Weinrich, H., Tempel, H., Kungl, H. and Eichel, R.A. (2022) 'CO_2/N_2 Separation on Highly Selective Carbon Nanofibers Investigated by Dynamic Gas Adsorption', *ChemSusChem*, 15(14), p. e202200761.

Serna-Guerrero, R. and Sayari, A. (2010) 'Modeling adsorption of CO_2 on amine-functionalized mesoporous silica. 2: Kinetics and breakthrough curves', *Chemical Engineering Journal*, 161(1-2), pp. 182-190.

Shafeeyan, M.S., Daud, W.M.A.W. and Shamiri, A. (2014) 'A review of mathematical modeling of fixed-bed columns for carbon dioxide adsorption', *Chemical engineering research and design*, 92(5), pp. 961-988.

Shafeeyan, M.S., Daud, W.M.A.W., Shamiri, A. and Aghamohammadi, N. (2015) 'Modeling of carbon dioxide adsorption onto ammonia-modified activated carbon: kinetic analysis and breakthrough behavior', *Energy & Fuels*, 29(10), pp. 6565-6577.

Shaul, S., Rabinovich, E. and Kalman, H. (2012) 'Generalized flow regime diagram of fluidized beds based on the height to bed diameter ratio', *Powder Technology*, 228, pp. 264-271.

Shen, T., Zhu, X., Song, T. and Shen, L. (2020) 'Fluidization of micro-interconnected fluidized beds for chemical looping', *Particuology*.

Shen, T., Zhu, X., Song, T. and Shen, L. (2021) 'Fluidization of micro-interconnected fluidized beds for chemical looping', *Particuology*, 54, pp. 136-145.

Shen, T., Zhu, X., Yan, J. and Shen, L. (2019) 'Design of micro interconnected fluidized bed for oxygen carrier evaluation', *International Journal of Greenhouse Gas Control*, 90.

Shi, X., Lan, X., Liu, F., Zhang, Y. and Gao, J. (2014) 'Effect of particle size distribution on hydrodynamics and solids back-mixing in CFB risers using CPFD simulation', *Powder Technology*, 266, pp. 135-143.

Shi, Y., Li, Y., Du, Y. and Ren, W. (2021) 'Experimental study on pressure drop characteristics and minimum fluidization velocity of gas-solid micro-fluidized bed', *Guocheng Gongcheng Xuebao/The Chinese Journal of Process Engineering*, 21(4), pp. 420-430.

Shrestha, S. and Zhou, Z. (2021) *EPJ Web of Conferences*. EDP Sciences.

Siagian, U.W.R., Raksajati, A., Himma, N.F., Khoiruddin, K. and Wenten, I.G. (2019) 'Membrane-based carbon capture technologies: Membrane gas separation vs. membrane contactor', *Journal of Natural Gas Science and Engineering*, 67, pp. 172-195.

Singh, D., Croiset, E., Douglas, P.L. and Douglas, M.A. (2003) 'Techno-economic study of CO_2 capture from an existing coal-fired power plant: MEA scrubbing vs. O_2/CO_2 recycle combustion', *Energy Conversion and Management*, 44(19), pp. 3073-3091.

Skrip, S., Das, G.K. and Chatterjee, S.G. (2013) 'Analytical expressions for the adsorbate breakthrough curve from a fixed bed of adsorbent with first-order and second-order kinetic models', *Indian Chemical Engineer*, 55(2), pp. 87-103.

Smolders, K. and Baeyens, J. (2001) 'Gas fluidized beds operating at high velocities: a critical review of occurring regimes', *Powder Technology*, 119(2-3), pp. 269-291.

Songolzadeh, M., Ravanchi, M.T. and Soleimani, M. (2012) 'Carbon dioxide capture and storage: a general review on adsorbents', *International Journal of Chemical and Molecular Engineering*, 6(10), pp. 906-913.

Suescum-Morales, D., Jiménez, J.R. and Fernández-Rodríguez, J.M. (2022) 'Review of the Application of Hydrotalcite as CO_2 Sinks for Climate Change Mitigation', *ChemEngineering*, 6(4), p. 50.

Sun, Z., Fan, M. and Argyle, M. (2011) 'Desorption kinetics of the monoethanolamine/macroporous TiO2-based CO_2 separation process', *Energy & fuels*, 25(7), pp. 2988-2996.

Szöllösi-Janze, M. (2001) 'Pesticides and war: the case of Fritz Haber', *European Review*, 9(1), pp. 97-108.

Tan, L., Roghair, I. and van Sint Annaland, M. (2017) 'Discrete particle simulations of bubble-to-emulsion phase mass transfer in single-bubble fluidized beds', *Particuology*, 33, pp. 80-90.

Tsutsumi, A., Nakamoto, S., Mineo, T. and Yoshida, K. (1995) 'A novel fluidized-bed coating of fine particles by rapid expansion of supercritical fluid solutions', *Powder Technology*, 85(3), pp. 275-278.

Ullah, A., Wang, W. and Li, J. (2013) '"Generalized Fluidization" Revisited', *Industrial & Engineering Chemistry Research*, 52(33), pp. 11319-11332.

Upendar, K., Sagar, T., Raveendra, G., Lingaiah, N., Rao, B., Prasad, R. and Prasad, P.S. (2014) 'Development of a low temperature adsorbent from karanja seed cake for CO_2 capture', *RSC Advances*, 4(14), pp. 7142-7147.

Vanni, F., Caussat, B., Ablitzer, C. and Brothier, M. (2015) 'Effects of reducing the reactor diameter on the fluidization of a very dense powder', *Powder Technology*, 277, pp. 268-274.

Vargas, A.M., Cazetta, A.L., Kunita, M.H., Silva, T.L. and Almeida, V.C. (2011) 'Adsorption of methylene blue on activated carbon produced from flamboyant pods (Delonix regia): Study of adsorption isotherms and kinetic models', *Chemical Engineering Journal*, 168(2), pp. 722-730.

Vasta, S. (2023) 'Adsorption Air Conditioning for Automotive Applications: A Critical Review'.

Veerabhadrappa, M.G., Maroto-Valer, M.M., Chen, Y. and Garcia, S. (2021) 'Layered double hydroxides-based mixed metal oxides: development of novel structured sorbents for CO_2 capture applications', *ACS Applied Materials & Interfaces*, 13(10), pp. 11805-11813.

Veneman, R., Li, Z.S., Hogendoorn, J.A., Kersten, S.R.A. and Brilman, D.W.F. (2012) 'Continuous CO 2 capture in a circulating fluidized bed using supported amine sorbents', *Chemical Engineering Journal*, 207-208, pp. 18-26.

Verougstraete, B., Martin-Calvo, A., Van der Perre, S., Baron, G., Finsy, V. and Denayer, J.F. (2020) 'A new honeycomb carbon monolith for CO_2 capture by rapid temperature swing adsorption using steam regeneration', *Chemical Engineering Journal*, 383, p. 123075.

Visser, J. (1989) 'An Invited Review Van der Waals and Other Cohesive Forces Affecting Powder Fluidization', *Powder Technology*, 58 (1), p. 10.

Vitillo, J.G., Smit, B. and Gagliardi, L. (2017) 'Introduction: Carbon Capture and Separation', *Chem Rev*, 117(14), pp. 9521-9523.

Vollmari, K., Jasevičius, R. and Kruggel-Emden, H. (2016) 'Experimental and numerical study of fluidization and pressure drop of spherical and non-spherical particles in a model scale fluidized bed', *Powder Technology*, 291, pp. 506-521.

Wang, C., Jia, L., Tan, Y. and Anthony, E. (2007a) *Challenges of Power Engineering and Environment: Proceedings of the International Conference on Power Engineering 2007*. Springer.

Wang, F. and Fan, L.-S. (2011) 'Gas−Solid Fluidization in Mini- and Micro-channels', *Industrial & Engineering Chemistry Research*, 50(8), pp. 4741-4751.

Wang, F., Zeng, X., Geng, S., Yue, J., Tang, S., Cui, Y., Yu, J. and Xu, G. (2017) 'Distinctive Hydrodynamics of a Micro Fluidized Bed and Its Application to Gas–Solid Reaction Analysis', *Energy & Fuels*, 32(4), pp. 4096-4106.

Wang, H., Li, Z., Li, Y. and Cai, N. (2021) 'Reduced-order model for CaO carbonation kinetics measured using micro-fluidized bed thermogravimetric analysis', *Chemical Engineering Science*, 229, p. 116039.

Wang, J., Huang, L., Yang, R., Zhang, Z., Wu, J., Gao, Y., Wang, Q., O'Hare, D. and Zhong, Z. (2014) 'Recent advances in solid sorbents for CO 2 capture and new development trends', *Energy & Environmental Science*, 7(11), pp. 3478-3518.

Wang, J., Tan, L., van der Hoef, M.A., van Sint Annaland, M. and Kuipers, J.A.M. (2011) 'From bubbling to turbulent fluidization: Advanced onset of regime transition in micro-fluidized beds', *Chemical Engineering Science*, 66(9), pp. 2001-2007.

Wang, Q., Feng, Y., Lu, J., Yin, W., Yang, H., Witt, P.J. and Zhang, M. (2015) 'Numerical study of particle segregation in a coal beneficiation fluidized bed by a TFM–DEM hybrid model: Influence of coal particle size and density', *Chemical Engineering Journal*, 260, pp. 240-257.

Wang, S., Li, Y. and Li, Z. (2020a) 'Fast Adsorption Kinetics of CO_2 on Solid Amine Sorbent Measured Using Microfluidized Bed Thermogravimetric Analysis', *Industrial & Engineering Chemistry Research*, 59(15), pp. 6855-6866.

Wang, X.S., Rahman, F. and Rhodes, M.J. (2007b) 'Nanoparticle fluidization and Geldart's classification', *Chemical Engineering Science*, 62(13), pp. 3455-3461.

Wang, Y., Guo, B., Guo, J., Zhang, M., Yang, H. and Jin, Y. (2020b) 'K_2CO_3-Impregnated Al/Si Aerogel Prepared by Ambient Pressure Drying for CO_2 Capture: Synthesis, Characterization and Adsorption Characteristics', *Materials*, 13(17), p. 3741.

Wang, Y. and LeVan, M.D. (2009) 'Adsorption equilibrium of carbon dioxide and water vapor on zeolites 5A and 13X and silica gel: pure components', *Journal of Chemical & Engineering Data*, 54(10), pp. 2839-2844.

Wang, Z. and Zhu, Z. (2021) 'Experimental study on the effects of different heating rates on coalbed methane desorption and an analysis of desorption kinetics', *ACS omega*, 6(50), pp. 34889-34903.

Webley, P.A. (2014) 'Adsorption technology for CO_2 separation and capture: a perspective', *Adsorption*, 20(2-3), pp. 225-231.

Weng, X., Cui, Y., Shaikhutdinov, S. and Freund, H.-J. (2018) 'CO_2 Adsorption on CaO (001): temperature-programmed desorption and infrared study', *The Journal of Physical Chemistry C*, 123(3), pp. 1880-1887.

Werther, J. (2000) 'Fluidized-bed reactors', *Ullmann's encyclopedia of industrial chemistry*.

Wijesiri, R.P., Knowles, G.P., Yeasmin, H., Hoadley, A.F. and Chaffee, A.L. (2019) 'Desorption process for capturing CO_2 from air with supported amine sorbent', *Industrial & Engineering Chemistry Research*, 58(34), pp. 15606-15618.

Wilberforce, T., Olabi, A.G., Sayed, E.T., Elsaid, K. and Abdelkareem, M.A. (2021) 'Progress in carbon capture technologies', *Sci Total Environ*, 761, p. 143203.

Wilkins, N.S., Rajendran, A. and Farooq, S. (2021) 'Dynamic column breakthrough experiments for measurement of adsorption equilibrium and kinetics', *Adsorption*, 27(3), pp. 397-422.

Wormsbecker, M. and Pugsley, T. (2008) 'The influence of moisture on the fluidization behaviour of porous pharmaceutical granule', *Chemical Engineering Science*, 63(16), pp. 4063-4069.

Wu, W., Duan, L., Li, L., Yang, Z., Liu, D. and Anthony, E.J. (2021) 'The gas interchange between bubble and emulsion phases in a pressurized fluidized bed by computational fluid dynamics simulations', *Industrial & Engineering Chemistry Research*, 60(10), pp. 4142-4152.

Wurzbacher, J.A., Gebald, C., Piatkowski, N. and Steinfeld, A. (2012) 'Concurrent separation of CO_2 and H_2O from air by a temperature-vacuum swing adsorption/desorption cycle', *Environmental science & technology*, 46(16), pp. 9191-9198.

Xu, X., Song, C., Andresen, J.M., Miller, B.G. and Scaroni, A.W. (2002) 'Novel polyethylenimine-modified mesoporous molecular sieve of MCM-41 type as high-capacity adsorbent for CO_2 capture', *Energy & Fuels*, 16(6), pp. 1463-1469.

Yaghoobi-Khankhajeh, S., Alizadeh, R. and Zarghami, R. (2018) 'Adsorption modeling of CO_2 in fluidized bed reactor', *Chemical Engineering Research and Design*, 129, pp. 111-121.

Yates, J. (2013) *Fundamentals of fluidized-Bed chemical processes: Butterworths monographs in chemical engineering*. Butterworth-Heinemann.

Yehuda, T. and Kalman, H. (2020) 'Geldart classification for wet particles', *Powder technology*, 362, pp. 288-300.

Yi, C.-K., Jo, S.-H., Seo, Y., Lee, J.-B. and Ryu, C.-K. (2007) 'Continuous operation of the potassium-based dry sorbent CO_2 capture process with two fluidized-bed reactors', *International Journal of Greenhouse Gas Control*, 1(1), pp. 31-36.

Yu, C.-H. and Tan, C.-S. (2013) 'Mixed alkanolamines with low regeneration energy for CO_2 capture in a rotating packed bed', *Energy Procedia*, 37, pp. 455-460.

Yu, J., Yao, C., Zeng, X., Geng, S., Dong, L., Wang, Y., Gao, S. and Xu, G. (2011) 'Biomass pyrolysis in a micro-fluidized bed reactor: Characterization and kinetics', *Chemical Engineering Journal*, 168(2), pp. 839-847.

Yu, J., Yue, J., Liu, Z., Dong, L., Xu, G., Zhu, J., Duan, Z. and Sun, L. (2010) 'Kinetics and mechanism of solid reactions in a micro fluidized bed reactor', *AIChE Journal*, 56(11), pp. 2905-2912.

Yu, J., Zeng, X., Zhang, G., Zhang, J., Wang, Y. and Xu, G. (2013) 'Kinetics and mechanism of direct reaction between CO_2 and $Ca(OH)_2$ in micro fluidized bed', *Environ Sci Technol*, 47(13), pp. 7514-20.

Yu, K.M.K., Curcic, I., Gabriel, J. and Tsang, S.C.E. (2008) 'Recent advances in CO_2 capture and utilization', *ChemSusChem: Chemistry & Sustainability Energy & Materials*, 1(11), pp. 893-899.

Zanco, S.E., Mazzotti, M., Gazzani, M., Romano, M.C. and Martínez, I. (2018) 'Modeling of circulating fluidized beds systems for post-combustion CO_2 capture via temperature swing adsorption', *AIChE Journal*, 64(5), pp. 1744-1759.

Zeinali, F., Ghoreyshi, A. and Najafpour, G. (2012) 'Removal of toluene and dichloromethane from aqueous phase by granular activated carbon (GAC)', *Chemical Engineering Communications*, 199(2), pp. 203-220.

Zeng, H., Qu, X., Xu, D. and Luo, Y. (2022) 'Porous adsorption materials for carbon dioxide capture in industrial flue gas', *Frontiers in Chemistry*, 10, p. 939701.

Zeng, X., Wang, F., Wang, Y., Li, A., Yu, J. and Xu, G. (2014) 'Characterization of char gasification in a micro fluidized bed reaction analyzer', *Energy & fuels*, 28(3), pp. 1838-1845.

Zhang, B., Liu, P., Huang, Z. and Liu, J. (2023) 'Adsorption Equilibrium and Diffusion of CH_4, CO_2, and N2 in Coal-Based Activated Carbon', *ACS omega*, 8(11), pp. 10303-10313.

Zhang, M. and Guo, Y. (2013) 'Rate based modeling of absorption and regeneration for CO_2 capture by aqueous ammonia solution', *Applied Energy*, 111, pp. 142-152.

Zhang, W., Liu, H., Sun, C., Drage, T.C. and Snape, C.E. (2014) 'Capturing CO_2 from ambient air using a polyethyleneimine–silica adsorbent in fluidized beds', *Chemical Engineering Science*, 116, pp. 306-316.

Zhang, W., Sun, C., Snape, C.E., Sun, X. and Liu, H. (2020) 'Cyclic performance evaluation of a polyethylenimine/silica adsorbent with steam regeneration using simulated NGCC flue gas

and actual flue gas of a gas-fired boiler in a bubbling fluidized bed reactor', *International Journal of Greenhouse Gas Control*, 95, p. 102975.

Zhang, Y., Goh, K.-L., Ng, Y.-L., Chow, Y. and Zivkovic, V. (2021a) 'Design and Investigation of a 3D-printed micro-fluidized bed', *ChemEngineering*, 5(3), p. 62.

Zhang, Y., Goh, K.-L., Ng, Y.L., Chow, Y., Wang, S. and Zivkovic, V. (2021b) 'Process intensification in micro-fluidized bed systems: A review', *Chemical Engineering and Processing - Process Intensification*, 164.

Zhang, Y., Ng, Y.L., Goh, K.-L., Chow, Y., Wang, S. and Zivkovic, V. (2021c) 'Fluidization of fungal pellets in a 3D-printed micro-fluidized bed', *Chemical Engineering Science*, 236, p. 116466.

Zhao, R., Wang, Q., Zhao, L., Deng, S., Bian, X. and Liu, L. (2021) 'Comparative study on energy efficiency of moving-bed adsorption for carbon dioxide capture by two evaluation methods', *Sustainable Energy Technologies and Assessments*, 44.

Zhipeng Qie , H.A., Fei Suna, Jihui Gao , Guangbo Zhao , Xiaolei Fan (2022) 'Characteristics and applications of micro fluidized beds (MFBs)', *Chemical Engineering Joumal*, 428 (2022) 131330, p. 17.

Zhou, Y. and Zhu, J. (2021) 'A review on fluidization of Geldart Group C powders through nanoparticle modulation', *Powder Technology*, 381, pp. 698-720.

Zhu, X., Liu, Y., Jiang, X., Wang, H., Wang, Z., Bai, Z. and Ocone, R. (2023) 'Effects of pressure and particle size on bubble behaviors in a pseudo 2D pressured fluidized bed with Geldart A/B, B and D particles', *Chemical Engineering Journal*, p. 143904.

Zivkovic, V. and Biggs, M.J. (2015) 'On importance of surface forces in a microfluidic fluidized bed', *Chemical Engineering Science*, 126, pp. 143-149.

Zivkovic, V., Biggs, M.J. and Alwahabi, Z.T. (2013) 'Experimental study of a liquid fluidization in a microfluidic channel', *AIChE Journal*, 59(2), pp. 361-364.

Zivkovic, V., Ridge, N. and Biggs, M.J. (2017) 'Experimental study of efficient mixing in a micro-fluidized bed', *Applied Thermal Engineering*, 127, pp. 1642-1649.